Engineered Fibrin Scaffolds for Cardiac Tissue Repair

Kassandra S. Thomson

A dissertation

submitted in partial fulfillment of the

requirements for the degree of

Doctor of Philosophy

University of Washington

2013

Reading Committee:

Marta Scatena, Co-Chair

Cecilia M. Giachelli, Co-Chair

Michael Regnier

Program Authorized to Offer Degree:

Bioengineering

Abstract

Engineered Fibrin Scaffolds for Cardiac Tissue Repair

Kassandra S. Thomson

University of Washington, Department of Bioengineering

Supervisory Committee:
Dr. Michael Regnier, Bioengineering (Co-Chair)
Dr. Marta Scatena, Bioengineering (Co-Chair)
Dr. Cecilia M. Giachelli, Bioengineering
Dr. Michael A. Laflamme, Pathology
Dr. William M. Mahoney Jr., Pathology (GSR)

Myocardial infarction (MI) causes significant cell loss and damage to myocardium. Cell-based therapies for treatment of MI aim to remuscularize the resultant scar, but the majority of transplanted cells do not survive or integrate with host tissue. Additionally, survival of tissue engineered constructs after implantation depends heavily on induction of a vascular response in host tissue in order to promote a quick anastomosis of the cellular graft. Scaffolds can improve cell retention following implantation, but often do little to enhance host-graft integration. Fibrin is an ideal biomaterial for cardiac tissue engineering as it is a natural, biodegradable polymer that can induce neovascularization, promote cell attachment, and has tunable mechanical properties. The research presented in this dissertation describes the development and characterization of a novel high density microtemplated fibrin scaffold with mechanical stiffness comparable to native myocardium, tunable degradation, and a microarchitecture designed to promote cellular organization within constructs. Acellular fibrin scaffolds demonstrated highly angiogenic properties when implanted. Cell seeding with a tri-cell mixture of cardiomyocytes, endothelial cells, and fibroblasts demonstrated the fibrin scaffolds promote cardiomyocyte alignment and the development of a pre-vascular network. The fibrin scaffolds are designed to promote graft cell organization and improve chances of construct survival and integration with host tissue upon implantation.

Table of Contents

List of Figures

List of Tables

Acknowledgements

Thank you to Sarah Dupras for performing animal implant surgeries, Galina Flint for performing cell isolations, Maria Razumova for instruction in mechanical testing, and Veronica Muskheli, Kareen Kreutziger, Mandy Lund, Matt Coons, Elizabeth Gay and Christopher Hargrave for assistance with histological sample preparations and analysis. Thanks to Michael Linnes, Lauran Madden, and Derek Mortisen for instruction in scaffold construction procedures, Ben van Biber for the supply and assistance with hESC cardiomyocytes, and Marc Takeno, Alex Chen, and Ron Seifert for assistance with polarized light and 2-photon imaging. I sincerely thank the members of the Regnier & Scatena labs for all of your friendship and support, especially Scott Lundy, Erik Feest, Sarah Nowakowski, Dan Wang, Anthony Rodriguez, Bree Robinson, Maria Razumova, Vijay Rao, and Steve Korte. Thank you to all of my friends for your support and love, especially Brittany Lundy. Finally, I would like to thank each of my committee members for their guidance in helping me to develop as a scientist, in particular my two advisors Michael Regnier and Marta Scatena for supporting me and allowing me to pursue the new avenues of research described in this dissertation.

Dedication

I dedicate this dissertation to my husband Adam, my parents, and my brother. Without the love and support of my family throughout my life I never would have made it this far, and I doubt I will ever be able to adequately express my love, gratitude and thanks to you. To my husband Adam, thank you for supporting and believing in me through the years, and for keeping me sane along this journey – I could not have done it without you.

Chapter 1:

Background

1.1. Significance

An estimated 84 million Americans suffer from some form of cardiovascular disease, with over 1 million patients diagnosed with a new or recurrent heart attack (myocardial infarction) each year in the United States (1). Myocardial infarction (MI) occurs when a coronary artery becomes occluded and tissue downstream begins to die within minutes due to lack of oxygen. Because cardiomyocytes cannot repair or regenerate themselves, dead tissue is quickly replaced with a dense fibrous scar (infarct) much stiffer and less compliant than intact myocardium and which can no longer propagate electrical signals. There are three phases describing tissue remodeling following MI (**Figure 1.1**). The first is the inflammatory phase, occurring hours to days after injury, in which cardiomyocyte death leads to the release of chemokines and cytokines that recruit inflammatory cells to the site of injury. This is followed by the proliferative phase (days to weeks), which is characterized by a high degree of angiogenesis and mesenchymal cell recruitment to the site of injury. Fibroblasts are highly proliferative and secrete a large amount of collagen-rich extracellular matrix (ECM). The third and final phase is maturation of the scar tissue as the newly deposited ECM is cross-linked and the majority of fibroblasts and endothelial cells present in the previous phases undergo apoptosis. Scar maturation occurs on the order of weeks to months after initial injury (2, 3).

MI leads to a dramatic increase in risk of repeated heart complications, chances of arrhythmias, and in severe cases can cause instant mortality. Scar tissue causes stiffening of the heart wall, decreasing effective blood pumping, particularly when located within the left ventricle. In some cases the body can temporarily stabilize the damaged heart in an attempt to maintain cardiac output, but these compensatory mechanisms eventually lead to deterioration of the heart and ultimately heart failure (4). Patients may be put on pharmacological regimens after an MI, but these typically only treat the symptoms and can slow but not prevent the progression to total heart failure. Coronary artery bypass surgery is a possibility for some patients as an attempt to restore blood perfusion to the tissue downstream of an occluded vessel. However, the only currently available treatment for these patients that addresses the loss of muscle function in the heart is to have a left ventricular assist device (LVAD) implanted, which is generally only intended for temporary use until the patient can receive a full heart transplant. Unfortunately, due to the severe lack of available donors, less than 1% of patients with end-stage heart failure ever receive a transplant (1, 4). There is therefore a large significant need for innovative new therapies that can address the loss of cardiac cells and tissue function for treatment of patients suffering from MI.

1.2. Cell-Based Therapies for MI

Current research in cell-based cardiac repair includes inducing resident adult cardiac stem cells (SCs) to initiate repair processes or injecting cells (such as bone marrow SCs, skeletal myoblasts, or SC-derived cardiomyocytes) into coronary vessels, with the hope that delivered cells will home in on damaged tissue and exert therapeutic effects (4-7). However, very few cells actually reach the infarct with these methods. Direct injection into the infarct zone also has very low cell survival and retention rates (<10%), most likely due to the ischemic conditions of the infarct (6). Alternatively, sheets of cells

have been stacked to form tissue grafts a few cell layers thick, but these are limited by diffusion of nutrients, low mechanical strength, and difficulty with implantation (5, 8). For cell-based therapies to successfully regenerate damaged myocardium, it is imperative to deliver enough viable cells to the infarct zone that function like normal cardiac cells and integrate with host tissue.

1.2.1. *Cardiac Tissue Engineering*

Tissue engineering as a field came about as a way to develop replacement tissues and organs for patients in lieu of transplant that would restore or regenerate damaged tissue. The basic principle of a tissue engineering construct is the development of a tissue or whole organ composed of cells from the patient (or from another compatible cell source) which may be grown on some form of scaffold in order to induce cellular organization and function mimicking that of the native tissue structure. Despite the large variety in tissue and organ targets being studied, there are certain critical challenges that apply to nearly all areas of tissue engineering. These include the need for organization of cells within scaffolds that mimics the native tissue-level organization, construct mechanical properties that match the target tissue, overall biocompatibility of the constructs, and the ability for constructs to fully integrate with host tissues upon implantation.

Cells respond differently when grown in 3D vs. 2D environments, and many cell types are anchorage-dependent, meaning they will not perform their normal functions when in suspension. Biomaterials are therefore desirable as delivery vehicles for cell therapies. Biomaterials for cardiac tissue engineering should enhance cell attachment and growth, promote cardiomyocyte alignment, encourage infiltration of host vasculature and integration with host tissue, and degrade into non-toxic byproducts easily cleared by the body. Additionally, biomaterials should have mechanical properties similar to native myocardium to avoid issues with mechanical mismatch and be non-immunogenic (4, 5, 9). Numerous synthetic and natural polymers are under investigation for use in cardiac tissue engineering

(10-18). Many of these are used to form scaffolds with an ECM-like structure on which cells are grown before implantation of the construct. There is a significant degree of cardiomyocyte and vascular alignment within the native cardiac tissue, which is directly correlated with the overall function of the organ (19). Therefore, constructs designed for cardiac tissue engineering applications should be able to induce cardiac cell alignment in order to achieve this tissue level structure-function relationship.

1.2.2. *Scaffold Material Considerations*

Synthetic scaffolds generally have more consistency in terms of reproducibility and are typically less expensive and easier to construct into a variety of architectures (11, 20). However, they typically have much greater mechanical stiffness than natural polymers and native tissues (19). Commonly used synthetic polymers include homo- or co-polymers of lactide, glycolide, and/or caprolactone, poly-(ethylene glycol) (PEG), and poly-(2-hydroxyethyl methacrylated) (pHEMA) (11, 19). The chemical compositions of these synthetic polymers allows for a high degree of control over material properties and degradation profiles, but issues with material toxicity must be taken into consideration (19).

Natural polymers very often have much lower mechanical stiffness and strength than synthetic polymers, but typically have improved biocompatibility. Some of the most commonly used natural materials include collagen, fibrin, gelatin, and alginate due to their inherent ability to promote cell adhesion and survival, and these typically show improved host responses upon implantation (10, 20-24). In particular, collagen and fibrin have shown enhanced cell adhesion and survival properties when used to deliver cells (21, 23). Alternatively, fusion proteins have been produced to enhance delivery of cells, growth factors, and/or genetic therapies by incorporating favorable binding sites to enhance loading and delivery within a scaffold (21, 23). Other scaffolds have been derived from decellularized cadaveric or xenogeneic tissues in order to seed cells onto a pre-formed ECM structure (9, 25). Currently, major

setbacks of scaffold-based cell therapies include issues with cell-seeding, mechanical mismatch, toxic degradation products, and unfavorable immune responses (4, 5, 9).

1.3. Wound Healing & the Foreign Body Response

The natural host tissue response to implantation of any material or device is to initiate a cascade of events intended to "heal" the wound and often leads to the formation of a fibrous capsule around implants, effectively sealing them off from the body. Tissue damage occurs during implantation which exposes the host blood supply to the material implant, allowing blood proteins to adsorb to the material surface within minutes to hours of exposure to form a provisional matrix or blood clot. This provisional matrix is mainly composed of fibrin, and is responsible for coordinating the angiogenic response and cellular infiltration into the site of wound healing by providing both structural and chemical cues to host cells (26, 27).

1.3.1. *Inflammation & Granulation Tissue Formation*

An inflammatory response is triggered upon tissue injury which is subsequently mediated by the host tissue and cellular responses to the material implant itself (**Figure 1.2**). Neutrophils are the first inflammatory cells to arrive at the site of injury and are typically present for the first hours to days of healing during the acute inflammatory phase. Neutrophils are soon replaced by monocytes/macrophages, the main cells responsible for coordinating the normal wound healing response in the foreign body reaction. Macrophages may persist in the wound for weeks depending on the extent of injury and the host responses to the biomaterial implant (27). Granulation tissue, which consists of macrophages, fibroblasts, and newly formed capillaries, begins to form as early as three to five days after implantation, and is part of the normal wound healing response to material implants.

Endothelial cells form new blood vessels in the process known as angiogenesis, and proliferating fibroblasts actively synthesize and deposit new extracellular matrix (ECM) proteins such as collagen (27).

1.3.2. *Foreign Body Response & Fibrous Capsule Formation*

Foreign body giant cells (FBGCs) can form when macrophages fuse together in an attempt to phagocytose a large implant. These macrophages and FBGCs are components of the foreign body response along with protein adsorption and collagen deposition in the area surrounding the implant. The extent of this response depends on many factors such as the implant size, surface architecture, shape, and material and chemical properties. All of these characteristics can induce differing responses in host inflammatory cells and therefore affect the outcome of healing. For example, implants with a smooth surface typically promote a greater degree of fibrosis than materials with higher surface to volume ratios, such as fabric meshes or porous implants, which generally result in greater numbers of macrophages and FBGCs at the tissue-material interface (26, 27). In addition, the size of the porous architecture of biomaterial implants has been shown to affect the vascularization response from the host tissue (11). These effects on the wound healing response of host tissue must be taken into consideration when designing biomaterial implants.

The final phase of the normal wound healing response to implanted materials is that of fibrosis and fibrous capsule formation. Fibroblasts proliferate in the granulation tissue and deposit collagen (mainly type I) which is organized into a fibrous capsule surrounding implants. This capsule can completely inhibit graft integration with host tissues by preventing host cells and vasculature from reaching the implant (27). In the field of tissue engineering, integration of cellular constructs with host tissue cells and vasculature is essential for implanted grafts to survive and provide functional benefit. Fibrous capsule formation is therefore an important consideration when designing biomaterial constructs. A material that can prevent or decrease the formation of a thick, acellular capsule and thus

promote a more physiological healing response by inducing vascularization of an implant could improve the chances for graft survival and integration, and would be of great benefit to the field of tissue engineering.

1.4. Vasculogenesis, Angiogenesis, & Vessel Maturation

1.4.1. *Vasculogenesis*

The cardiovascular system consists of a highly ordered network of branching vessels which work in concert to deliver oxygen and nutrients to every living cell in the body while simultaneously removing waste products, circulating immune cells, and transporting other substances from cell to cell (28). This intricate system is one of the first to develop during embryogenesis (29). The term vasculogenesis is traditionally defined as the *de novo* formation of vessels from angioblasts or endothelial progenitor cells (EPCs) during the process of embryonic development (**Figure 1.3**)(30-32). Vasculogenesis was originally thought to occur solely in the developing embryo. However, many recent discoveries have shown bone marrow-derived endothelial progenitor cells circulate through the adult blood supply (33, 34) and are involved in areas of active vascular remodeling in the adult body, including processes of wound healing (29), tumor vascularization (33, 35, 36) and repair of ischemic tissues (30, 31, 35, 37). It is now widely accepted that vessel formation in the adult occurs via both angiogenesis and vasculogenesis (30-32).

1.4.2. *Angiogenesis*

Once the primitive vascular plexus is formed during vasculogenesis, capillaries branch off to form additional vessels in a process known as angiogenesis (30-32). In addition, existing immature vessels may be remodeled to form a more mature vascular network. Extensive research has led to the description of a series of events that occur during angiogenesis (30, 31). The first of these is the

activation of endothelial cells (ECs) within an existing vessel, thought to be induced by hypoxia in the surrounding tissue. Activated ECs begin secreting factors to degrade the surrounding basement membrane (BM) and extracellular matrix (ECM) via expression of certain matrix metalloproteinases (MMPs) (29-31, 38, 39). MMP-9 is associated with pericyte migration to the vessel wall, and MMP-2 is involved in the process of endothelial lumen formation (30, 39). ECs are then free to migrate towards the angiogenic signals being secreted by cells in the area in need of vascularization (31). These activated ECs, or "tip cells," are the first to migrate outwards, following a gradient of the growth factors and other chemokines which specify the direction of migration (29), while ECs that follow behind begin proliferating to form the new vessels. As the tip cells continue to migrate, the ECs in the newly formed capillaries begin to re-differentiate back to a non-proliferating (quiescent) state. During the whole process of angiogenesis new vessels are being constantly remodeled and reorganized, leading to the formation of a complex, interconnected capillary network (30-32).

1.4.3. *Vessel Maturation*

The final stages of angiogenesis involve the remodeling of capillary networks into more mature vascular structures (30). As tip cells make contact with each other or existing capillaries, the structures fuse and cells become more quiescent (29). In order to develop a mature, stable vasculature, ECs must recruit and interact with mural cells (40). Association of these supporting cells with the nascent endothelial structures decreases EC proliferation and leads to the deposition of ECM and basement membrane components, ultimately establishing mature functional vessel structures (30-32, 41). Without these supporting cells, vessels remain immature, leaky, and tend to regress (29, 42). Pericytes form direct contacts with ECs as they attach to the outer surface of capillaries, while more mature, larger diameter vessels (such as arteries and veins) are separated from supporting mural cells by a layer of deposited basement membrane (29, 41).

1.5. Vascularization of Tissue Engineering Constructs

In the native myocardium, cardiomyocytes are never further than 200µm away from a capillary (19). In order to deliver a high density of metabolically active cardiomyocytes that require a large supply of oxygen and nutrients to survive and function, cardiac tissue engineering constructs of significant size would benefit from the development of a vascular network within constructs. This would likely increase the chances of a quick vascular integration with host tissue and therefore improve the likelihood of graft survival. The development of an effective vascular strategy for thicker tissue constructs remains a major challenge in the field of tissue engineering (19, 43). Many groups are researching different ways to incorporate vasculature within cell-seeded constructs. The most common method is to deliver pro-angiogenic factors either in conjunction with or incorporated within constructs (43). Others rely on the architecture of the scaffold to induce an angiogenic response from the host tissue, as the size and geometry of the scaffold has been shown to affect vascularization of grafts (11, 43). Scaffolds have also been fabricated with open channels designed to induce vascular infiltration after implantation (44, 45).

Alternatively, co-culture of constructs with vascular cell components, such as ECs and supporting pericyte cells, has been shown to improve the formation of vascular networks (43, 46-50). The first reported pre-vascularized tissue construct was a collagen scaffold designed for skin tissue engineering which contained keratinocytes, dermal fibroblasts, and human umbilical vein ECs (HUVECs) (51). Multilayered constructs of cell sheets containing cardiomyocytes and ECs have been shown to form vascular networks that survive and integrate with host myocardium after implantation (50). Co-culture of cardiomyocytes with ECs and a third supporting cell type such as a fibroblast or mesenchymal stem cell has been shown to improve cardiomyocyte and ECs survival and proliferation, as well as form more stable vascular networks within tissue engineered constructs (20, 43, 46). These pre-vascular networks have been shown to anastomose with host vasculature upon implantation, leading to functionally

vascularized implants at a much earlier time point than constructs implanted without pre-formed vascular networks (43, 52). All of these strategies are aimed at shortening the time required to fully vascularize an implanted tissue construct in order to improve overall graft survival and integration.

1.6. Fibrin as an Angiogenic Scaffold Material

1.6.1. *Fibrin Formation*

Fibrin is a natural protein that has long been used as an effective scaffolding material to grow cells and tissue constructs due to its cell adhesive properties and natural non-toxic degradation products (10, 53-60). Physiologically, fibrin is the major protein component of the blood clot. In the coagulation cascade the fibrin precursor fibrinogen (340kDa, approximately 3mg/mL in plasma) (**Figure 1.4**) is cleaved by thrombin to remove two fibrinopeptides (A and B) from the fibrinogen molecule (61-63), forming the fibrin monomer that will spontaneously polymerize into long polymer chains that intertwine to form the fibrin clot (10, 64). In addition to cleaving fibrinogen, thrombin (in the presence of extracellular Ca^{2+}) activates the zymogen factor XIII (FXIII, approximately 10µg/mL in plasma)(65). Activated FXIII (FXIIIa) covalently cross-links the unstable fibrin network at glutamine and lysine residues to form the insoluble fibrin clot (**Figure 1.4 & 1.5**)(64).

1.6.2. *Fibrinolysis*

The process of fibrinolysis describes the natural degradation of fibrin clots, and occurs via multiple parallel pathways *in vivo*. Plasminogen, an inactive proenzyme in the plasma (approximately 2µM), is converted to plasmin, a serine protease. Plasmin binds to fibrin at lysine and arginine residues, breaking the matrix into a number of fibrin degradation products (FDPs) that are easily cleared by the body. FDPs include fibrin E-fragments, D-fragments, and D-dimer fragments (two cross-linked D-

fragments) (**Figure 1.5**). Plasmin is also the most potent activator of matrix metalloproteinases (MMPs), a family of enzymes that degrades most components of the ECM (66-69). MMPs play a role in normal tissue turnover, but are also responsible for tissue destruction in many disease processes (54). During tissue remodeling, cells excrete MMPs which, in combination with the plasminogen-plasmin pathway, play a major role in normal wound healing (54, 67, 68). In particular, MMP-1, -2, -3, and -9 have shown increased expression in human, rat, and porcine cardiac tissue after MI, indicating their role in the tissue remodeling process (69). Multiple MMPs have been shown to degrade cross-linked fibrin (including MMP-2, -3, and -9) independently of plasmin, leading to the formation of D-dimer fragments similar to those produced during plasmin degradation (54, 67). Fibrinolysis can be inhibited with the use of protease and/or MMP inhibitors, including the serine protease inhibitor aprotinin (6.5kDa)(54, 70) and the broad-spectrum MMP inhibitor galardin (Ilomastat, GM6001)(54, 69).

1.6.3. *Fibrin as an Angiogenic Scaffold Material*

As a biomaterial, fibrin is generally utilized as a hydrogel in varying concentrations in which suspended cells rearrange the fibers and lay down their own extracellular matrix (ECM). In the cardiac repair arena, Christman *et al*. were the first to demonstrate improved cell survival when transplanted cells were injected in combination with fibrin hydrogels (53). Fibrin is able to bind many growth factors directly (including bFGF, PDGF, & TGF-β) and indirectly via heparin binding, allowing many angiogenic growth factors (including VEGF & FGFs) to bind (71-75). Degradation products of fibrin (FDPs) have been shown to have angiogenic properties. FDPs are able to recruit cells involved in vasculogenesis, increase proliferation, migration, and differentiation of endothelial cells, and promote smooth muscle cell proliferation and migration (76-80). Fibrin was shown to induce neovascularization within the ischemic myocardium and reduce infarct expansion (57). Others have reported enhanced neovascularization in ischemic myocardium following injection of fibrin gels alone or in combination with cells (58-60). The

observed neovascularization effects of fibrin fit with the well-established role of FDPs in the induction of angiogenesis (81).

1.7. Overall Hypothesis & Project Goals

The research described in this dissertation details the development of an engineered fibrin scaffold targeted for cardiac tissue engineering applications. Issues with many current cardiac tissue engineering constructs typically include construct stiffness that does not match that of the native myocardium, inadequate construct vascularization, lack of cardiomyocyte alignment, and relatively low cell density and/or unevenly distributed cells within constructs. The design of the engineered fibrin constructs described in this dissertation was developed to mimic certain characteristics of native myocardial tissue in order to address many of these issues. Design parameters taken into consideration included the native tissue stiffness, the dense network of vasculature, the large degree of cellular alignment, and the high cell density within the native myocardium. The overall project hypothesis was that a templated high density fibrin scaffold would promote seeded cell alignment and the development of a pre-vascular network within constructs, and that these design parameters would enhance construct integration with host myocardium. This hypothesis was investigated with four project goals: the development of a microtemplated high density fibrin scaffold with mechanical and degradation properties tailored for cardiac tissue engineering applications (Aim 1); the evaluation of host tissue responses to the engineered fibrin scaffold material (Aim 2); demonstrating the scaffolds can promote cell survival and organization within constructs (Aim 3); and the development of a perfusion seeding system to improve overall seeding efficiency, distribution, and cell density within constructs (Aim 4).

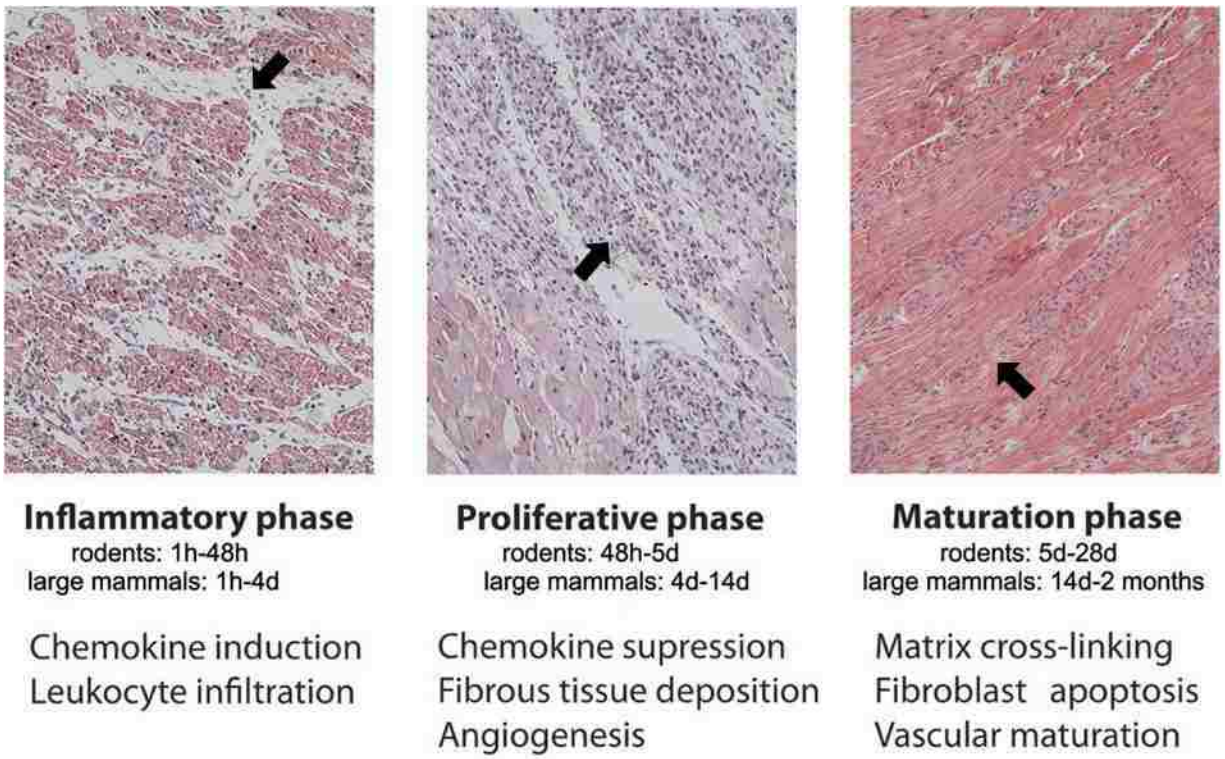

Figure 1.1. The phases of infarct healing (adapted from Dobaczewski *et al.* 2010)(2). Arrows indicate infiltrating leukocytes (left), granulation tissue (middle), and fibrous scar tissue deposition (right).

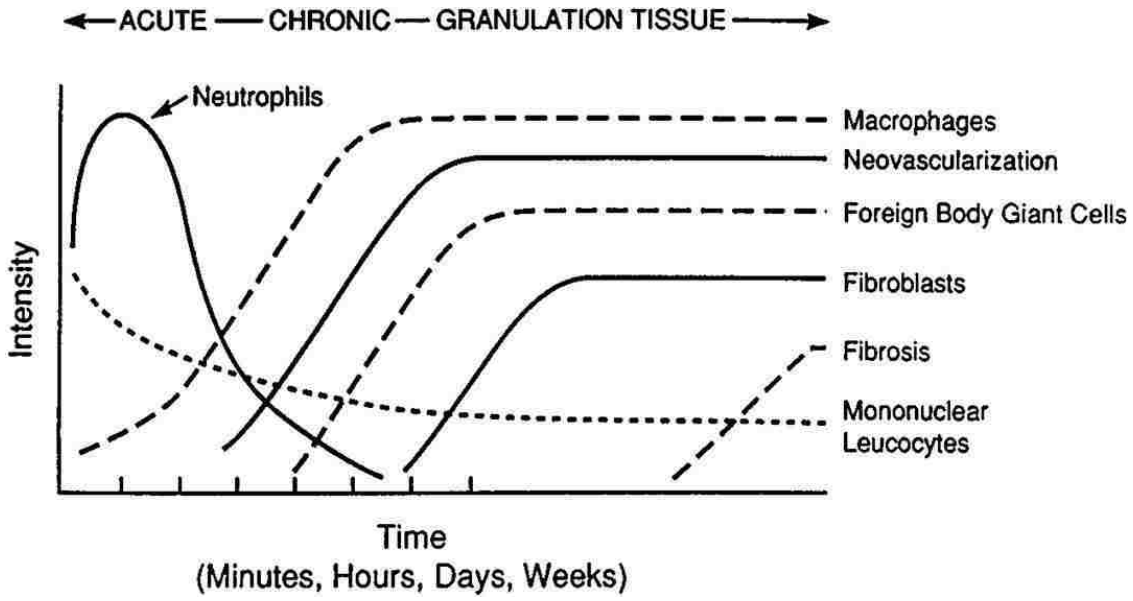

Figure 1.2. Temporal changes in cellular responses during wound healing and foreign body responses to biomaterial implants (adapted from Anderson 2001)(27).

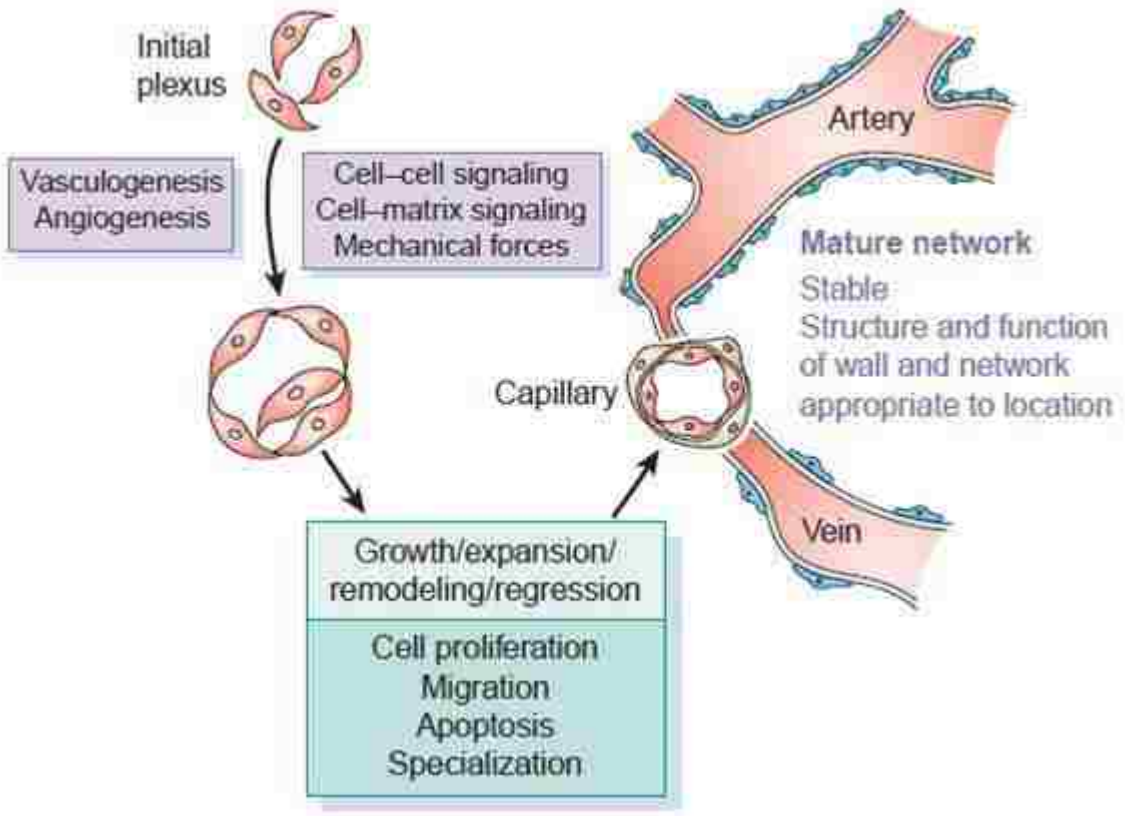

Figure 1.3. Processes of normal vasculogenesis and angiogenesis (adapted from Jain 2003)(30).

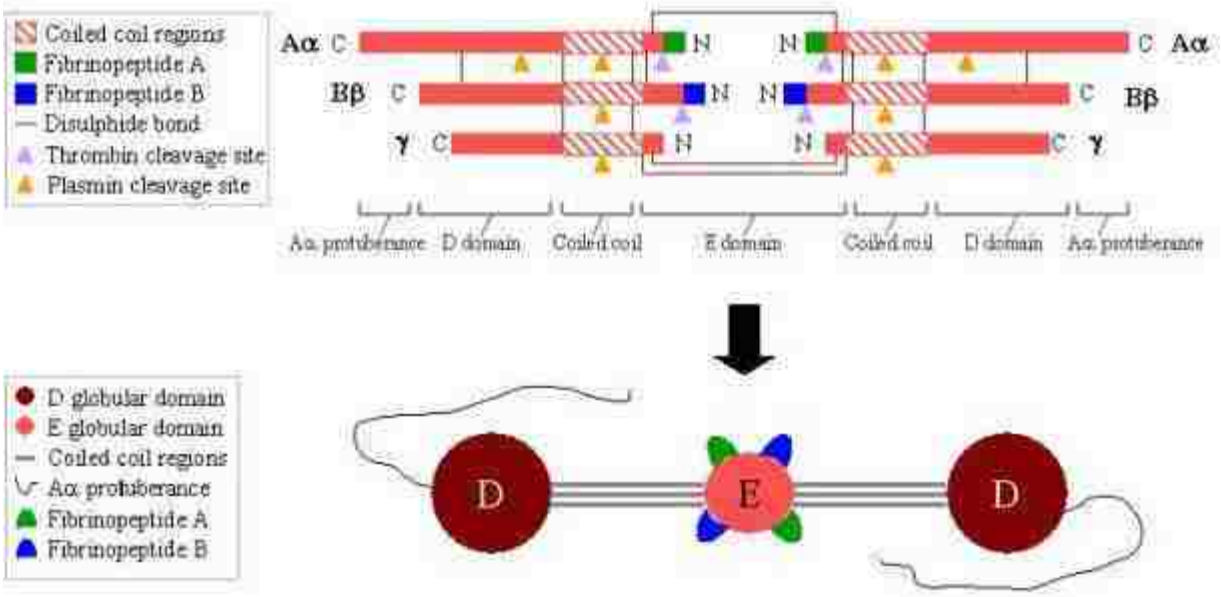

Figure 1.4. The polypeptide (top) and domain (bottom) organization of fibrinogen (adapted from Hunter *et al.* 2012)(63).

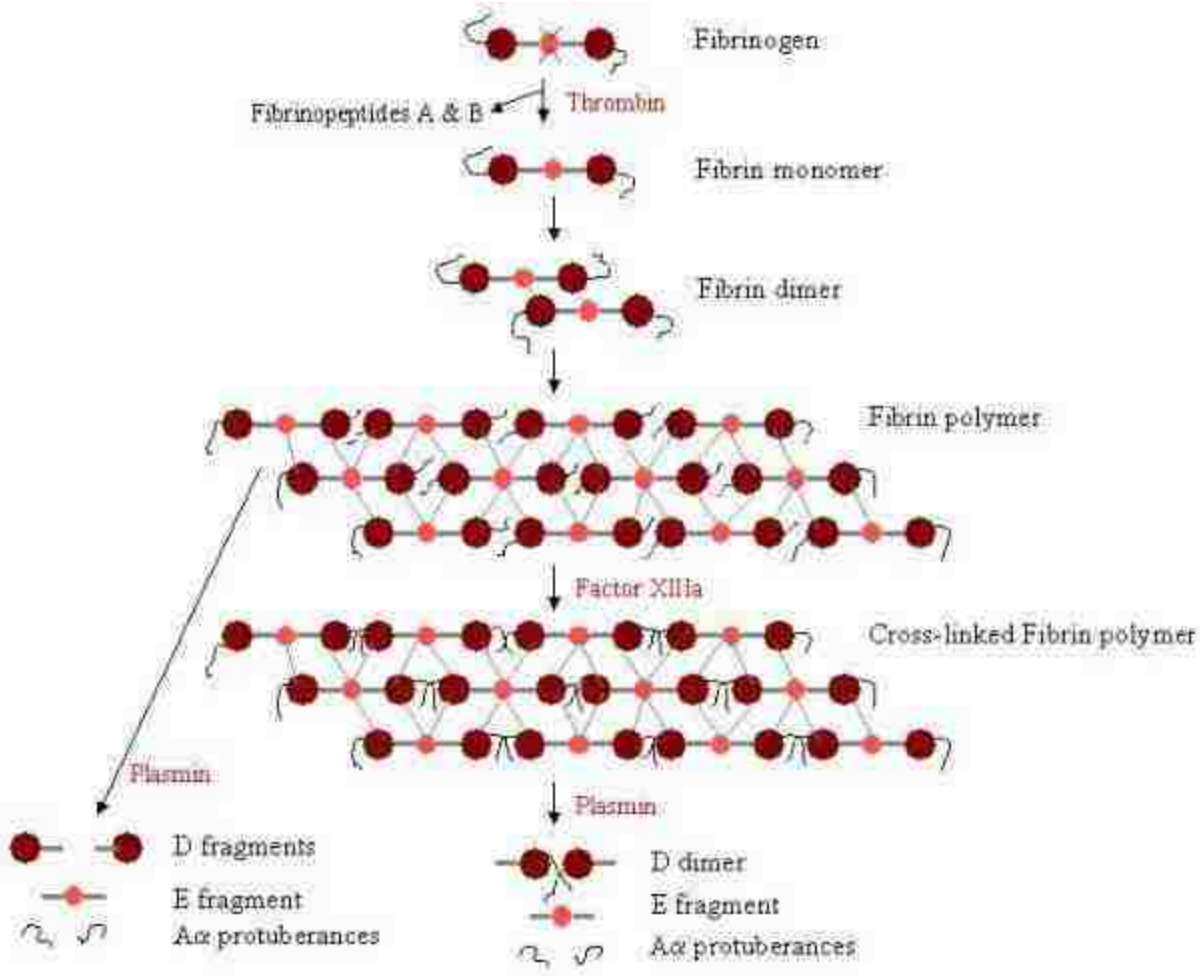

Figure 1.5. Fibrin clot formation and fibrinolysis (adapted from Hunter *et al.* 2012)(63).

Chapter 2:

Development, Modification, & Characterization of a Microchanneled & Microporous Fibrin Scaffold for Cardiac Tissue Engineering Applications

2.1. Introduction

Current cell-based therapies for myocardial infarction (MI) in human trials include direct injection of cells (such as bone marrow stem cells, skeletal myoblasts, or stem cell-derived cardiomyocytes) into infarcted myocardium or surrounding tissue or coronary vessels. The hope is that these delivered cells will home in on damaged tissue and exert therapeutic effects. However, few cells reach the infarct with these methods and cell retention and survival remain extremely low (< 10%) (5, 11, 20, 82). In addition, cells delivered in suspension can be disorganized and often lack cell-cell and cell-matrix contacts. Cells respond differently when grown in a 2D vs. 3D environment, and the function of many cell types is anchorage-dependent. Sheets of cells have been stacked to form thicker tissue grafts, but these are limited by diffusion of nutrients and low mechanical strength (5, 8). For cell-based therapies to successfully regenerate damaged myocardium, it is imperative to deliver enough viable cells to the infarct zone that function like normal cardiac cells and integrate with the host tissue. For these reasons, biomaterials are desirable as delivery vehicles to help improve cell retention. However, issues with immune rejection, degradation, and mechanical integration have limited the success of many biomaterials in cardiac repair (5, 20).

An effective cellular construct for the treatment of MI should (1) enhance cell attachment and promote cellular organization to increase the number of functional cells being delivered, (2) encourage infiltration of and integration with the host vasculature to improve construct survival upon implantation, (3) be non-immunogenic, and (4) degrade into non-toxic byproducts. Additionally, constructs should have a mechanical strength similar to native myocardium in order to support grafted cell function and to avoid issues with mechanical mismatch upon implantation. Both synthetic and natural polymers are being investigated for use in cardiac tissue engineering applications. Many of these are used to form scaffolds mimicking an extra-cellular matrix (ECM)-like structure on which cells are grown before implantation of the construct (5).

Fibrin is a natural protein used as an effective scaffolding material to grow cells and tissue constructs due to its cell adhesive properties and natural non-toxic degradation products (10, 55, 83). Fibrin is the major protein component of blood clots, and is formed when the precursor, fibrinogen, is cleaved by thrombin, which also activates the zymogen factor XIII (FXIII) to covalently cross-link the unstable fibrin network to form an insoluble fibrin clot. These clots are naturally degraded by plasmin into D-dimers and other degradation products that are easily cleared by the body (10, 64). Fibrin hydrogels have been utilized to deliver cells (56, 60, 84), with Christman *et al.* being the first to demonstrate transplanted cell survival was improved when injected with fibrin hydrogels (53). Additionally, fibrin induces neovascularization within ischemic myocardium and reduces infarct expansion, with enhanced neovascularization in ischemic myocardium observed following injection of fibrin gels alone or in conjunction with cells (53, 58-60). The observed neovascularization effects of fibrin fit with the well-established role of fibrin degradation products in the induction of angiogenesis (81), and further demonstrate the suitability of fibrin as a scaffold biomaterial.

The main issue with fibrin hydrogels for cardiac tissue engineering applications is that they are mechanically weak (< 10kPa (10)), limiting their ability to adequately support dynamically contracting cardiomyocytes and constantly working native myocardium. In contrast, high-concentration fibrin glues are too dense for cells to penetrate, limiting their use as cell delivery vehicles. Ideally, the scaffold-cell construct should have similar biomechanical properties to ventricular wall tissue. Linnes *et al.* developed a method of microtemplating high-density fibrin into an interconnected microporous architecture with controllable pore size and mechanical stiffness closer to cardiac tissue than fibrin gels (10). A sphere-templated microporous architecture with pores of equal size is ideal for promoting nutrient delivery, gas exchange, and neovascularization within the construct (11), but is limited by low density cell-seeding and random cellular alignment. Madden *et al*. overcame these limitations by incorporating a microchannel network into a similar microporous scaffold construction, producing bimodal synthetic scaffolds for use as cardiac constructs (11).

The construct described here is a novel high density templated fibrin scaffold with a microchanneled and microporous architecture with mechanical properties tailored for cardiac tissue engineering applications. The hypothesis was that a scaffold designed to mimic native cardiac tissue structure would address many of the issues described above. The microarchitecture of the scaffold is designed to promote cellular alignment and pre-vascular network formation within channels after seeding (the subject of Chapter 4), and will help facilitate nutrient exchange and waste removal within constructs. In addition, the high density fibrin material will provide adequate and tunable mechanical strength to support graft cells, and is designed to promote overall construct integration with the host tissue upon implantation.

2.2. Materials & Methods

2.2.1. *Fibrin Scaffold Construction*

Scaffolds were constructed according to published methods with modifications (10, 11), summarized in **Figure 2.1**. Briefly, optical fibers (Paradigm Optics, Vancouver, WA) with a 60µm diameter inner polycarbonate (PC) core and a 30µm thickness poly(methyl methacrylate) (PMMA) outer shell were bundled in Teflon shrink tubing and sintered at 145^{o}C overnight to form a solid PMMA matrix containing PC cores spaced 60µm apart. After sectioning into 1-3mm length disks and immobilizing the ends of the PC cores with cyanoacrylate, the PMMA matrix was selectively dissolved with xylene washes over 5 days. The resulting void space around the PC cores was then filled with PMMA microbeads (27µm diameter, Microbeads, Skedsmokorset, Norway) in a close-packed arrangement via sonic sifting. The beads were sintered in place at 180^{o}C for 24h to obtain a pore neck diameter 50% of the bead diameter.

The polymer template was infiltrated with a 200mg/mL fibrinogen solution (bovine fibrinogen Type 1-S, Sigma-Aldrich, St. Louis, MO; in 0.9% NaCl) via centrifugation. The fibrinogen solution was pre-warmed in a 37^{o}C water bath for 45-90minutes to allow the fibrinogen to completely dissolve. After centrifuging the fibrinogen solution into the templates and after scraping all surfaces to remove excess fibrinogen, concentrated thrombin solution (13.25U/mL thrombin, Sigma-Aldrich, St. Louis, MO; 8.3mM $CaCl_2$; DMEM, Gibco, Grand Island, NY) warmed to 37^{o}C was used to polymerize the fibrinogen into fibrin around the polymer template overnight at room temperature. After scraping the exterior of the scaffolds to remove excess fibrin, the polymer template was dissolved with two 24 hour washes in a 90% dichloromethane/10% hexanes solution followed by a 24h acetone wash on an orbital shaker at room temperature. Scaffolds were treated with 100% ethanol rinses for 1 week before rehydration with a graded ethanol series into sterile phosphate-buffered saline (PBS).

2.2.2. *Scaffold Modifications*

Additional cross-linking of fibrin scaffolds was achieved by adding the human Factor XIII (FXIII, Innovative Research, Novi, MI) at 10µg/mL (physiological) or 100µg/mL (high) to the fibrinogen solution before centrifugation into polymer templates. Inhibition of scaffold degradation by proteases was tested by adding the serine protease inhibitor aprotinin (3000U/mL, Sigma-Aldrich, St. Louis, MO) to the fibrinogen solution. Inhibition of scaffold degradation by matrix metalloproteinases (MMPs) was tested by adding the broad-spectrum MMP inhibitor galardin (GM6001, EMD Millipore, Billerica, MA) at 5µM or 25µM to the fibrinogen mixture before centrifugation into templates. These scaffold modifications were tested alone and in combination with each other to determine their effects on stiffness and *in vitro* degradation rates of the fibrin scaffolds.

2.2.3. *Architecture Evaluation*

Scaffold architecture was evaluated with scanning electron microscopy (SEM) and 2-photon microscopy. For SEM imaging, scaffolds were fixed in 0.5% glutaraldehyde overnight at room temperature followed by dehydration in a graded ethanol series and critical point drying to maintain pore and channel structures. Samples were cut to different depths and Au/Pd sputter-coated for 60s before imaging with an FEI (Hillsboro, OR) Sirion field-emission microscope under high vacuum conditions at an accelerating voltage of 10kV. Multiphoton microscopy of hydrated scaffolds was performed using an Olympus FV1000 MPE multiphoton microscope equipped with a 25x SuperObjective (Olympus) and Mai Tai laser (Spectra Physics). Images were compiled using Imaris Imaging Software (version 6.3, Bitplane). Multiphoton imaging studies were supported in part by the Mike and Lynn Garvey Cell Imaging Lab at the University of Washington Institute for Stem Cell and Regenerative Medicine.

2.2.4. *Acellular Scaffold Myocardial Implants*

After rehydration and equilibration in sterile PBS, acellular fibrin scaffolds (unmodified, FXIII-treated (high), or aprotinin-treated) were cut into 300-400µm diameter x 1-2mm length strips and kept in sterile PBS at 4°C until implantation. All animal procedures were conducted in accordance with the US National Institutes of Health Policy on Humane Care and Use of Laboratory Animals and were approved by the University of Washington (UW) Animal Care Committee. Rats were housed in the Department of Comparative Medicine at UW and cared for in accordance with the UW Institutional Animal Care and Use Committee (IACUC) procedures. Adult male Fischer 344 rats (200-300g) were sedated with isoflurane before implanting scaffold strips into the wall of the left ventricle as described previously (11). Briefly, after intubating for ventilation with supplemental oxygen at 2L/min and 60breaths/min, rats were kept on a heating pad to maintain an internal body temperature of 37°C. A lateral thoracotomy was performed along the 3rd to 5th rib to open the chest and expose the beating heart. Scaffold implants were delivered via guide wire from a 20 gauge needle into a pocket in the uninfarcted left ventricular wall made by a 16 gauge needle, and the implant site was closed off with a purse string suture. Animals were monitored for 48-72 hours following surgery and given IP injections of buprenorphine for pain. At endpoints of 1, 7, and 14 days, rats were euthanized via pentobarbital overdose (120-150 mg/kg) administered via IP injection, followed by pneumothorax before rapidly dissecting the hearts. This method of euthanasia is in accordance with recommendations of the Panel on Euthanasia of the American Veterinary Medical Association.

2.2.5. *Histological Analysis*

Hearts from acellular implant studies were sliced into 2mm sections beginning with a cut through the center of the implant site (determined by suture location), and then immersion-fixed in Methyl Carnoy's (MC) fixative. Samples were processed, embedded in paraffin, and sectioned (5µm) for

histology. Serial sections of samples were stained with H&E, Masson's trichrome stain, and with immunohistochemical staining using hematoxylin as the nuclear counterstain. Immunostaining was performed with primary antibodies against rat endothelial cell antigen (RECA-1, mouse anti-rat (1:10), AbD Serotec, Raleigh, NC), leukocyte marker CD45 (mouse anti-rat (1:100), BD Biosciences, San Jose, CA), and macrophage marker CD68 (mouse anti-rat (1:100), AbD Serotec, Raleigh, NC). Samples were then labeled with a biotinylated horse anti-mouse (1:400) secondary antibody (Vector, Burlingame, CA) and developed with DAB (Sigma-Aldrich, St. Louis, MO).

2.2.6. *Mechanical Stiffness &* in vitro *Degradation Analysis*

To assess the tensile strength and degradation time-course of the fibrin scaffolds, scaffold stiffness was measured using a custom built biomechanical analysis setup in the Regnier lab (85-87). Briefly, scaffolds were cut into strips (0.2-0.4mm diameter x 1.0mm length) and mounted with aluminum foil T-clips between a force transducer and a servomotor tuned for a 300μs step response (**Figure 2.2a**). Step changes in length (4%-24% of scaffold strip length) and resulting changes in tension (**Figure 2.2b**) were measured and recorded by a custom LabVIEW software program. Resulting tension (mN) and force normalized to cross-sectional area (mm^2) were plotted against percent length change, and the slope of the resulting linear regression line was used as a measure of stiffness in kPa (**Figure 2.2c**). Scaffolds were measured at different time points (0, 3, 6, & 10 days) after incubation at 37^{o}C in sterile PBS.

2.2.7. *Statistical Analysis*

All values are reported as mean ± S.E.M. When comparing scaffold modifications, statistical significance from unmodified scaffold values was determined with a One-Way ANOVA test using the

Dunnett method. Statistical significance between other scaffold modifications was tested using a Student's t-test ($\alpha = 0.05$). Differences at a *p*-value < 0.05 were considered statistically significant.

2.3. Results

2.3.1. *Fibrin Scaffold Construction*

High density (200mg/mL) fibrin scaffolds were constructed using the polymer templates described above. Success of fibrin scaffold formation was assessed with SEM imaging at different depths through the scaffold, confirming an interconnected microporous network (27µm diameter pores) surrounding open microchannels (60µm diameter) that spanned the length of the construct. Initially, templates were formed using 30-38µm PMMA beads. However, beads of this diameter were unable to be packed between the PC cores (60µm spacing) consistently throughout the template, as indicated by SEM imaging showing pores/beads mainly located in the outer edges of the scaffold/template (data not shown). It was therefore decided that a smaller bead diameter (27µm) would be necessary to ensure consistent formation of the desired architecture. SEM and 2-photon microscopy confirmed consistent formation of this microtemplated architecture with 27µm beads, resulting in regularly-shaped and evenly-spaced channels and pores throughout the fibrin scaffold (**Figure 2.3**).

2.3.2. *Acellular Scaffold Myocardial Implants*

An initial study was performed to determine how host cardiac tissue would respond to the scaffold material and to assess the time course of degradation of scaffolds *in vivo*. Unmodified, FXIII, and aprotinin scaffolds were implanted in the ventricular wall of adult rat hearts. Scaffolds located at the site of implantation were completely infiltrated with host cells after 1 day (**Figure 2.4a, f**).

Histological analysis indicated these were mainly neutrophils, suggesting a normal early inflammatory response to the fibrin scaffolds as expected for this early time point. Scaffolds were significantly degraded by 7 days post-implantation (**Figure 2.4b-d, g-i**). Histological analysis of day 7 samples showed an area of inflammation immediately surrounding the implants, characterized by RECA-1+ endothelial cell-lined lumens (**Figure 2.5a, d**), CD45+ leukocytes (**Figure 2.5b, e**) and CD68+ macrophages (**Figure 2.5c, f**), and an area of newly deposited loose collagen (**Figure 2.4b-d, g-i**), consistent with a normal wound healing response. Unmodified and FXIII-treated scaffolds showed a similar host response at the 7-day time point. Aprotinin-treated scaffolds appeared to have less collagen deposition in the area of implantation at the 7-day time point (**Figure 2.4c, h**), and 3 of 6 aprotinin-treated implants were located after 7 days (as compared to 1 of 6 unmodified, and 2 of 6 FXIII-treated implants). Unmodified and aprotinin-treated scaffolds could not be located 14 days post-implantation, suggesting complete scaffold degradation by this time. Although significantly degraded, 2 of 8 FXIII-treated scaffolds were located at the site of implantation after 14 days (**Figure 2.4e, j**) versus 0 of 5 unmodified scaffolds and 0 of 6 aprotinin-treated scaffolds, suggesting FXIII modification may slow fibrin scaffold degradation *in vivo*.

2.3.3. *Mechanical Stiffness &* in vitro *Degradation Analysis*

Following the *in vivo* study, it was necessary to determine whether scaffold modifications that may slow degradation *in vivo* would affect the material stiffness, as it will be important to maintain an initial scaffold stiffness comparable to that of native tissues (neonatal rat myocardium = 39 ± 9 kPa; adult rat myocardium = 273 ± 100 kPa (87, 88)). Scaffolds were mechanically tested *in vitro* to determine material stiffness and degradation rates with and without material modifications (± FXIII (10µg/mL or 100µg/mL), ± aprotinin (3000U/mL), ± galardin (5µM or 25µM)). The stiffness and degradation time course for each treatment tested is summarized in **Figure 2.6** and material stiffness values are reported in **Table 2.1**.

Unmodified fibrin scaffolds had an average stiffness of 80.9 ± 6.0 kPa, a value comparable to native cardiac tissues. This stiffness rapidly decreased to 38.3 ± 3.5 kPa (47.3 ± 5.6% stiffness retention, significantly different from day 0, $p < 0.05$) after 3 days and to 30.3 ± 2.7 kPa (37.5 ± 4.3%) after 6 days, with a continuing significant drop in stiffness to 16.1 ± 2.9 kPa (19.9 ± 3.9%, $p < 0.05$) after 10 days in sterile PBS at 37^{o}C. During testing of the day 10 samples, 10 of the unmodified scaffold strips tore before they could be measured due to a high extent of degradation. The stiffness value reported for the day 10 unmodified scaffolds includes these 10 samples as zero passive force. Without the inclusion of these samples, the day 10 stiffness was 22.8 ± 3.1 kPa (28.2 ± 4.4% stiffness retention). This data in combination with the results of the *in vivo* implant study indicate a fast degradation time course for these unmodified fibrin scaffolds.

Addition of FXIII at 10µg/mL did not affect overall scaffold degradation properties compared to unmodified scaffolds (data not shown), most likely due to contaminating physiological levels of FXIII in the fibrinogen used to make the scaffolds. Addition of FXIII at 100µg/mL (hereafter referred to as FXIII) did not significantly change initial scaffold stiffness (90.8 ± 8.4 kPa), but did significantly decrease the overall extent of scaffold degradation (45.8 ± 5.9% after 10 days, $p < 0.05$) compared with unmodified scaffolds. A significant decrease in FXIII scaffold stiffness was observed between the 3 and 6 day time points (68.3 ± 7.5% down to 43.9 ± 5.8%, $p < 0.05$).

Addition of aprotinin to the fibrin material also did not significantly change initial material stiffness (68.0 ± 4.7 kPa), and significantly decreased the rate of scaffold degradation *in vitro* (60.9 ± 5.2% after 10 days, $p < 0.05$) compared to unmodified scaffolds, with no significant decrease in stiffness observed past the 3-day time point. The combination of FXIII with aprotinin produced a scaffold with a stiffness of 89.0 ± 5.9 kPa and, as with aprotinin alone, significantly decreased the overall extent of scaffold degradation (76.4 ± 7.6% after 10 days, $p < 0.05$), with no significant decrease in stiffness past

the 3-day time point. The degradation rates of aprotinin with FXIII and aprotinin-only scaffolds were not significantly different.

Addition of galardin to the fibrin scaffold did not significantly change scaffold stiffness at either the 5µM or 25µM concentrations (72.3 ± 11 kPa and 73.6 ± 7.0 kPa, respectively). Scaffolds with 5µM galardin significantly decreased the rate of scaffold degradation *in vitro* (48.7 ± 6.6% stiffness retention after 10 days, $p < 0.05$) compared with unmodified scaffolds. Interestingly, scaffolds with 25µM galardin showed a significant improvement in stiffness retention after 3 days (91.7 ± 17%, $p < 0.05$) compared to unmodified scaffolds, but after this time point the scaffold stiffness decreased to unmodified scaffold levels (43.3 ±7.3% by day 6, 25.8 ± 4.6% by day 10).

2.4. Discussion

Fibrin is a natural protein ideally suited for tissue engineering, as it has been shown to promote cellular adhesion, has tunable mechanical and degradation properties, and naturally degrades into non-toxic bioactive molecules that induce neovascularization. Linnes *et al*. developed a method of sphere-templating fibrin at a high density to produce stable and non-toxic porous scaffolds with mechanical stiffness that could be controlled by altering fibrinogen concentration, time in acetone, and time of exposure to an external crosslinker (genipin) (10). Madden *et al*. developed a method of incorporating parallel microchannels within the porous network to align seeded cardiomyocytes within synthetic scaffolds (11). Modification of these two templating procedures allowed the production of a high density templated fibrin scaffold with 60µm parallel microchannels surrounded by an interconnected 27µm porous network. The choice of channel diameter was based on studies done by Madden *et al*. that determined 60µm channels were optimal for cell-seeding, while minimizing mass transport issues within

the channel, while channel spacing was chosen so that pores in the range of 20-40μm diameter could be incorporated around the channels, as this range of pore sizes has been shown to induce a greater extent of host vascular infiltration and reduced fibrous capsule formation in myocardial implants (11, 15).

The *in vivo* degradation studies confirmed a normal host response to the fibrin implants with no indications of calcification or foreign body giant cell formation. An area of granulation tissue was observed surrounding acellular implants after 1 and 2 weeks. The acellular unmodified fibrin scaffold had a stiffness of 80.9 ± 6.0 kPa, a value comparable to native cardiac tissues (87, 88). However, these unmodified fibrin scaffolds had a rapid degradation profile both *in vitro* (likely due to contaminating levels of plasmin in the fibrinogen) and *in vivo*. It was hypothesized that a slower degradation profile would be necessary to maintain structural support for grafted cells until they had sufficient time to deposit their own replacement ECM. Therefore, modifications to the fibrin material were tested in an attempt to slow the scaffold degradation while maintaining the material stiffness within the range of native cardiac tissues.

During coagulation, fibrin clots are stabilized and protected from rapid fibrinolysis by FXIII cross-linking (10, 64, 89). Therefore, the addition of FXIII to the fibrinogen solution at a physiological concentration and at a concentration approximately 5-10x that normally found in mammalian plasma (89, 90) was tested as a method to retain material stiffness. Contrary to other studies (89, 91, 92), a significant increase in material stiffness was not found for FXIII-treated scaffolds (90.8 ± 8.4 kPa) compared to unmodified scaffolds (80.9 ± 6.0 kPa). An explanation for this could be that the extremely high density of the fibrin (200mg/mL) masked any moderate effects on stiffness that resulted from addition of FXIII. Additionally, the fibrin scaffolds are exposed to a series of water-free solvents during production that are most likely further increasing material stiffness (10, 93). The effect of FXIII treatment on scaffold degradation was unclear from *in vivo* implant studies, but seemed to indicate it may be

slowing scaffold degradation. Further investigation with *in vitro* degradation studies showed an intermediate level of stiffness retention (45.8 ± 5.9%) that was significantly improved from unmodified fibrin scaffolds (19.9 ± 3.9%) over 10 days *in vitro*.

The addition of the protease inhibitor aprotinin also significantly reduced scaffold degradation (60.9 ± 5.2%) over 10 days *in vitro*, and appeared to decrease collagen deposition *in vivo* 7 days after implantation. Aprotinin is commonly incorporated in fibrin glue-based tissue sealants for surgical applications to increase the material durability (91). In addition, aprotinin has been indicated as an anti-inflammatory agent that reduces activation and chemotaxis of neutrophils and macrophages, therefore lessening the release of inflammatory cytokines and the resulting cell and tissue damage they cause (94, 95). It was necessary to determine whether aprotinin would remain in the high-density fibrin material and retain its activity after undergoing the scaffold processing required to remove the polymer template. The slowing of degradation seen in the *in vitro* study suggests aprotinin is still present and is not denatured by the scaffold processing procedures.

As hypothesized, the combination of FXIII with aprotinin also had a significant effect on slowing scaffold degradation compared to the unmodified and FXIII-only groups, maintaining 76% of scaffold stiffness after 10 days *in vitro*. However, this was not significantly different from the degradation rate of the aprotinin-only group. Based on these *in vitro* results, it was expected that aprotinin implants would perform equally as well as or better than FXIII implants. However, while more aprotinin implants were located after 7 days than in the unmodified and FXIII groups, no aprotinin implants could be located at the 14-day time point. One possible explanation for this may be that the dose of aprotinin delivered with the implant was sufficient to prolong the scaffold life for 7 days, but not for 14 days due to the relatively small size of the implants. Since the degradation studies showed most of the retained stiffness occurred with aprotinin scaffolds for up to 10 days *in vitro*, it is hypothesized that the addition of

aprotinin to the high-density fibrin scaffolds will extend the scaffold life *in vivo* in the presence of cell seeding and the inflammatory environment of the infarct when a larger scaffold size is implanted. Optimal degradation time will depend on a variety of factors, such as how quickly the construct mechanically integrates, forms vascular anastomoses, and how much fibrin needs to degrade to promote neovascularization.

Addition of the broad-spectrum MMP inhibitor galardin to the fibrin scaffolds at a low dose of 5μM showed an intermediate degradation profile similar to that of FXIII scaffolds, allowing significant retention of scaffold stiffness over 10 days *in vitro*. These results indicate that a low dose of galardin could be retained in the scaffold and released as the scaffold degraded. However, when added at a high dose of 25μM, galardin scaffolds degraded to the same extent as unmodified scaffolds by the 10 day time point. While this larger dose of galardin had significant effects on stiffness retention at an early time point (Day 3), it appears the fibrin material was unable to retain this high dose of galardin over the course of the experiment. The significant effect on stiffness retention at the 3 day time point was likely due to a bulk release of galardin.

These *in vitro* and *in vivo* studies demonstrate the development of a high density microtemplated fibrin scaffold with a highly organized microchanneled and microporous architecture designed to mimic the native cardiac ECM structure in order to promote seeded cell organization. In addition, these studies demonstrate the ability to tune the material properties of these fibrin scaffolds in terms of matching initial stiffness to that of native cardiac tissues and tailoring the rate of degradation to target desired scaffold properties for future *in vivo* implant studies.

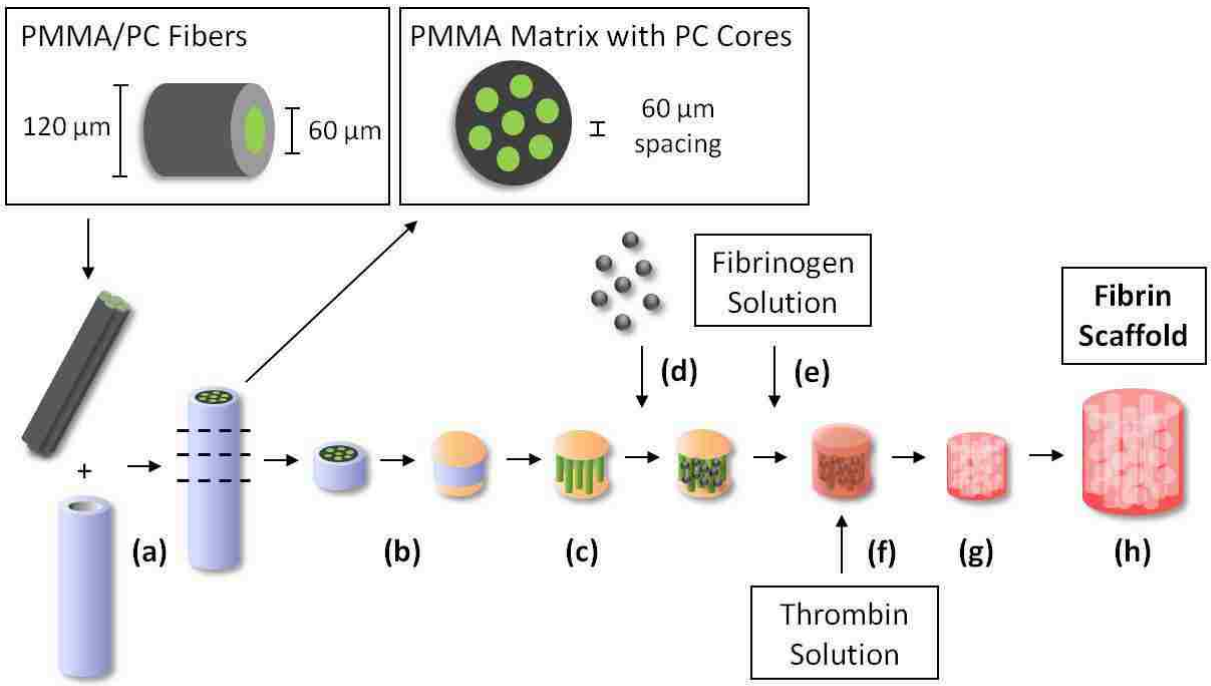

Figure 2.1. Microtemplated fibrin scaffold construction. **(a)** Bundle PMMA/PC fibers & sinter to form PMMA matrix with PC cores spaced 60 µm apart, **(b)** section & immobilize ends of PC cores, **(c)** selectively remove PMMA matrix, **(d)** pack PMMA beads around PC cores and sinter, **(e)** add fibrinogen solution via centrifugation, **(f)** polymerize with thrombin solution, **(g)** remove synthetic polymers, and **(h)** rehydrate fibrin scaffold.

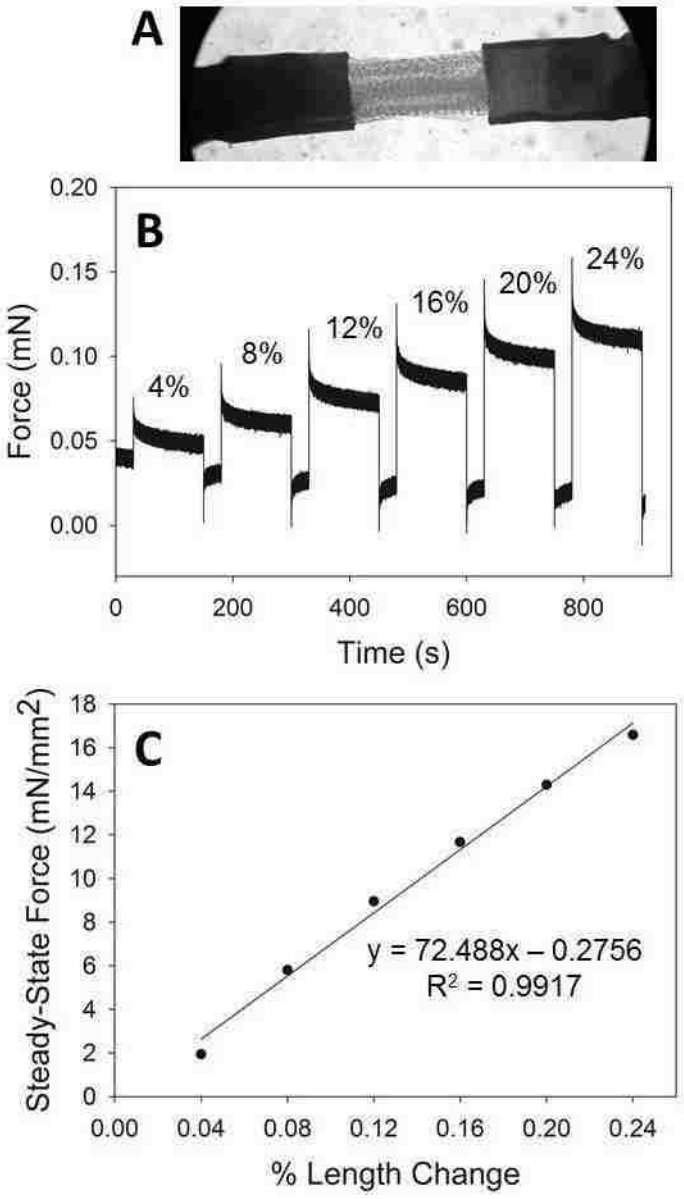

Figure 2.2. Mechanical stiffness testing of fibrin scaffolds. **(a)** Strip of scaffold mounted between a force transducer and a motor (10x magnification). **(b)** Step length changes (4-24%) with resulting tension measured as force (mN). **(c)** Normalized steady-state force (mN/mm^2) is plotted against % length change, and the slope of the resulting regression line is the material stiffness (kPa).

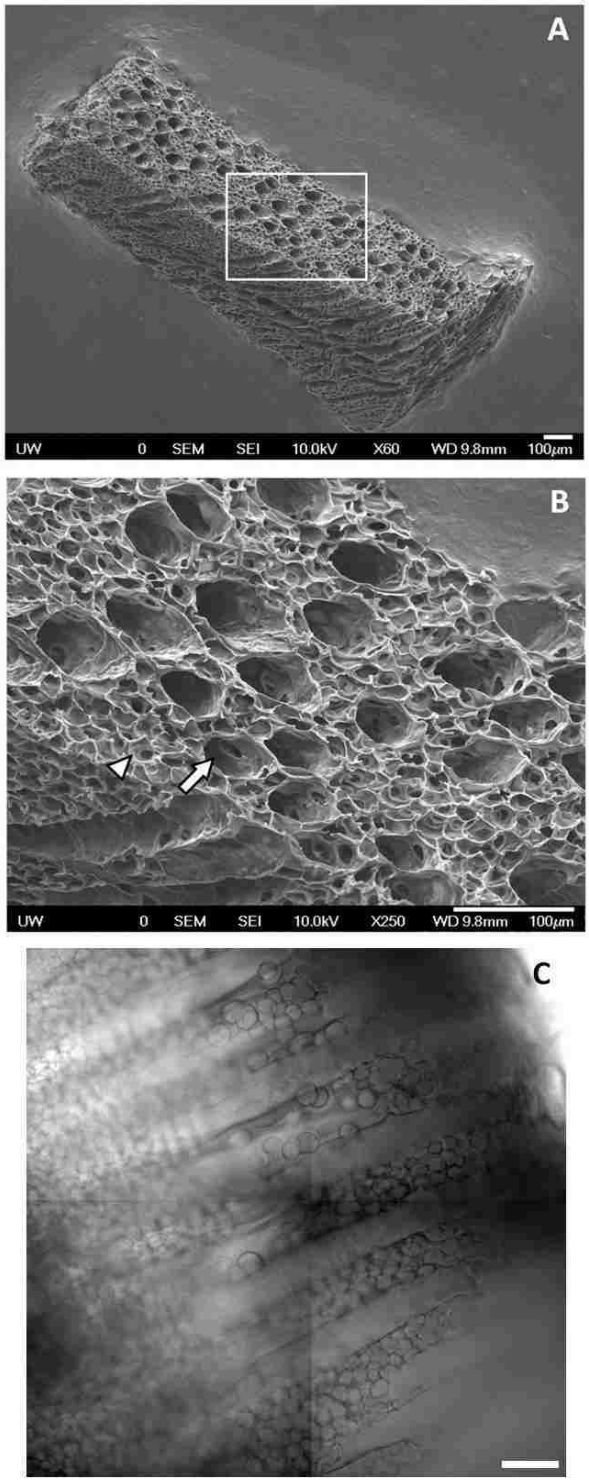

Figure 2.3. High density microtemplated fibrin scaffold architecture with a uniform 27µm porous network (arrowhead) surrounding evenly spaced 60µm channels (arrow). SEM images at **(a)** 60x and **(b)** 250x magnification. **(c)** Composite of 2-photon microscopy brightfield images. Scale bars = 100µm.

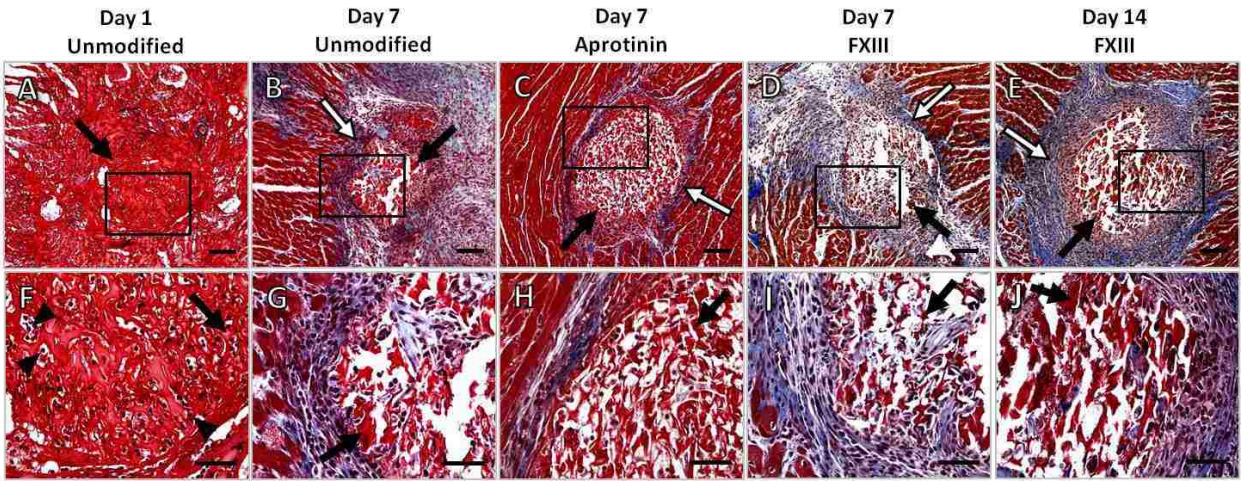

Figure 2.4. Acellular fibrin scaffold implants in adult rat myocardium. Masson's trichrome staining of scaffold implants in cross-section. Unmodified scaffolds after **(a & f)** 1 day and **(b & g)** 7 days, aprotinin scaffolds after **(c & h)** 7 days, and FXIII scaffolds after **(d & i)** 7 days and **(e & j)** 14 days of implantation. Black arrows indicate fibrin implant material, white arrows indicate loose collagen deposition, arrowheads indicate examples of infiltrated neutrophils. Scale bars = 100µm in **(a-e)**, 50µm **(f-j)**.

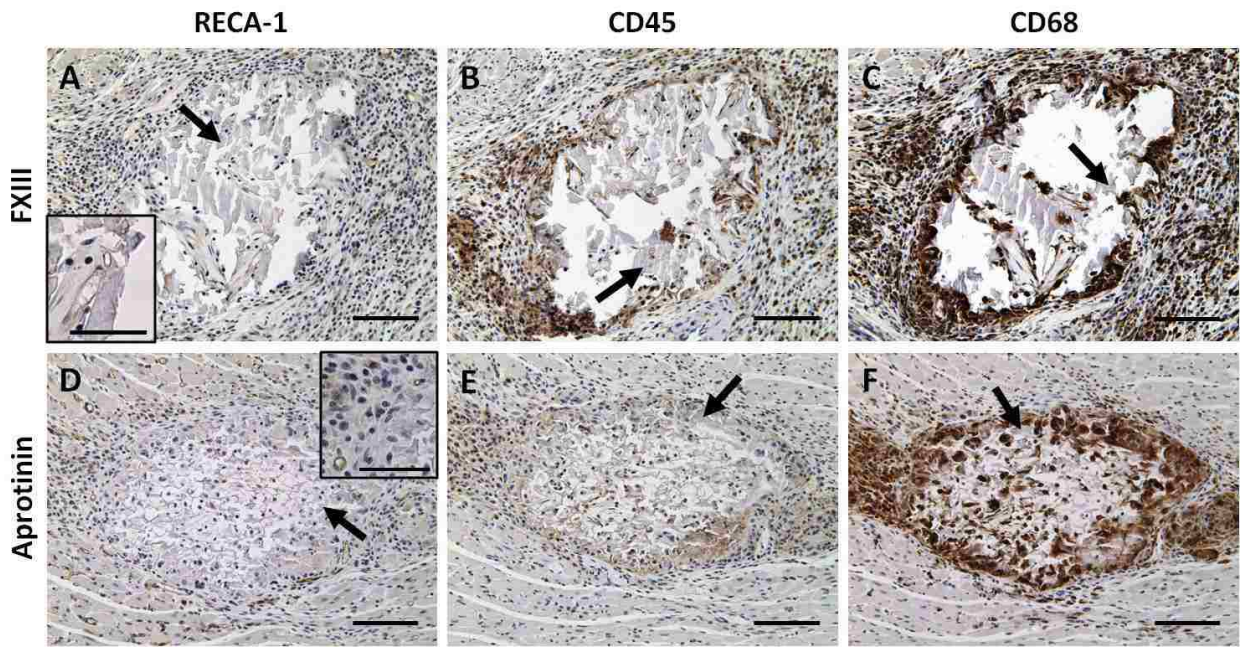

Figure 2.5. Acellular fibrin scaffold implants in adult rat myocardium. Immunohistological staining of FXIII **(a-c)** and aprotinin **(d-f)** scaffold implants in cross-section after 7 days of implantation. RECA-1 **(a & d)**, CD45 **(b & e)**, and CD68 **(c & f)** staining indicate a normal wound healing response to implants. Inset images in **(a)** and **(d)** show RECA-1+ cells (indicated by arrowheads) within and adjacent to fibrin scaffolds. Black arrows in all panels indicate fibrin implant material. Scale bars = 100µm (50µm in insets).

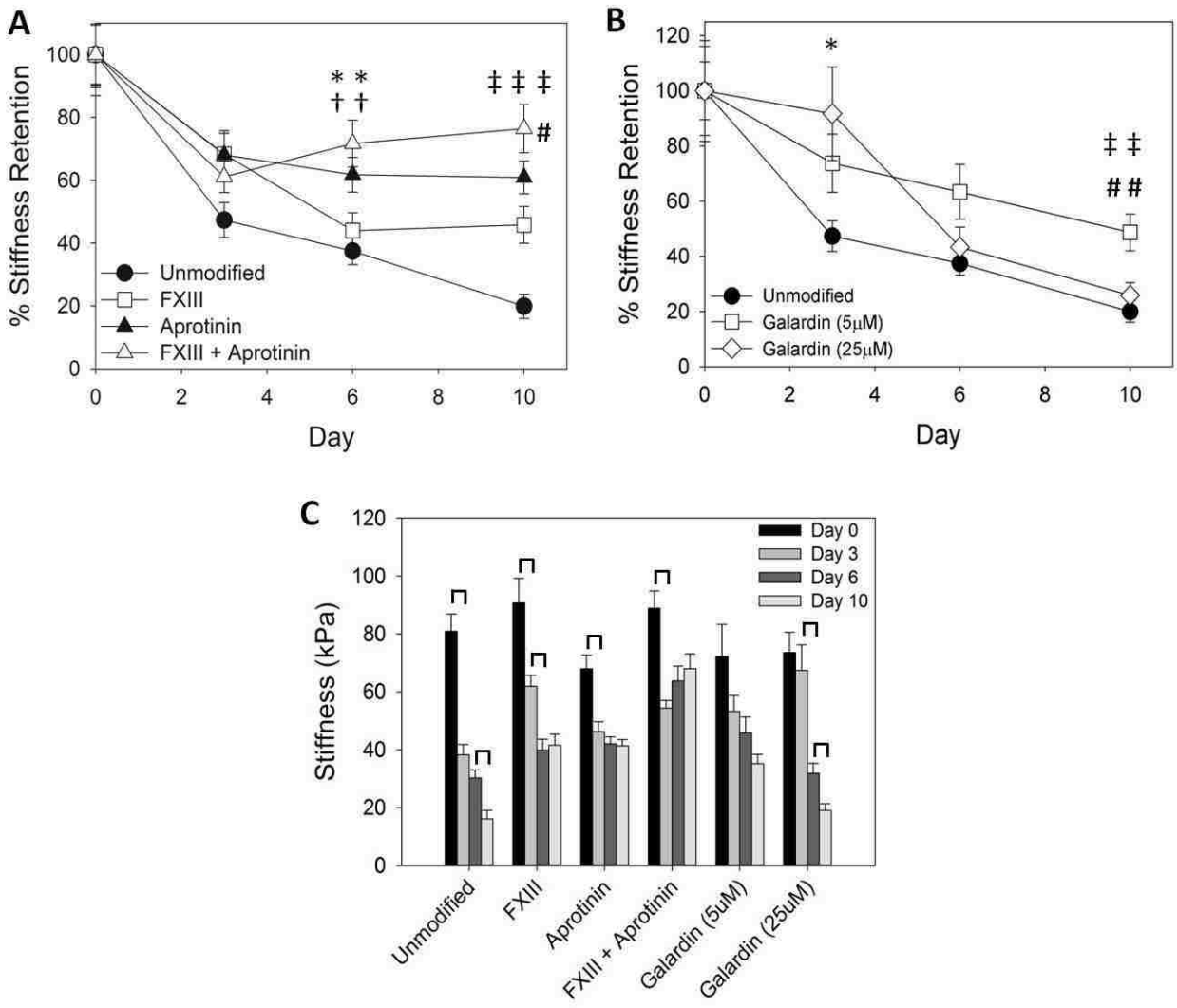

Figure 2.6. Acellular scaffold degradation studies. **(a)** and **(b)** % stiffness retention *in vitro.* **(a)** FXIII and aprotinin degradation studies. Statistically significant difference from unmodified scaffolds on day 6 (*****) or on day 10 (**‡**) (One-Way ANOVA, Dunnett method, $p < 0.05$); statistically significant difference from FXIII scaffolds on day 6 (**†**) or on day 10 (**#**) (2-sided Student's t-test, $p < 0.05$). **(b)** Galardin degradation studies. Statistically significant difference from unmodified scaffolds on day 3 (*****) or on day 10 (**‡**) (One-Way ANOVA, Dunnett method, $p < 0.05$); statistically significant difference from 25μM galardin on day 10 (**#**) (2-sided Student's t-test, $p < 0.05$). **(c)** Stiffness values of scaffold formulations over 10 days *in vitro*. Brackets indicate significant difference from previous time point within each group (2-sided Student's t-test, $p < 0.05$).

Table 2.1. Stiffness (kPa) of fibrin scaffold formulations over 10 days *in vitro*.

	Stiffness in kPa (n)			
Scaffold Treatment	**Day 0**	**Day 3**	**Day 6**	**Day 10**
Unmodified	80.9 ± 6.0 (40)	38.3 ± 3.5 (35)	30.3 ± 2.7 (37)	16.1 ± 2.9 (34)*
FXIII	90.8 ± 8.4 (35)	62.0 ± 3.7 (35)	39.9 ± 3.7 (35)	41.6 ± 3.7(35)
Aprotinin	68.0 ± 4.7 (49)	46.3 ± 3.4 (35)	42.0 ± 2.4 (48)	41.4 ± 2.1 (35)
FXIII + Aprotinin	89.0 ± 5.9 (35)	54.4 ± 2.6 (36)	63.8± 5.1 (35)	68.0 ± 5.1 (34)
Galardin (5μM)	72.3 ± 11 (10)	53.3 ± 5.4 (8)	45.8 ± 5.5 (8)	35.2 ± 3.2 (8)
Galardin (25μM)	73.6 ± 7.0 (10)	67.5 ± 8.8 (8)	31.9 ± 3.4 (7)	19.0 ± 2.3 (7)

* Indicates that the unmodified day 10 stiffness value includes 10 preps that yielded zero passive force, which did not occur in other groups.

Chapter 3:

Evaluation of Fibrin Scaffold Formulations for Promotion of Angiogenesis in a Subcutaneous Implant Model

3.1. Introduction

In the field of tissue engineering, scaffold materials that can support cell seeding and survival, promote tissue-level organization, have mechanical properties matching those of the target tissue, and induce a positive angiogenic response from host tissues are ideal (10, 96, 97). Implantation of any material initiates an inflammatory response from the host tissue, which is characterized by a coordinated and complex series of cellular events intended to heal the wound. The normal host response to constructs implanted for any significant amount of time is to deposit a fibrous capsule of collagen around the implant, known as the foreign body response, which can impede vascularization and integration with host tissue (27). Therefore, the development of biomaterials that can promote a more physiological healing response by decreasing fibrous capsule formation and inducing vascularization could improve the success of tissue engineered implants.

The ability to induce vascularization and anastomosis with the host tissue is critical for the survival of graft cells being delivered in tissue engineered constructs, especially for cells with high metabolic demand such as cardiomyocytes, and is a major factor in the extent of graft integration with the host tissue (97). A variety of scaffold materials have been investigated for their ability to promote vascular infiltration of implants, but a sufficient extent of graft vascularization is still one of the main

challenges in tissue engineering (97-99). In the previous chapter, a microtemplated high density fibrin scaffold for cardiac tissue engineering applications was described. In the event of tissue injury, platelets release the enzyme thrombin which cleaves fibrinogen into fibrin which aggregates into a fibrin mesh and is further stabilized by factor XIII (FXIII) crosslinking. This crosslinked fibrin forms the major protein component of blood clots. Fibrin is naturally degraded by the serine protease plasmin, which leads to the formation of various fibrin degradation products (FDPs), including D-dimers, fibrin D-fragments, and fibrin E-fragments (76, 77). These FDPs have been shown to induce angiogenesis *in vivo* (76), and are naturally cleared by the body (10, 64).

Fibrin has been used by many groups as a hydrogel scaffolding material to deliver cells due to its natural cell adhesive properties, tunable architecture, and non-toxic degradation products (10, 55, 56, 60, 83, 84). Fibrin has been shown to improve survival of transplanted cells (53, 100), induce neovascularization and reduce infarct expansion when injected into ischemic myocardial tissue (53, 58-60). The need for a scaffolding material that can promote a favorable angiogenic response from the host tissue is significant in the field of tissue engineering, and fibrin is a promising biomaterial for this type of application. One issue with using fibrin for certain tissue engineering applications is the low mechanical strength of a fibrin hydrogel (10, 101). Increasing the density of fibrinogen used to form the fibrin gel has been shown to increase mechanical strength (10). In order to match the stiffness of some tissues (such as cardiac muscle), an extremely high concentration of fibrinogen is needed. However, these high concentration fibrin gels are too dense for cells to penetrate and are therefore not ideal for use as cell delivery vehicles.

To address this issue, the microtemplating technique for high density fibrin was developed, which allows fabrication of fibrin scaffolds with much higher stiffness than fibrin gels while maintaining void space in the form of microchannels and an interconnected microporous network to promote high

density cell-seeding and nutrient exchange within scaffolds (96). The addition of a high concentration of FXIII and aprotinin (a serine protease inhibitor), alone and in combination, were tested in the previous chapter to determine their effects on scaffold stiffness and degradation *in vitro*. Significant differences were found in the rate of degradation between scaffold modification groups in these *in vitro* studies, which indicated the potential for scaffold modifications to alter the *in vivo* degradation profile of the microtemplated fibrin.

The main goal of this study was to assess whether different scaffold modifications would induce different tissue responses by evaluating these high density microtemplated fibrin scaffold formulations in a subcutaneous implant model. The hypothesis was that the addition of aprotinin to the fibrin material would slow the degradation of the scaffold *in vivo*, in much the same way as was observed for *in vitro* experiments, and that the fibrin scaffolds would promote a vascular response from the host tissue. Parameters that were investigated include the rate of scaffold degradation, the extent of host angiogenic response to scaffolds, the distribution of infiltrating vasculature within implants, and the effects on fibrous capsule formation around scaffolds over a two week implantation period.

3.2. Materials & Methods

3.2.1. *Fibrin Scaffold Construction*

Scaffold templates and fibrin scaffolds were constructed as described in Chapter 2, with some modifications. Briefly, the polymer templates were infiltrated with a 200mg/mL fibrinogen solution (bovine fibrinogen Type 1-S, Sigma-Aldrich, St. Louis, MO; in 0.9% NaCl) via centrifugation. The fibrinogen solution was pre-warmed in a 37^{o}C water bath for 45-90min to allow the fibrinogen to completely dissolve. Concentrated thrombin solution (13.25U/mL thrombin, Sigma-Aldrich, St. Louis,

MO; 8.3mM $CaCl_2$; DMEM, Gibco, Grand Island, NY) warmed to 37°C was used to polymerize the fibrinogen into fibrin around the polymer template overnight at room temperature. After scraping the exterior of the scaffolds to remove excess fibrin, the polymer template was dissolved with two 24 hour washes in a 90% dichloromethane/10% hexanes solution followed by a 24h acetone wash on an orbital shaker at room temperature. Scaffolds were treated with 100% ethanol rinses for 1 week before rehydration with a graded ethanol series into sterile phosphate-buffered saline (PBS).

3.2.2. *Scaffold Modifications*

Additional cross-linking of fibrin scaffolds was achieved by adding human Factor XIII (FXIII, 100µg/mL, Innovative Research, Novi, MI) to the fibrinogen solution before centrifugation into polymer templates. Inhibition of scaffold degradation by proteases was tested by adding the serine protease inhibitor aprotinin (3000U/mL, Sigma-Aldrich, St. Louis, MO) to the fibrinogen solution. These scaffold modifications were tested alone and in combination with each other to determine their effects on *in vivo* degradation and tissue responses to the fibrin scaffolds.

3.2.3. *Acellular Scaffold Subcutaneous Implants*

After rehydration and equilibration in sterile PBS, acellular fibrin scaffolds (unmodified, FXIII, aprotinin, and FXIII + aprotinin) were cut into 2mm diameter x 3mm length cylinders for subcutaneous implantation and kept in sterile PBS at 4°C until use. All animal procedures were conducted in accordance with the US National Institutes of Health Policy on Humane Care and Use of Laboratory Animals and were approved by the University of Washington (UW) Animal Care Committee. Rats were housed in the Department of Comparative Medicine at UW and cared for in accordance with the UW Institutional Animal Care and Use Committee (IACUC) procedures. Adult male Fischer 344 rats (200-300g) were sedated with isoflurane before implantation following previously described procedures

(102). Briefly, rats (n = 12) received 4 subcutaneous hindlimb implants (2 on each side), one from each scaffold modification group. Sterile scaffolds were implanted into subcutaneous pockets in the left and right hindlimb regions. Rats were euthanized via pentobarbital overdose (120-150 mg/kg) administered via IP injection at endpoints of 7 and 14 days (n = 6 per time point), after which subcutaneous implants with an area of tissue surrounding the suture site were retrieved. This method of euthanasia is in accordance with recommendations of the Panel on Euthanasia of the American Veterinary Medical Association.

3.2.4. *Sample Preparation & Histology*

Subcutaneous implants were immediately immersion-fixed in Methyl Carnoy's fixative after retrieval. Samples were processed, embedded in paraffin, and sectioned (5µm) for histology. Cross-sectional sections were cut from the center (midpoint sections) and both distal ends of samples (approximately 200-300µm apart), and serial sections were stained with Masson's trichrome stain, picrosirius red stain, and with immunohistochemical staining using methyl green as the nuclear counterstain. Immunostaining was performed with primary antibodies against rat endothelial cell antigen (RECA-1, mouse anti-rat (1:10), AbD Serotec, Raleigh, NC) and macrophage marker CD68 (mouse anti-rat (1:100), AbD Serotec, Raleigh, NC). Samples were then labeled with a biotinylated secondary antibody (horse anti-mouse (1:400), Vector, Burlingame, CA) and developed with DAB (Sigma-Aldrich, St. Louis, MO).

3.2.5. *Histological Analysis*

Histological analysis of subcutaneous implants was performed using ImageJ analysis software v1.46 (NIH, Bethesda, MD, USA). All analyses were performed on midpoint and distal end sections (3-4 sections/sample) and then averaged for each sample unless otherwise noted. All samples were imaged

and analyzed in a blinded fashion. The cross-sectional area of implant remaining was determined from Masson's trichrome staining. The density of RECA-1+ lumen structures was determined both within scaffold implants and in an area of tissue between the scaffold and the outer edge of the fibrous capsule on the skin side of implants, and normalized to area (mm^2). Only midpoint sections were used for analysis of RECA-1+ lumen structure density in Day 14 samples due to the extent of scaffold degradation in these end sections. The percent area of CD68+ staining was determined by thresholding images of CD68 stained samples using ImageJ, and then averaging the percent positive area for 3 separate fields of equal size (at 20x magnification) within each scaffold section while avoiding the edges of the implants, as well as in an area of tissue between the scaffold and the outer edge of the fibrous capsule on the skin side of implants. Fibrous capsule thickness was determined from Masson's trichrome staining by taking 4 measures of capsule thickness on the skin side of the implant in each section. Capsule location and thickness measurements were verified with picrosirius red stained samples, both with brightfield and polarized light imaging using previously described protocols (46). In order to measure fibrous capsule cellularity, an area of capsule on the skin side of implants was analyzed for the total number of cells (all nuclei) and normalized to area (mm^2).

3.2.6. *Vascular Distribution Analysis*

To assess whether aprotinin scaffolds induced vascular infiltration to a greater extent than unmodified fibrin, a vascular distribution analysis was done on RECA-1 stained images using ImageJ and Adobe Illustrator. An outline of the remaining scaffold in cross-section was drawn in ImageJ and used to calculate the centroid. A vector outline of the remaining scaffold area was then re-drawn using Adobe Illustrator, and resized around the centroid to delineate three concentric rings, each one third of the distance between the centroid and the initial outline. The number of RECA-1+ lumen structures within each ring was counted, and the percentage of total structures in each ring was calculated.

3.2.7. *Statistical Analysis*

All values are reported as mean ± S.E.M. When comparing multiple scaffold modification groups, statistical significance from unmodified scaffolds was determined with a One-Way ANOVA test using the Dunnett method. When comparing aprotinin and unmodified scaffold groups to each other, statistical significance was determined using a paired Student's t-test with $p < 0.05$ considered significant.

3.3. Results

3.3.1. *Aprotinin Decreases Scaffold Degradation* in vivo

The cross-sectional area of implants remaining after 7 and 14 days of implantation was used to indicate extent of scaffold degradation in the subcutaneous implant model. No significant difference in cross-sectional area was found between scaffold groups at the one week time point, with the remaining scaffold areas averaging approximately 1.4-1.5mm^2 (cross-sectional area of implants on Day 0 was calculated to be 3.1mm^2). However, at the two week time point a significantly greater amount of scaffold was found for the groups containing aprotinin. While unmodified and FXIII scaffolds were almost completely degraded by this time (0.042 ± 0.01mm^2 and 0.010 ± 0.007 mm^2, respectively), aprotinin and FXIII + aprotinin scaffolds were significantly less degraded (0.30 ± 0.05 mm^2 and 0.25 ± 0.04 mm^2, respectively) (**Figure 3.1a**). Representative Masson's trichrome images of Day 14 unmodified and aprotinin scaffold midpoint sections are shown in **Figure 3.1b, c**.

3.3.2. *Aprotinin Scaffolds Increase Angiogenic Response*

To assess effects on host tissue angiogenic response to the four scaffold modification groups, samples were analyzed for total number of RECA-1+ lumen structures per area of scaffold, as well as extent of macrophage infiltration (%CD68+ area). A significantly greater number of RECA-1+ lumen structures were found in aprotinin scaffolds after 7 days of implantation (200 ± 40 lumens/mm^2) as compared to any other scaffold group at this time point (36 ± 30 lumens/mm^2 for unmodified scaffolds, 27 ± 10 lumens/mm^2 for FXIII scaffolds, and 23 ± 10 lumens/mm^2 for FXIII + aprotinin scaffolds), as shown in **Figure 3.2a**. Representative images of the vascularization response in 7 day unmodified and aprotinin implants are shown in **Figure 3.3**. The vascularization response was similar at the 14 day time point, with a significantly greater number of RECA-1+ lumen structures in aprotinin scaffolds (1.3 x 10^3 ± 100 lumens/mm^2) as compared to unmodified scaffolds (0.57 x 10^3 ± 300 lumens/mm^2), as shown in **Figure 3.2b**. To determine whether these differences might be attributed to a differing inflammatory response in the surrounding tissue, the number of RECA-1+ lumen structures in an area of tissue surrounding the scaffolds was also assessed. No significant differences in lumen structure density were found in the surrounding tissue at Day 7 (**Figure 3.2c**). Surprisingly, at the 14 day time point a significantly lower number of RECA-1+ lumen structures per area were found in the tissue surrounding aprotinin scaffolds (3.0 x 10^3 ± 100 lumens/mm^2) as compared to unmodified scaffolds (4.0 x 10^3 ± 300 lumens/mm^2) (**Figure 3.2d**).

The percent area of CD68+ staining was determined for 7 day unmodified and aprotinin scaffold implants, both from the interior of the implant material (excluding edge regions) and in an area of tissue surrounding the implant. A significantly greater amount of CD68+ staining was found within aprotinin scaffold implants (8.6 ± 0.5% CD68+ area) as compared to unmodified scaffold implants (6.2 ± 0.3% CD68+ area) (**Figure 3.4a**). In contrast, a significantly lower amount of CD68+ staining was found in the

surrounding tissue for aprotinin scaffold implants (27 ± 2% CD68+ area) as compared to unmodified scaffold implants (36 ± 1% CD68+ area) (**Figure 3.4b**). Representative images of CD68+ staining in unmodified and aprotinin implants and the resulting threshold level used for analysis are shown in **Figure 3.4c-f**.

3.3.3. *Aprotinin Induces Vascular Infiltration of Scaffolds*

To assess whether aprotinin scaffolds were inducing lumen structure infiltration further into the interior regions of implants, a vascular distribution analysis (**Figure 3.5a**) was performed on Day 7 unmodified and aprotinin samples. For midpoint sections, a significantly greater average number of RECA-1+ lumen structures were found in the outer and middle rings of aprotinin scaffolds when compared with unmodified scaffolds (41 ± 20 lumens (outer ring) & 5.2 ± 3 lumens (middle ring) for aprotinin scaffolds; 3.0 ± 1 lumens (outer ring) & 0.0 ± 0 lumens (middle ring) for unmodified scaffolds) (**Figure 3.5b**). Representing these values as percentages of the total number of lumens found within the implants, approximately 72% of lumens were found in the outer ring, 20% in the middle ring, and 8% in the inner ring for midpoint sections of aprotinin scaffolds. For unmodified scaffolds, 100% of lumen structures were found in the outer ring. In contrast to the results for midpoint sections, no significant differences in lumen structure distribution were found in distal end sections for unmodified and aprotinin scaffolds at this time point (**Figure 3.5c**).

3.3.4. *Fibrous Capsule Thickness is Reduced by Aprotinin Scaffolds*

Fibrous capsule thickness was measured for unmodified and aprotinin scaffolds at the 7 and 14 day time points (**Figure 3.6a**) from trichrome stained sections, and results were confirmed with picrosirius red staining. No significant difference in capsule thickness was seen between unmodified and aprotinin scaffolds at the 7 day time point. However, after 14 days of implantation aprotinin scaffolds showed significantly thinner fibrous capsules (0.064 ± 0.003mm) when compared to unmodified

scaffolds (0.11 ± 0.004mm). In addition, unmodified scaffold capsule thickness significantly increased from day 7 to day 14, while the capsule thickness surrounding aprotinin scaffolds significantly decreased between time points. Representative picrosirius red staining of 14 day unmodified and aprotinin scaffolds demonstrating the differences in fibrous capsule thickness are shown with both brightfield (**Figure 3.6c, d**) and polarized light imaging (**Figure 3.6e, f**).

Capsule cellularity was investigated by determining the total number of cell nuclei in a selected area of capsule on the skin side of implants for unmodified and aprotinin scaffold groups (**Figure 3.6b**). No significant difference was found in the number of cells per area of capsule for these two scaffold groups at the 7 day time point ($6.1 \times 10^4 \pm 0.6 \times 10^4$ cells/mm^2 for unmodified scaffolds, $5.4 \times 10^4 \pm 0.8 \times 10^4$ cells/mm^2 for aprotinin scaffolds). However, although not statistically significant, there appears to be a greater number of cells per area of capsule surrounding aprotinin implants after 14 days ($3.3 \times 10^4 \pm 0.8 \times 10^4$ cells/mm^2) as compared to unmodified scaffolds ($1.1 \times 10^4 \pm 0.07 \times 10^4$ cells/mm^2). Capsule cellularity for both of these scaffold groups decreased from 7 to 14 days.

3.4. Discussion

Aprotinin is a broad spectrum 6.5kDa competitive serine protease inhibitor naturally derived from bovine lung tissue, and has well-known anti-fibrinolytic properties as an inhibitor of plasmin (54, 70, 103). Due to this ability to prevent fibrin clot degradation aprotinin has been used as a haemostatic agent during cardiac surgical procedures (94, 95) and as a component of fibrin glues and tissue sealants (91, 104, 105). In addition, many groups have demonstrated slowed degradation of fibrin hydrogels with the addition of aprotinin to the culture media (54, 70, 106) or into the fibrin material itself (105, 107). Aprotinin was utilized to modify fibrin scaffold degradation properties *in vitro* in the studies discussed in the previous chapter, in which addition of aprotinin to high density microtemplated fibrin scaffolds was

able to significantly increase scaffold stiffness retention when compared to unmodified fibrin scaffolds or scaffolds with additional FXIII crosslinking alone (96).

One of the goals of modifying the fibrin material was to try and extend the lifetime of the scaffold after implantation, as unmodified fibrin scaffolds were found to degrade very quickly both *in vitro* and *in vivo* (96). In this study, four different fibrin scaffold modification groups were evaluated in a subcutaneous implant model. The amount of scaffold cross-sectional area remaining was measured after 1 and 2 weeks of implantation, and the results showed significantly more scaffold area remaining after 14 days in both scaffold groups containing aprotinin. This follows with the well-established role of aprotinin as an inhibitor of fibrin degradation, and indicates that aprotinin can be loaded into the microtemplated fibrin, retains its function during scaffold processing procedures, and is subsequently released in active form into the surrounding tissue. The stability of the aprotinin molecule against many forms of denaturation is attributable to its highly compact tertiary protein structure (108, 109), which accounts for the retention of its protease inhibitor activity even after organic solvent processing of the scaffolds during template removal.

Previous studies have shown pore size can have a significant effect on the extent of vascular infiltration of biomaterial scaffolds, and observed the greatest extent of vascularization in scaffolds with an average pore size of 35µm (110). In addition, the natural degradation products of fibrin have been shown to promote angiogenesis (77, 80, 111, 112). It was therefore expected that the fibrin scaffolds would be able to elicit a vascular response from the host tissue even at the relatively early time point of 7 days due to the 27µm diameter porous architecture and release of fibrin degradation products. Interestingly, aprotinin scaffolds induced a significantly greater average number of lumen structures infiltrating the microtemplated fibrin implants at both the 7 and 14 day time points compared to unmodified implants. Aprotinin scaffolds also induced vascularization further into the interior regions of

implants than did unmodified scaffolds, as shown by the results of the concentric rings analysis on day 7 implants.

Aprotinin has been shown to induce angiogenesis in a chicken embryo chorioallantoic membrane assay, as well as induce endothelial cell activation and migration *in vitro* (103, 113). One proposed mechanism by which it may promote angiogenesis is by the inhibition of angiostatin generation by platelets (113, 114). Angiostatin induces apoptosis in and inhibits migration of endothelial cells (114), and is formed by the auto-proteolysis of plasmin (113). As an inhibitor of serine proteases (including plasmin), aprotinin has been shown to inhibit angiostatin generation by platelets and subsequently induce an increased angiogenic response (113). Another mechanism by which aprotinin might be affecting the angiogenic response is by increasing levels of the growth factor pleiotrophin, which directly induces endothelial cell migration (103). Aprotinin has been shown to increase levels of pleiotrophin both by inhibiting its degradation by plasmin and by inducing its expression via transcriptional activation of the pleiotrophin gene (103). Since aprotinin is a relatively small molecule that can freely diffuse out of lower density fibrin hydrogels (105), it was hypothesized that in the high density fibrin constructs aprotinin molecules would be entrapped within the dense fibrin network and released as the scaffold was degraded. One effect observed in this study was that additional FXIII crosslinking appeared to result in significant delay in the release of aprotinin, as no effects on the overall vascularization response with scaffolds containing both aprotinin and FXIII at the 7 day time point were seen. The results of this study, along with the results discussed in the previous chapter on the *in vitro* degradation data of these scaffold formulations, support this hypothesis.

When the macrophage response was investigated, a significantly greater amount of CD68+ staining was found within aprotinin implants as compared to unmodified scaffolds at the 7 day time point. Macrophages coordinate the foreign body response and induce the infiltration of other cell types

into the wound, including fibroblasts and endothelial cells (11). Therefore, an increased amount of macrophage infiltration into aprotinin implants correlates with the increased vascularization response seen in this implant group. Interestingly, when the vascular and macrophage responses in the tissue surrounding implants were investigated, aprotinin implants showed significant decreases in these cell types as compared to unmodified scaffolds (decreased CD68+ area at 7 days, decreased RECA-1+ lumen structures at day 14). Additionally, aprotinin implants had significantly thinner (but apparently more cellular) fibrous capsules at the day 14 time point compared to unmodified scaffolds. These results indicate aprotinin release from the fibrin material may be affecting the inflammatory and wound healing responses to the scaffold implants.

As neutrophils and later monocytes/macrophages are recruited to the site of healing, they release both pro- (including TNF-α, IL-1, and IL-6) and anti-inflammatory (including IL-10) cytokines which coordinate the wound healing response (115, 116). Aprotinin has been shown to induce expression of anti-inflammatory cytokines, which in turn inhibit release of pro-inflammatory cytokines from both macrophages and neutrophils (115, 117). In addition, aprotinin inhibits expression of endothelial cell receptors for neutrophils (ICAM-1)(115, 117) and inhibits production of pro-inflammatory cytokines which attract neutrophils (118), and therefore decreases accumulation of these inflammatory cells at the site of wound healing. Previous studies have shown an increase in anti-inflammatory macrophages (M2 phenotype) within and around microporous implants when compared to non-porous implants, and that this macrophage switch corresponded with an increased extent of porous implant vascularization (11). An increase in M2 macrophage phenotype has also been associated with improved tissue remodeling and host response to implanted scaffolds (119). One potential explanation for the results found in this study could be that aprotinin is inducing a differential macrophage phenotype profile, which would affect the overall cellular responses and remodeling in the tissue surrounding implants.

An interesting finding of this study was the decreased capsule thickness found for aprotinin implants at the 14 day time point when compared to unmodified scaffolds. While fibrin is known to attract fibroblasts and stimulate their proliferation and collagen secretion during normal wound healing, fibrin sealants (which typically contain aprotinin) have been shown to decrease tissue fibrosis and scar formation *in vivo* (104). Transforming growth factor beta (TGF-β) is one of the main factors responsible for promoting fibroblast proliferation and subsequent collagen deposition by these cells during wound healing (104), and is produced by different cell types including macrophages and epithelial cells (120). Aprotinin has been shown to completely inhibit the activation of TGF-β, and therefore reduce tissue fibrosis and capsule formation *in vivo* (120, 121). Therefore, a potential explanation for the reduced fibrous capsule thickness observed surrounding aprotinin implants is the interaction of aprotinin with TGF-β activation via this pathway, resulting in decreased collagen deposition by fibroblasts.

This study describes the host tissue responses to different modifications of high density microtemplated fibrin scaffolds. The addition of the protease inhibitor aprotinin significantly decreased implant degradation and significantly increased vascular and macrophage infiltration of scaffolds. Additionally, aprotinin release from scaffolds decreased the extent of inflammation in the surrounding tissue, and promoted the formation of a thinner and more cellular fibrous capsule. Future studies will need to further investigate the host cell responses to aprotinin scaffolds, and eventually determine their effect on cell-seeded scaffold integration with host tissues.

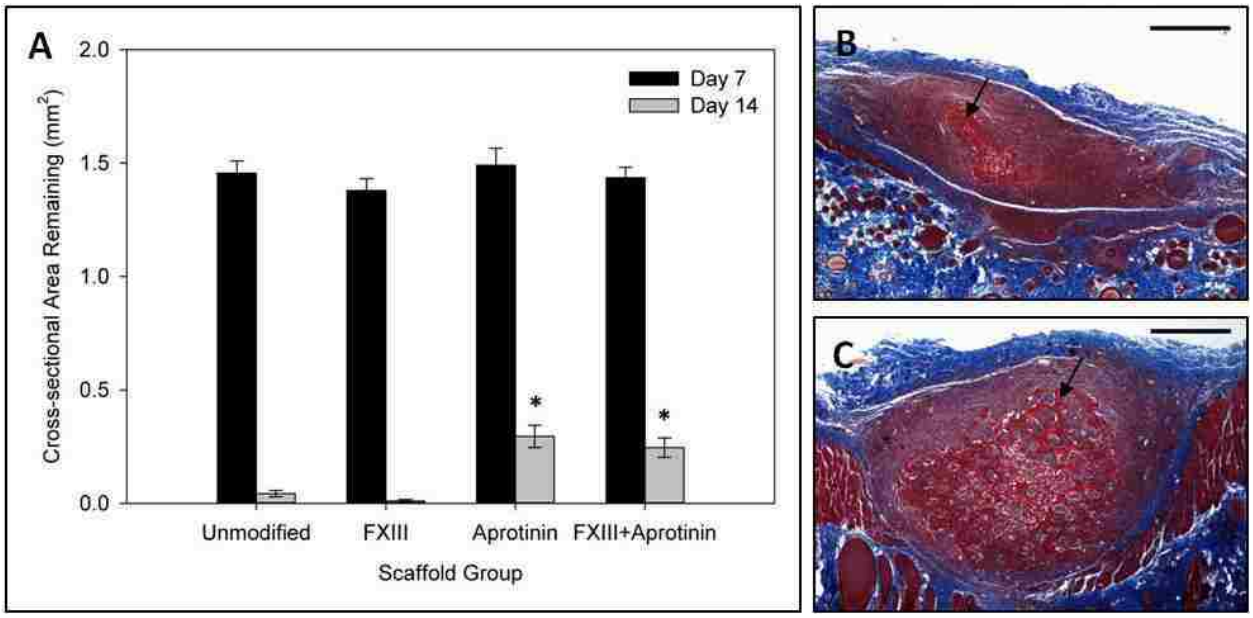

Figure 3.1. Degradation of scaffold formulations *in vivo*. **(a)** Cross-sectional area of scaffolds remaining after 7 & 14 days of subcutaneous implantation. Cross-sectional area of scaffolds at the time of implantation (Day 0) estimated as 3.1mm^2. Representative Masson's trichrome images for day 14 **(b)** unmodified scaffolds and **(c)** aprotinin scaffolds demonstrating the extent of scaffold degradation. Black arrows indicate fibrin scaffold material. ***** Indicates statistical significance from day 14 unmodified scaffolds (Student's t-test, $p < 0.05$). Scale bars = 500µm.

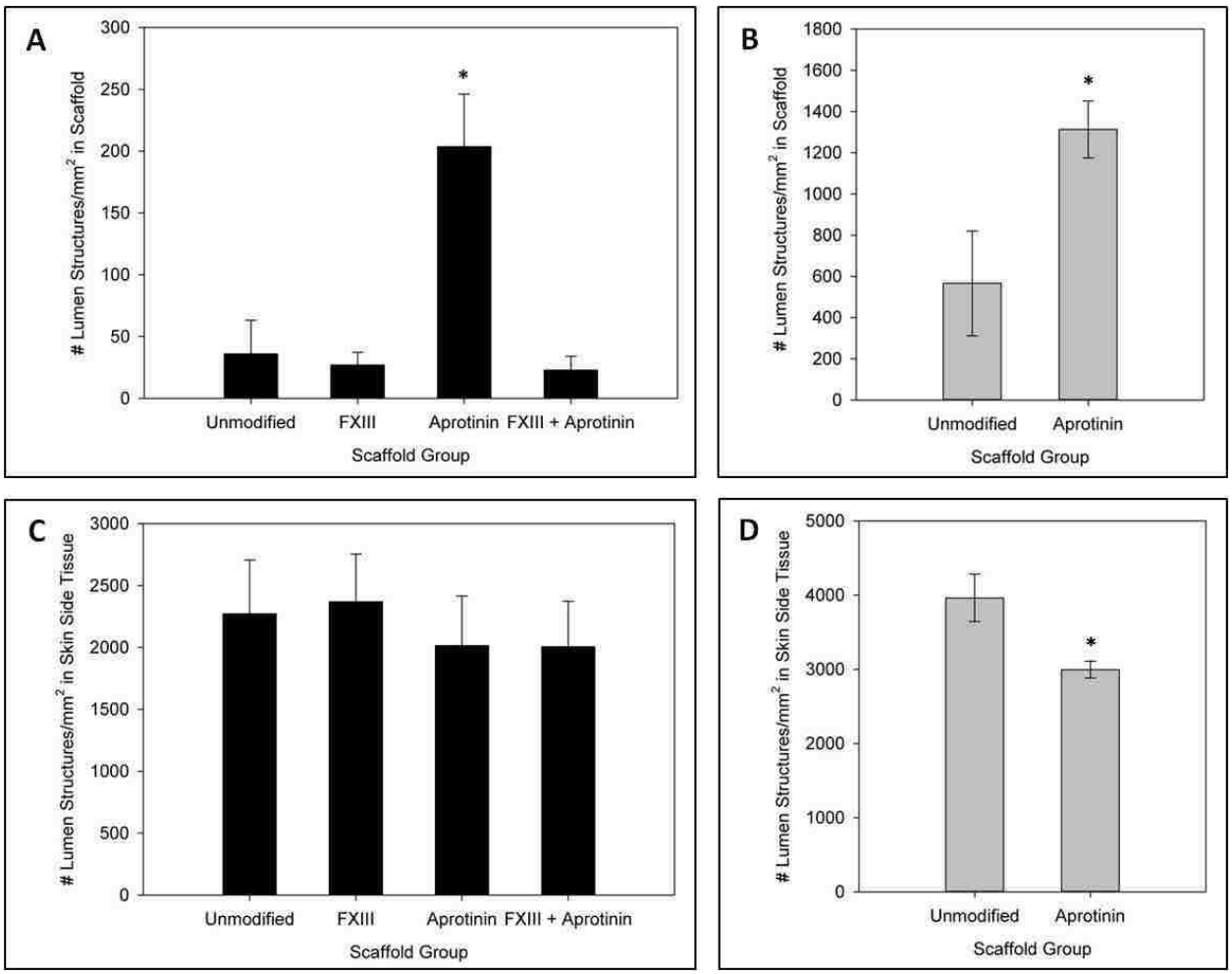

Figure 3.2. Induction of vascularization response by fibrin scaffold formulations. Average number of RECA-1+ lumen structures/mm^2 within scaffolds at **(a)** 7 days and **(b)** 14 days post-implantation. Average number of RECA-1+ lumen structures/mm^2 in an area of surrounding tissue on the skin side of implants at **(c)** 7 days and **(d)** 14 days post-implantation. ***** Indicates statistical significance from unmodified scaffolds (Student's t-test, $p < 0.05$).

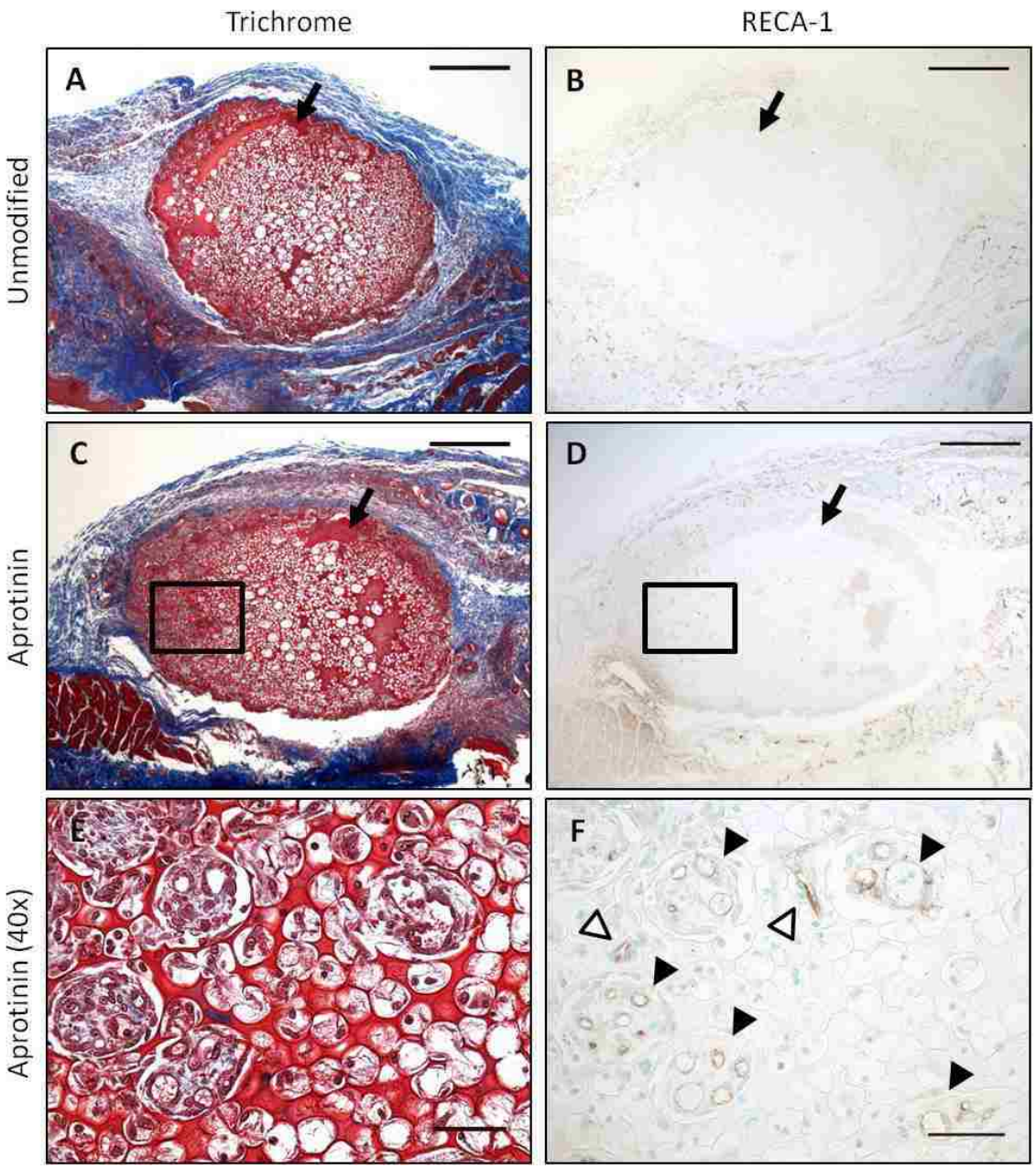

Figure 3.3. Vascularization response to implanted scaffolds. Representative images of **(a & b)** unmodified and **(c-f)** aprotinin scaffold implants after 7 days of implantation. **(a, c, & e)** Masson's trichrome staining with **(b, d, & f)** RECA-1+ staining of a consecutive section. Outlined areas in **(c)** and **(d)** are shown at higher magnification in **(e)** and **(f)**, respectively. Arrows indicate fibrin material, black arrowheads indicate RECA-1+ lumen structures in scaffold channels, white arrowheads indicate RECA-1+ lumen structures in scaffold pores. Scale bars in **(a-d)** = 500µm. Scale bars in **(e)** and **(f)** = 50µm.

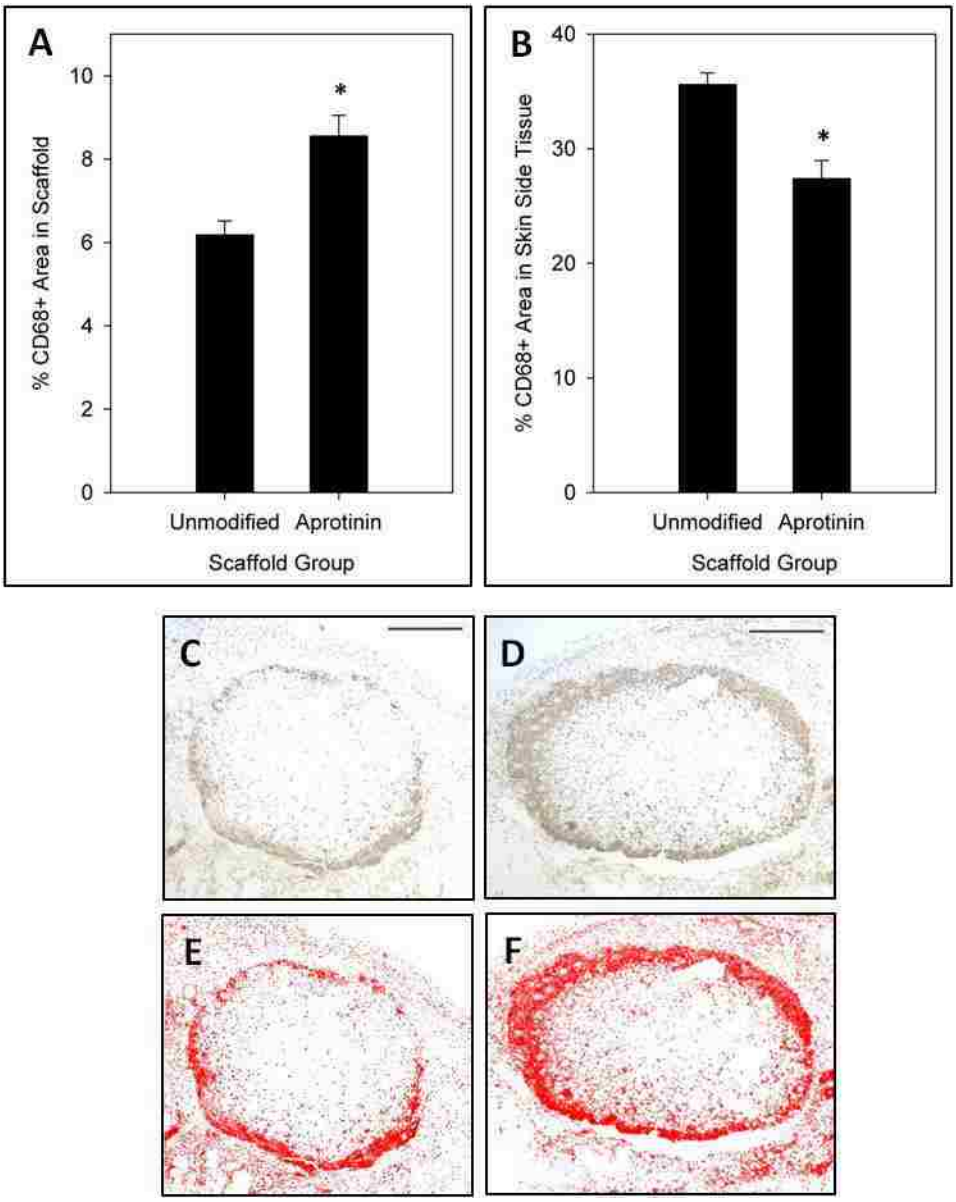

Figure 3.4. Macrophage response to 7 day scaffold implants. %CD68+ area **(a)** within scaffolds and **(b)** in an area of surrounding tissue on the skin side of implants. Representative CD68+ stained **(c)** unmodified and **(d)** aprotinin scaffolds, with corresponding threshold analysis images **(e & f)**. * Indicates statistical significance from unmodified scaffolds (Student's t-test, $p < 0.05$). Scale bars = 500µm.

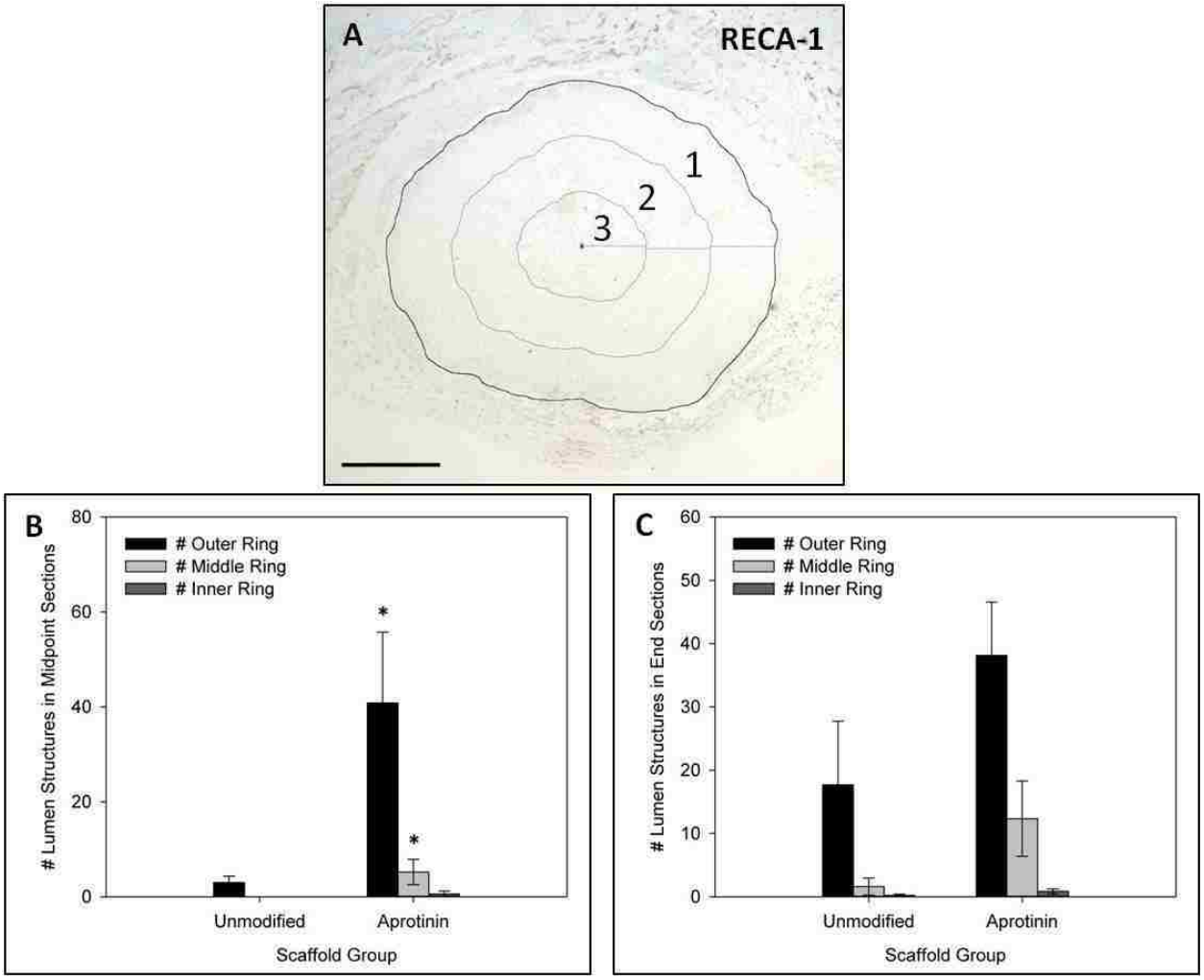

Figure 3.5. Concentric rings analysis to determine vascular distribution within 7 day implants. **(a)** Representative image showing concentric rings and centroid used for analysis. 1 = Outer ring; 2 = Middle ring; 3 = Inner ring. Average number of RECA-1+ lumen structures within each ring for unmodified and aprotinin scaffolds in **(b)** midpoint sections and **(c)** distal end sections. ***** Indicates statistical significance from corresponding ring in unmodified scaffolds (Student's t-test, $p < 0.05$). Scale bar = 500µm.

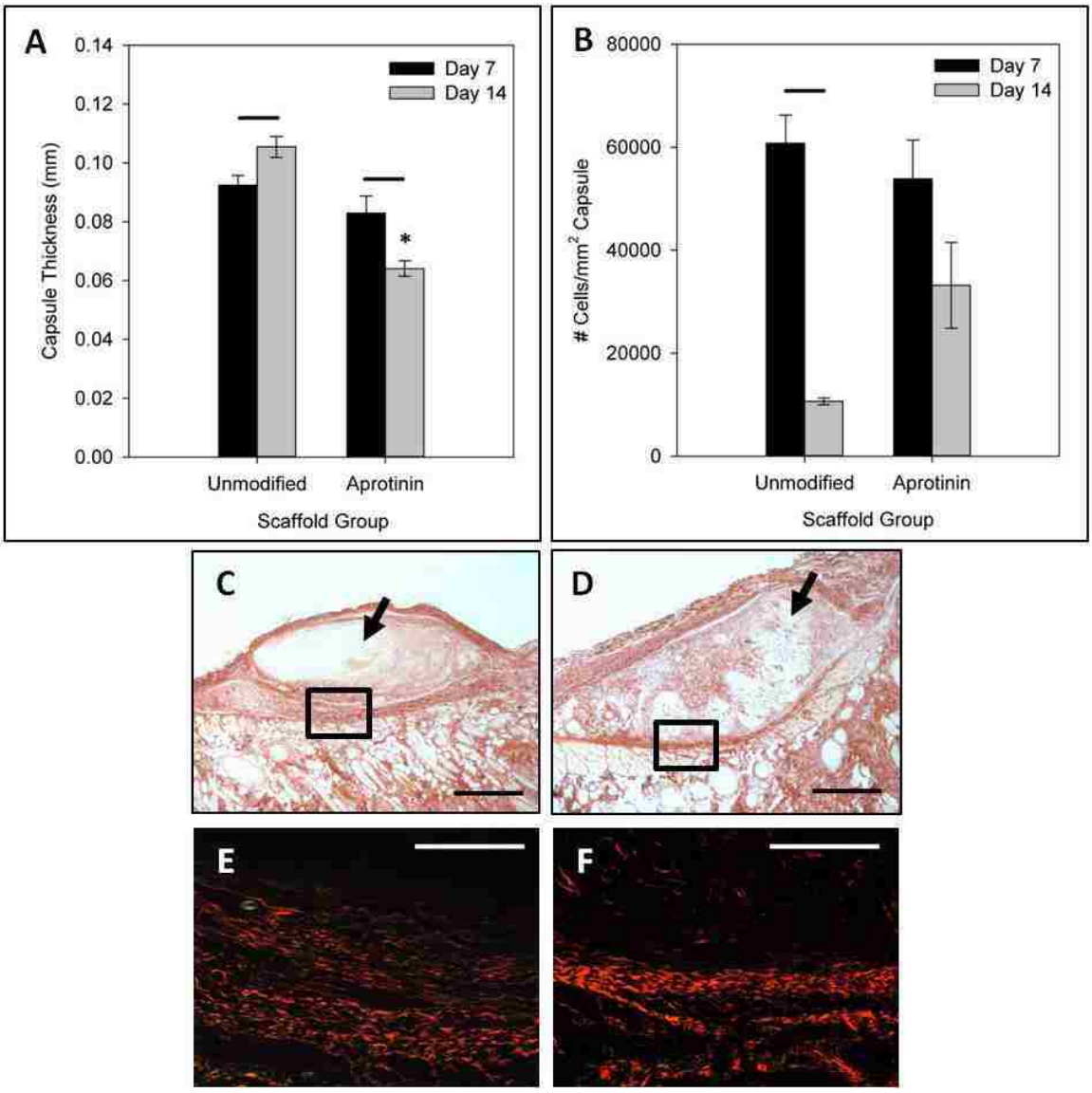

Figure 3.6. Fibrous capsule analysis of unmodified and aprotinin scaffold implants. **(a)** Average fibrous capsule thickness measured for scaffold groups at 7 and 14 days. **(b)** Average number of cells/mm^2 of capsule for 7 and 14 day implants. * Indicates statistical significance from 14 day unmodified scaffolds, bars indicate statistical significance from previous time point within a group (Student's t-test, $p < 0.05$). Representative brightfield images of picrosirius red staining of 14 day **(c)** unmodified scaffolds and **(d)** aprotinin scaffolds. Polarized light images of outlined areas in **(c)** and **(d)** are shown in **(e)** and **(f)**, respectively. Scale bars in **(c)** and **(d)** = 500µm, in **(e)** and **(f)** = 200µm.

Chapter 4:

Optimization & Characterization of Cell-Seeding of Microtemplated Fibrin Scaffolds

4.1. Introduction

Characteristics of an effective cellular construct for the treatment of myocardial infarction include the ability to enhance cell attachment and promote cellular organization in order to increase the number of functional cells being delivered to the site of implantation. Additionally, constructs should have a mechanical strength similar to native myocardium in order to support grafted cell function and to avoid issues with mechanical mismatch upon implantation. The construct described in the previous chapters is a novel high density templated fibrin scaffold with a microchanneled and microporous architecture with mechanical properties tailored for cardiac tissue engineering applications. This scaffold is designed to mimic native cardiac tissue structure in order to promote improved cellular organization *in vitro* with the goal of increasing graft integration with host tissue upon implantation. The microarchitecture of the scaffold is designed to promote cellular alignment and pre-vascular network formation within channels after seeding, as well as facilitate nutrient exchange and waste removal within constructs. In addition, the high density fibrin material will provide adequate and tunable mechanical strength to support graft cells until they can replace the scaffold with their own ECM.

Cardiac muscle fibers consist of highly aligned cardiomyocytes containing myofibrils oriented parallel to the fiber axis, and successive cardiomyocytes are interconnected at their ends through specialized junctional complexes (intercalated disks). McDevitt *et al.* showed that cardiomyocytes patterned in lanes of laminin responded to the spatial constraints by forming elongated, rod-shaped cells aligning parallel to the lanes. Patterned cardiomyocytes displayed bipolar localization of the junction molecules that resembled intercalated disks. Further, lanes of cardiomyocytes contracted synchronously (122). More recently, Black *et al*. showed that twitch force in aligned cardiomyocyte constructs was greater than in non-aligned conditions (123). Therefore, the microtemplated fibrin scaffolds described here were designed to direct the organization of cardiomyocytes in order to more closely resemble the organized alignment found *in vivo*.

The main components of healthy heart tissue are mature contracting cardiomyocytes coupled with an extensive capillary network. Thus, a cardiac repair construct requires cardiomyocytes and the components of capillaries, endothelial cells and supporting cells. It is well established that co-culture of endothelial cells and fibroblasts or mesenchymal stem cells generates stable vascular networks in 3D cultures (124). Studies by the Davis group have shown neovessel formation is a complex process requiring a sequential set of events modulated by cell-cell and cell-matrix interaction (125). Trophic function and differentiation potential of 3D cultures composed of three different cell types has also been shown *in vivo* and *in vitro* for cultures of keratinocytes, dermal fibroblasts and endothelial cells, and for cultures of skeletal myoblasts, embryonic fibroblasts and endothelial cells in chitosan/collagen and PLLA/PLGA porous scaffolds, respectively (47-49). When implanted *in vivo* these constructs exhibited continuous differentiation and were invaded by host blood vessels (47-49). When hESC-derived cardiomyocytes were seeded together with hESC-derived endothelial cells or human umbilical vein endothelial cells (HUVECs) with embryonic fibroblasts on a PLLA/PLGA scaffold, they generated a synchronously contracting construct containing a well-developed neovessel network *in vitro*. Fibroblasts

stabilized the formed neovessels by reducing endothelial cell death and increasing their proliferation (126). Tulloch *et al.* demonstrated tri-cell culture increased lumen structure formation in collagen constructs containing hESC-derived cardiomyocytes as compared to bi-cell constructs, and the presence of capillaries augmented cardiomyocyte proliferation (46). For these reasons, a tri-cell seeding strategy was adopted for the microtemplated fibrin scaffolds. The hypothesis was that the use of a mixture of rat or human cardiomyocytes, endothelial cells, and fibroblasts or mesenchymal stem cells seeded into scaffolds would promote the development of a pre-vascularized and aligned cardiac tissue construct.

4.2. Centrifugation Seeding Optimization

The main method of seeding cells into fibrin construct microchannels was centrifugation. There were many parameters that required optimization for cell seeding of the microtemplated fibrin scaffolds, including scaffold, cell, and seeding protocol considerations (**Table 4.1**). The main parameters that were investigated are discussed in this section, with what was determined to be the most optimal set described in detail in the Materials and Methods section following.

4.2.1. *Optimization of Scaffold Parameters*

Certain scaffold parameters needed optimization in order to increase the chances of successful cell seeding. It was hypothesized that cells were flowing through and out of scaffolds and not being held within scaffold channels during centrifugation. Therefore, in order to help retain cells a fibrin cap formed on the bottom (non-seeding) end of scaffolds was tested and compared to centrifugation seeding without a fibrin cap. Fibrin caps were found to increase cell retention in scaffolds, and were therefore used for the majority of unidirectional centrifugation seeding experiments.

Another scaffold parameter that needed optimization was that of scaffold pre-treatment. Initially, scaffolds were rehydrated into sterile PBS and kept in this solution until use for seeding. It was hypothesized that pre-treating scaffolds by incubating in either FBS or seeding media for a period of time before seeding would allow protein and growth factor adsorption to the fibrin material, which might improve cell attachment and retention. Some improvements were seen when scaffolds were pre-treated with seeding media for approximately 1 hour before seeding.

The method of cutting scaffolds with biopsy punches was a critical factor in the success of cell seeding with centrifugation. If scaffolds were not cut to fit exactly within the biopsy punch tubes, the majority of the cell solution flowed around scaffolds rather than through construct channels resulting in poor seeding. Initially, scaffolds were cut in a fully hydrated state. This often resulted in uneven cutting and "flaring out" of the bottom end of scaffolds. The most consistent method found was to slightly compress the scaffolds before cutting to try and remove some (but not all) liquid, and then cutting with the biopsy punches in this slightly dehydrated state. When the scaffold within the tube next came in contact with seeding media, it would absorb the liquid and become more tightly fitted within the biopsy punch tube. However, the fibrin material must not be allowed to completely dehydrate, as this sometimes led to a loss of the ordered architecture of the material. This method reduced but did not completely eliminate the issues with uneven scaffold cutting.

4.2.2. *Optimization of Cell Parameters*

There were multiple cell parameters that needed to be optimized for the cell seeding protocol. One of the main issues encountered with cell seeding was the low density of cells obtained within constructs. Therefore, the total attempted number of seeded cells was tested at concentrations ranging from 1-4x10^6 cells/scaffold (approximately 1.3-5.3x10^8 cells/cm^3). Contrary to what was initially hypothesized, seeding with the higher cell densities generally resulted in less successful seeding. This

was likely due to excessive clogging of scaffold channels by the dense cell solution, preventing seeding further into constructs. The most optimal cell concentration of those tested was $2x10^6$ cells/scaffold.

Another important parameter investigated was the ratio of the three cell types being seeded. Initial cell seeding experiments were done using a ratio of 1:1:1 (cardiomyocytes : endothelial cells : fibroblasts or MSCs). It was hypothesized that increasing the ratio of cardiomyocytes relative to one or both of the other cell types would increase the chances for gap junction formation and therefore development of synchronous contraction within constructs. Therefore, cell ratios of 2:1:1, 2:2:1, and 4:2:1 were also tested. The cell ratio that promoted cardiomyocyte and endothelial cell organization to the greatest extent was 4:2:1, the results of which are discussed in detail in later sections.

The third main cell parameter that was optimized was that of cell pre-treatment. In early cell seeding experiments cardiomyocytes were not pre-conditioned in any way before seeding, which resulted in very few constructs with contracting cells. Heat shock treatment of cells was hypothesized to provide a protective effect in the ischemic conditions encountered in this high cell density seeding system by upregulating heme oxygenase-I (HO-1), an enzyme shown to improve cardiomyocyte survival (127, 128). Heat shock pre-treatment of cardiomyocytes 24 hours before seeding was tested, and resulted in significantly more contracting cardiomyocytes after seeding. Therefore, heat shock pre-treatment of cardiomyocytes was used for all subsequent seeding experiments.

4.2.3. *Optimization of Seeding Protocol*

Once cell and scaffold parameters were established, optimization of the seeding protocol was investigated. Static seeding was used previously to seed microporous fibrin scaffolds (10), and was therefore tested with the microchanneled architecture. As discussed in detail in later sections, static seeding resulted in very little cell penetration into the interior regions of scaffolds and was therefore not

the main method of seeding used for this system. Centrifugation seeding typically resulted in cell seeding further into the microchannels, and therefore became the focus of further optimization experiments.

The main parameter of the seeding protocol that needed optimization was the centrifugation speed used. Centrifugation of cells into scaffolds at 1000rpm was used previously for pHEMA scaffolds with the microchanneled and microporous architecture (11). However, when this speed was used for seeding of the fibrin constructs it resulted in very poor cell seeding. It was hypothesized that due to the compliant material properties of the fibrin material compared to those of the pHEMA, the fibrin scaffolds could not withstand high centrifugation speeds and were being compressed, thus preventing cell seeding. Therefore, much lower centrifugation speeds were tested, and the most optimal speed found for seeding of fibrin scaffolds was approximately 7xg (200rpm).

In an attempt to improve cell seeding distribution, experiments were done testing unidirectional versus bidirectional centrifugation seeding of constructs, in which scaffolds were carefully removed from biopsy punch tubes after 2 rounds of centrifugation, and re-inserted in the other direction before 2 more rounds of centrifugation seeding. No significant improvements in cell seeding were seen with this method, and it was hypothesized that cell loss and scaffold damage were occurring during the re-insertion process. Therefore, unidirectional seeding was used for the remainder of seeding experiments.

Finally, the media used for seeding and plating was optimized for the tri-cell constructs. Initial experiments were done using a 50:50 mixture of cardiomyocyte and endothelial cell media for both seeding and plating media. This resulted in excellent endothelial cell organization within construct channels, but very little cardiomyocyte contraction within constructs and in tissue culture dishes. Experiments done with different media mixtures indicated that the greatest degree of cardiomyocyte survival occurred when 100% cardiomyocyte media was used for both seeding and plating with media

changes every day, and that this did not have significant detrimental effects on endothelial cell organization. For human tri-cell seeding with hESC-CMs, significant issues with cell clumping were encountered during the seeding protocol. It was therefore determined that the addition of DNAse to the seeding media to help prevent cell clumping was necessary for the human cell seeding protocol.

4.3. Materials & Methods

4.3.1. *Fibrin Scaffold Construction*

Scaffold templates and fibrin scaffolds were constructed as described in Chapter 2, with some modifications. Briefly, the polymer templates were infiltrated with a 200mg/mL fibrinogen solution (bovine fibrinogen Type 1-S, Sigma-Aldrich, St. Louis, MO; in 0.9% NaCl) via centrifugation. The fibrinogen solution was pre-warmed in a 37^{o}C water bath for 45-90min to allow the fibrinogen to completely dissolve. For some constructs, a fibrin cap was formed on one end of the scaffold to assist with retention of cells during centrifugation seeding. After centrifuging the fibrinogen solution into the templates and scraping all surfaces to remove excess fibrinogen, a drop of fibrinogen solution was added to one end of a template sitting in an empty well of a 24-well plate before carefully pipetting the thrombin solution around the template. Concentrated thrombin solution (13.25U/mL thrombin, Sigma-Aldrich, St. Louis, MO; 8.3mM $CaCl_2$; DMEM, Gibco, Grand Island, NY) warmed to 37^{o}C was used to polymerize the fibrinogen into fibrin around the polymer template overnight at room temperature. After scraping the exterior of the scaffolds to remove excess fibrin (without removing the fibrin cap when applicable), the polymer template was dissolved with two 24 hour washes in a 90% dichloromethane/10% hexanes solution followed by a 24h acetone wash on an orbital shaker at room

temperature. Scaffolds were treated with 100% ethanol rinses for 1 week before rehydration with a graded ethanol series into sterile phosphate-buffered saline (PBS).

4.3.2. *Rat Cell Sources & Culture*

For rat tri-cell constructs, neonatal rat ventricular cardiomyocytes (NRVCs), rat aortic endothelial cells (RAECs), and neonatal rat cardiac fibroblasts (NRCFs) were used. Primary NRVCs and NRCFs were isolated from 1–3 day-old Fischer 344 rats using standard protocols reported previously (87). Cardiomyocytes were separated from fibroblasts by preplating the primary cell suspension, and the two cell types were kept separately in tissue culture flasks for 2–4 days before use. Rat aortic endothelial cells (RAECs, a gift from Dr. Nicosia, VA hospital Seattle, WA) were grown in culture according to standard protocols. Rat cardiac cell media was NRC plating media used during the primary isolation protocol, described previously (129). Rat endothelial cell media was EBM-2 basal medium with EGM-2 SingleQuot supplement kit (Lonza, Walkersville, MD). Rat fibroblast media was DMEM with 10% FBS and penicillin/streptomycin (Gibco, Grand Island, NY).

4.3.3. *Human Cell Sources & Culture*

For human tri-cell constructs, human embryonic stem cell-derived cardiomyocytes (hESC-CMs, H7 line), human umbilical vein endothelial cells (HUVECs), and neonatal human dermal fibroblasts (NHDFs) or human mesenchymal stem cells (hMSCs) were used. Differentiated and expanded hESC-CMs expressing the genetically encoded calcium sensor GCaMP3 were generously provided by the Laflamme lab (University of Washington)(130). Human cardiac cell media was RPMI 1640 (no glutamine, no HEPES) with L-glutamine (200mM) and B27 serum-free supplements added (Gibco, Grand Island, NY). HUVECs (Lonza, Basel, Switzerland), NHDFs (a gift from Dr. Reinecke, University of Washington), and hMSCs (Lonza, Basel, Switzerland) were grown in culture according to standard protocols. Human endothelial

cell media was EBM-2 basal medium with EGM-2 SingleQuot supplement kit (Lonza, Walkersville, MD). Human fibroblast media was DMEM with 10% FBS and penicillin/streptomycin (Gibco, Grand Island, NY). Human mesenchymal cell media was MSCGM basal medium with MSCGM BulletKit supplement (Lonza, Walkersville, MD).

4.3.4. *Cell Pre-Treatments*

Cardiomyocytes were heat shocked at 42^{o}C for 40 min, 24 h before seeding, as this has been shown to enhance cell survival after transplantation and it was believed this treatment would be important in this system due to the stress of seeding and the high density of cells being used (87, 131). For some rat cell constructs, NRVCs were labeled with a fluorescent lipophilic tracer dye (CM-DiI, Vybrant Cell-Labeling Solutions; Molecular Probes, Eugene, OR) during heat shock treatment.

4.3.5. *Cell Seeding & Culture of Fibrin Constructs*

After rehydration into sterile PBS and incubating in seeding media for approximately 1hr, scaffolds were cut using sterile 2-mm-diameter biopsy punch tubes in which the scaffolds remained for the duration of seeding. Scaffolds constructed with a fibrin cap were cut keeping the fibrin cap at the bottom of the tube. Cells were seeded at a 4:2:1 ratio (cardiomyocytes : endothelial cells : supporting cell type) at a density of $2x10^{6}$ cells per scaffold (2mm diameter x 3mm length). Bi-cell constructs were seeded at a 2:1 ratio (cardiomyocytes : endothelial cells), keeping the number of cardiomyocytes the same as in tri-cell constructs.

For static seeding, cell mixtures were pipetted directly onto one end of the open microchannels of fibrin scaffolds after slight compression of the scaffolds, allowing the wicking action which occurred after removal of the compression to pull cells into the channels. This seeding method only allowed for one application of cells total, after which constructs sat in an incubator (37^{o}C, 5% CO_2) for 15–30 min to

allow cells to infiltrate scaffolds before pipetting 2mL of plating media around each scaffold. For centrifugation seeding, cell mixtures were pipetted into the top of the biopsy punch tubes and centrifuged into the scaffolds over 3–4 rounds of centrifugation at 7xg (200rpm) for 5 min per round, with a fresh application of cell mixture for each round (20µL cell mixture/scaffold/round). For human cell seeding, DNAse I (from bovine pancreas, Invitrogen, Grand Island, NY) was added to the seeding media at 200U/mL to help prevent cell clumping during seeding. After seeding, scaffolds were removed from the biopsy punch tubes, placed in 12-well tissue culture plates, and kept in an incubator (37^{o}C, 5% CO_2) for 0–30 min to allow cells to adhere to scaffolds before pipetting 2mL of warmed plating media around each scaffold. Cell-seeded constructs were maintained in static culture with cardiac media, which was changed every 1-2 days.

4.3.6. *Live Imaging of Fluorescent Constructs*

Live cell-seeded constructs containing CM-DiI-labeled cardiomyocytes or GCaMP3-expressing hESC-CMs were imaged under fluorescent light using a Zeiss AxioObserver microscope with Axiocam and AxioVision software (Carl Zeiss, Inc., Oberkochen, Germany) every day of culture.

4.3.7. *Sample Preparation, Histology & SEM*

Cell-seeded constructs were immersion-fixed in formalin or Methyl Carnoy's fixative at different time points from 0-14 days after seeding. Samples were processed, embedded in paraffin, and sectioned (5µm) for histology. Serial sections of samples were stained with H&E, Masson's trichrome stain, and with immunohistochemical staining using hematoxylin as the nuclear counterstain. Immunostaining was performed with primary antibodies against sarcomeric myosin (clone MF-20, Developmental Studies Hybridoma Bank), rat endothelial cell antigen (RECA-1, mouse anti-rat (1:10), AbD Serotec, Raleigh, NC), human endothelial cell marker (CD31, mouse anti-human (1:100), Dako, Carpinteria, CA), and desmin

(rabbit anti-rat (1:20), Dako Carpinteria, CA). Samples were then labeled with secondary antibodies using either a biotinylated horse anti-mouse (1:400) secondary antibody (Vector, Burlingame, CA) and developed with DAB (Sigma-Aldrich, St. Louis, MO), or with fluorescently-labeled secondary antibodies (Alexa Fluor 488 goat anti-mouse (1:100) or Alexa Fluor 594 goat anti-rabbit (1:100), Molecular Probes, Eugene, OR) and counterstained with 4',6-diamidino-2-phenylindole, dilactate (DAPI, dilactate, 300nM, Molecular Probes, Eugene, OR). For SEM imaging, scaffolds were fixed in 0.5% glutaraldehyde overnight at room temperature followed by dehydration in a graded ethanol series and critical point drying to maintain pore and channel structures. Samples were cut through the center of constructs and Au/Pd sputter-coated for 60s before imaging with an FEI (Hillsboro, OR) Sirion field-emission microscope under high vacuum conditions at an accelerating voltage of 10kV.

4.3.8. *Mechanical Stiffness Measurements of Cell-Seeded Constructs*

Stiffness changes of cell-seeded constructs were measured over 10 days in culture using methods described in Chapter 2. Briefly, areas of cell-seeded constructs were cut into strips (0.2-0.4mm diameter x 1.0mm length) and mounted with aluminum foil T-clips between a force transducer and a servomotor. Step changes in length (4%-24% of scaffold strip length) and resulting changes in tension were measured and recorded by a custom LabVIEW software program. Resulting tension (mN) and force normalized to cross-sectional area (mm^2) were plotted against percent length change, and the slope of the resulting linear regression line was used as a measure of stiffness in kPa. Scaffolds were measured at different time points (0, 3, 6, & 10 days) after incubation at 37^{o}C in culture medium.

4.3.9. *Statistical Analysis*

All values are reported as mean ± S.E.M. Statistical significance between time points for scaffold stiffness measurements were tested using a Student's t-test ($\alpha = 0.05$). Differences at a p-value < 0.05 were considered statistically significant.

4.4. Results

4.4.1. *Static vs. Centrifugation Seeding*

Static seeding of constructs resulted in the majority of cells remaining in a large clump on the seeding end of constructs, with little to no cell penetration into the interior of scaffolds over time in culture (**Figure 4.1a, b**). In contrast, constructs that were successfully seeded with centrifugation resulted in cells seeded at a significantly greater depth into construct channels (**Figure 4.1c, d**), indicating the necessity for a dynamic seeding method for high density cell seeding of the microtemplated scaffolds. These results were obtained from live fluorescent imaging of GCaMP3 cardiomyocytes and verified with histological analysis.

4.4.2. *Rat Tri-Cell Seeding*

Cell seeding of scaffolds with the rat tri-cell mixture (NRVCs, RAECs or HUVECs, and NRCFs) via centrifugation resulted in constructs containing viable cells, as indicated by images of live fluorescently labeled (CM-DiI) cardiomyocytes 2 hours after seeding into scaffolds (**Figure 4.2a**). Histological analysis showed viable cells seeded through the width of the constructs (**Figure 4.2b**) and down the length of the microchannels (**Figure 4.2c**) in 8-day constructs. Cardiomyocytes were seen contracting within

microchannels 2–4 days after seeding, as were non-seeded cardiomyocytes on the bottom of culture dishes (data not shown), demonstrating cardiac cell survival and viability. Constructs seeded with only cardiomyocytes or endothelial cells resulted in poor cell survival (data not shown). Histological analysis of tri-cell constructs indicated cardiomyocytes (sarcomeric myosin, MF-20+ or desmin+) survived seeding and were localized in scaffold channels (**Figure 4.2a, d, g**), and that they elongated within channels over time in culture (**Figure 4.2g**). This analysis suggests that the cardiomyocytes may be beginning to form columnar structures through the construct parallel to the microchannel orientation. Endothelial cells (RECA-1+ or CD31+) also survived seeding, became elongated within channels, and consistently formed lumen structures within and aligned parallel with channels, as indicated by histological staining both in cross-sectional (**Figure 4.2e**) and in longitudinal sections (**Figure 4.2f, h**). Fluorescent double-staining (desmin & CD31, **Figure 4.2g-i**) of a tri-cell seeded scaffold in the longitudinal section confirmed these cells were co-localized and aligned within scaffold channels.

4.4.3. *Human Tri-Cell Seeding*

Seeding of fibrin constructs with the human tri-cell mixture (hESC-CMs, HUVECs, and hMSCs or NDHFs) with centrifugation resulted in viable cells within construct channels (**Figure 4.3a, b**). Cardiomyocyte viability before and after seeding was also verified with fluorescent imaging of live cell-seeded constructs containing GCaMP3 cardiomyocytes which typically began contracting within 2-4 days of culture. As was seen with rat cell constructs, cardiomyocytes (sarcomeric myosin, MF-20+) (**Figure 4.3d**) and endothelial cells (CD31+) (**Figure 4.3c**) were located within construct channels, and endothelial cells readily formed lumen structures, seen in both cross-sectional and longitudinal sections (**Figure 4.4a, c**). In 7 day human tri-cell constructs seeded with MSCs, these lumen structures were surrounded by SMA+ cells (**Figure 4.4b, d**), indicating the fibrin scaffolds were promoting further pre-vascular network development. Taken together, the results from both rat and human tri-cell seeding

experiments indicate the scaffold microarchitecture promoted the development of a prevascular cell network adjacent to columns of elongated and aligned cardiomyocytes throughout the parallel construct channels, mimicking the cell orientation present in native cardiac tissue.

4.4.4. *Bi-Cell vs. Tri-Cell Seeding*

Constructs seeded with human bi-cell or tri-cell mixtures (containing NDHFs) were assessed with live fluorescent imaging of the GCaMP3 cardiomyocytes over 1-2 weeks in culture. Areas of fluorescent cardiomyocytes were seen throughout construct channels in both bi-cell and tri-cell constructs after 1-2 days of culture, indicating relatively even dispersion of cardiomyocytes after seeding (**Figure 4.5a, b, e, f**). However, significant differences in cardiomyocyte organization were seen after longer culture periods. In bi-cell constructs, non-synchronous islands of cells remained separated and never synchronized during the 2 week observation period (**Figure 4.5a-d**). In contrast, tri-cell constructs showed increasing synchronicity over time in culture, with synchronous lines of fluorescent signal within construct channels as early as day 2, and physical contraction along the longitudinal axis of scaffolds after 4-5 days (**Figure 4.5e-h**). While sufficient experimental replicates could not be analyzed due to issues with consistent seeding via centrifugation (discussed in further detail in Chapter 5), these results potentially indicate a vital role for a third supporting cell type such as a fibroblast in cardiomyocyte coupling and the development of synchronously contracting cardiac constructs.

4.4.5. *Mechanical Stiffness Measurements of Cell-Seeded Constructs*

Scaffolds seeded with the rat tri-cell mixture were mechanically tested over 10 days to determine the effect of cell seeding on scaffold degradation. Stiffness of day 0 unseeded scaffolds was used as the baseline stiffness value. In contrast to the *in vitro* degradation profile of acellular scaffolds (discussed in Chapter 2), the stiffness of cell-seeded scaffolds did not drop initially and instead

significantly increased between days 6 and 10, up to 209% ± 32% ($p < 0.05$) of initial stiffness (**Figure 4.6a**). Masson's trichrome staining of 8 day constructs (**Figure 4.6b**) and SEM imaging of 3 and 6 day constructs (**Figure 4.6c-e**) confirmed the presence of newly deposited collagen by cells within construct channels, providing a potential explanation of the observed increase in construct stiffness during culture.

4.5. Discussion

For tissue engineered cardiac constructs, it is essential for grafted cardiomyocytes within a scaffold to survive after implantation in infarcted myocardium and become rapidly vascularized by the host tissue. By using fibrin for the scaffold material and by developing a microtemplated architecture to promote the development of a prevascular network within constructs *in vitro*, it is hypothesized that these constructs will encourage rapid anastomosis of the graft with host vasculature and improve the overall chances of graft survival in future implant studies. The design of the microtemplated scaffold architecture promoted cell survival and organization by allowing seeding into parallel microchannels in order to more closely resemble the organized cellular alignment found *in vivo*. The microporous network consisting of 27μm pores that surround the channels was designed to aid in exchange of nutrients and waste removal, and may also elicit further host angiogenesis and a weaker or more pro-healing inflammatory response (discussed in Chapter 3) when constructs are implanted into hearts (11, 20, 132-134). In addition, this architecture allowed for a greater extent of cell seeding, alignment, and organization than other traditional methods of seeding cells into biomaterial scaffolds.

Fibrin constructs seeded with cardiomyocytes alone showed poor cell survival in this system. Conversely, within 8 days of *in vitro* culture the tri-cell constructs consistently developed endothelial

cell-lined lumen structures within scaffold microchannels, which were co-localized with viable cardiomyocytes oriented parallel to scaffold channels. In addition, seeded cells began depositing their own ECM in the form of collagen within construct microchannels during this time period, as indicated by histological and SEM analysis, resulting in increased construct stiffness over 10 days *in vitro*. This is a desirable attribute for a degradable cellular construct, as the newly deposited ECM will provide structural support to the cells and assist in maturation of the tissue as the scaffold is degraded. The rate of scaffold degradation and ECM deposition should be balanced to prevent transfer to the newly deposited matrix too soon.

Both static and centrifugation methods were investigated for seeding of the high density tri-cell mixture into the microtemplated fibrin scaffolds. While static seeding resulted in little to no cell penetration into the interior regions of scaffolds, constructs that were successfully seeded with centrifugation typically showed greater cell seeding deeper into construct channels. Successful seeding of constructs required the optimization of scaffold, cell, and seeding protocol parameters, including scaffold and cell pre-treatments, cell numbers and ratios, centrifugation speeds, and culture conditions. While the optimal set of parameters established by these experiments did result in successful seeding, the efficiency of seeding in terms of the number of successfully seeded constructs remained fairly low (estimated < 20%). In addition, with the centrifugation method the distribution and overall seeding density within constructs remained sub-optimal. Therefore, it was determined that a different form of dynamic seeding developed specifically for these microtemplated fibrin scaffolds that would improve cell seeding efficiency, distribution and density within scaffold constructs was needed (Chapter 5).

Table 4.1. Cell seeding optimization parameters considered for tri-cell seeding of microtemplated fibrin scaffolds.

Scaffold Parameters	
Scaffold construction	+/- Fibrin cap
Scaffold pre-treatment	PBS, FBS, or seeding media
Scaffold cutting technique	Hydrated vs. partially dehydrated
Cell Parameters	
Total cell number	1-4x10^6 cells/scaffold
Cell ratios (CMs:ECs:FBs)	1:1:1, 2:1:1, 2:2:1, 4:2:1
Cell pre-treatment	+/- Heat shock treatment
Seeding Protocol Parameters	
Seeding method	Static vs. centrifugation
Centrifugation speed	200-1000rpm
Direction of seeding	Unidirectional vs. bidirectional
Seeding media	CM media only vs. 50/50 mix CM & EC media, +/- DNAse
Plating media	CM media only vs. 50/50 mix CM & EC media

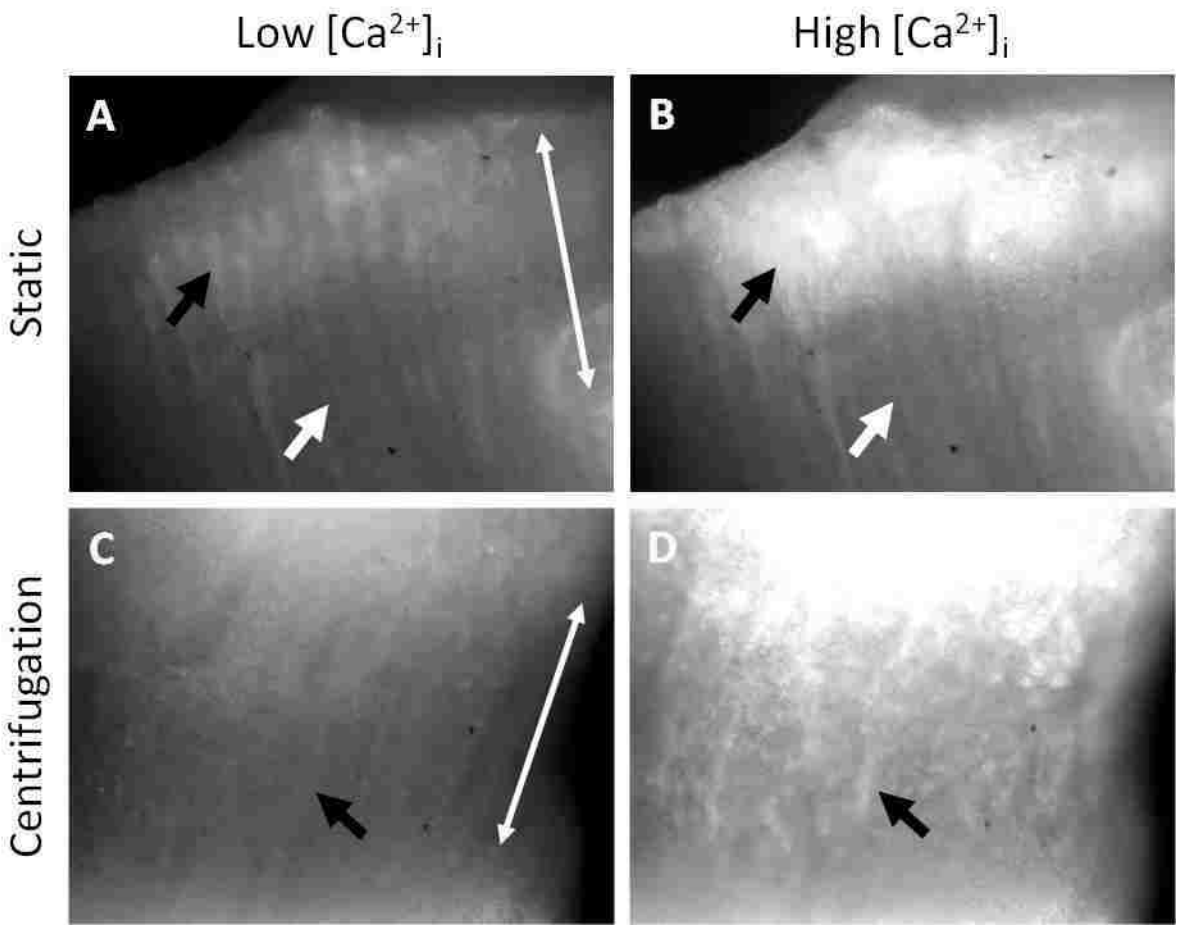

Figure 4.1. Static vs. centrifugation seeding of fibrin scaffolds. Human tri-cell seeded constructs with GCaMP3 cardiomyocytes 2 days after seeding showing rhythmic GCaMP3 signal in **(a, c)** low intracellular calcium ($[Ca^{2+}]_i$) and **(b, d)** high $[Ca^{2+}]_i$ states. **(a, b)** Static seeding resulted in the formation of a cell clump on the seeding end of the scaffold (black arrows), with little to no cell penetration into the interior of the construct (white arrows). **(c, d)** Centrifugation seeding resulted in cell seeding deeper into the interior of scaffolds (black arrows). White double-headed arrows in **(a, c)** indicate the direction of microchannel alignment. 5x magnification.

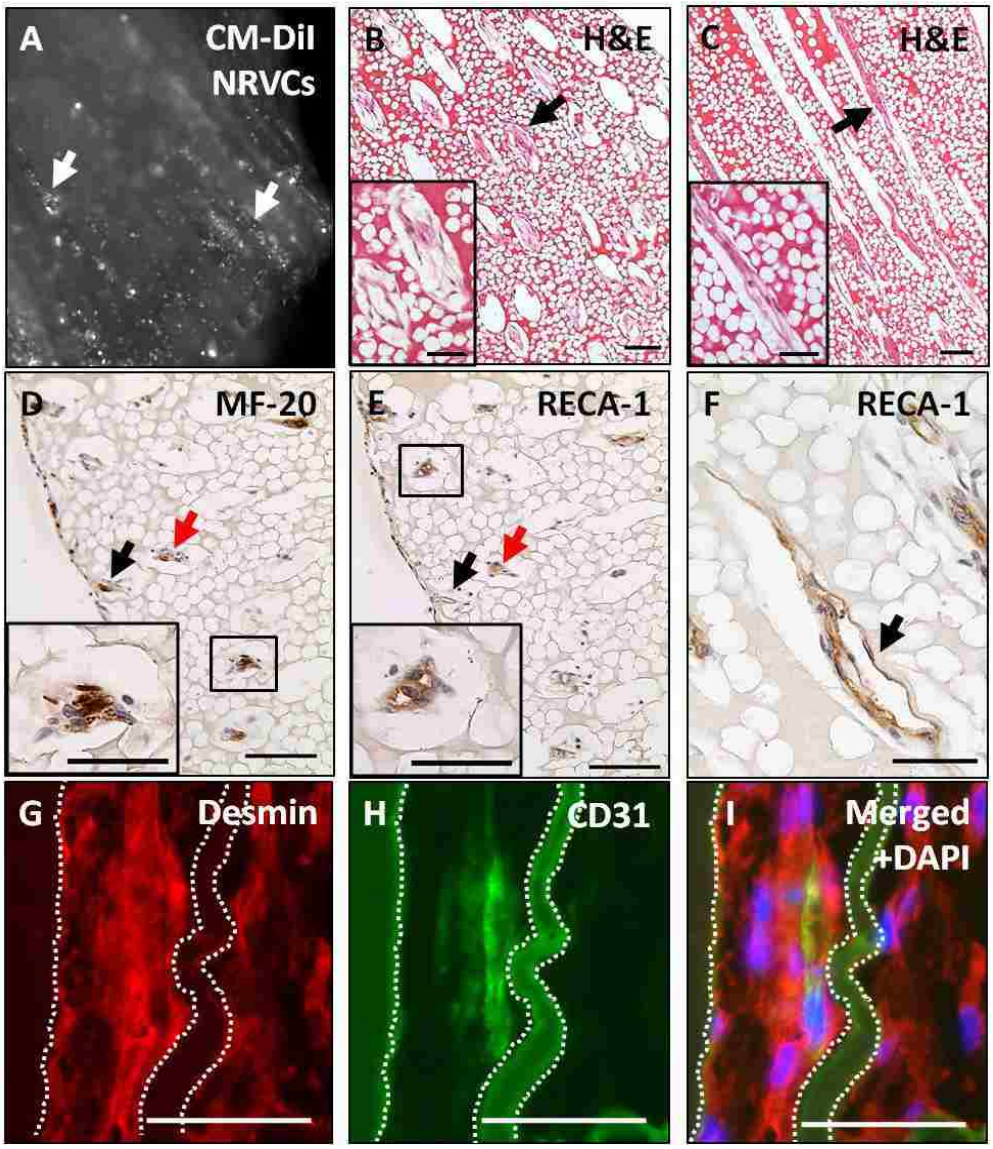

Figure 4.2. Rat tri-cell seeding of fibrin scaffolds. **(a)** Scaffold 2 hours after seeding showing fluorescently labeled (CM-DiI) cardiomyocytes (NRVCs) seeded in microchannels (white arrows). Histological analysis of 8 day samples cut in **(b, d, e)** cross-section and **(c, f-i)** longitudinal section. **(b, c)** H&E staining showing viable cells within construct channels (black arrows). **(d)** NRVCs (MF-20+, sarcomeric myosin) and **(e)** endothelial cells (RECA-1+) co-localized within channels (representative channels shown by black and red arrows). **(e, f)** Endothelial cells formed lumen structures within channels (black arrows). Fluorescent double-staining with **(g)** desmin and **(h)** CD31 confirming cardiomyocytes and endothelial cells are co-localized and elongated within scaffold channels (channel walls outlined with dotted lines, fibrin material is autofluorescent). **(i)** Merged images with DAPI nuclear stain. **(a)** 5x magnification. Scale bars in **(b-e)** = 100µm (50µm in insets), scale bars in **(f-i)** = 50µm.

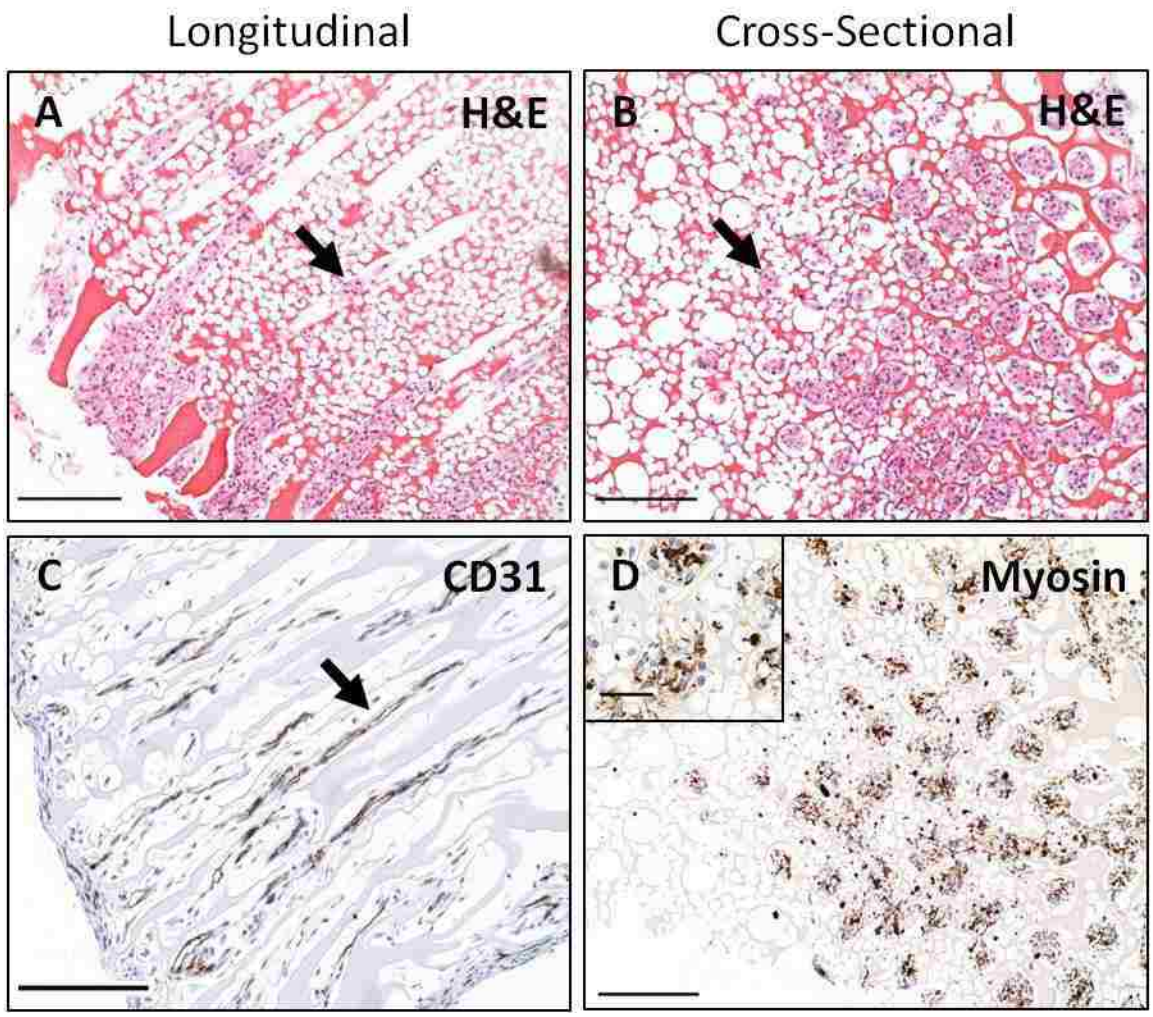

Figure 4.3. Human tri-cell seeding of fibrin scaffolds. Histological analysis of constructs 8 days after seeding shown in **(a, c)** longitudinal section and **(b, d)** cross-section. **(a, b)** H&E staining showing viable cells within construct channels (black arrows). **(c)** Endothelial cells (CD31+) formed lumen structures within channels (black arrow), and **(d)** viable cardiomyocytes were found throughout seeded channels. Scale bars = 200µm (50µm in inset).

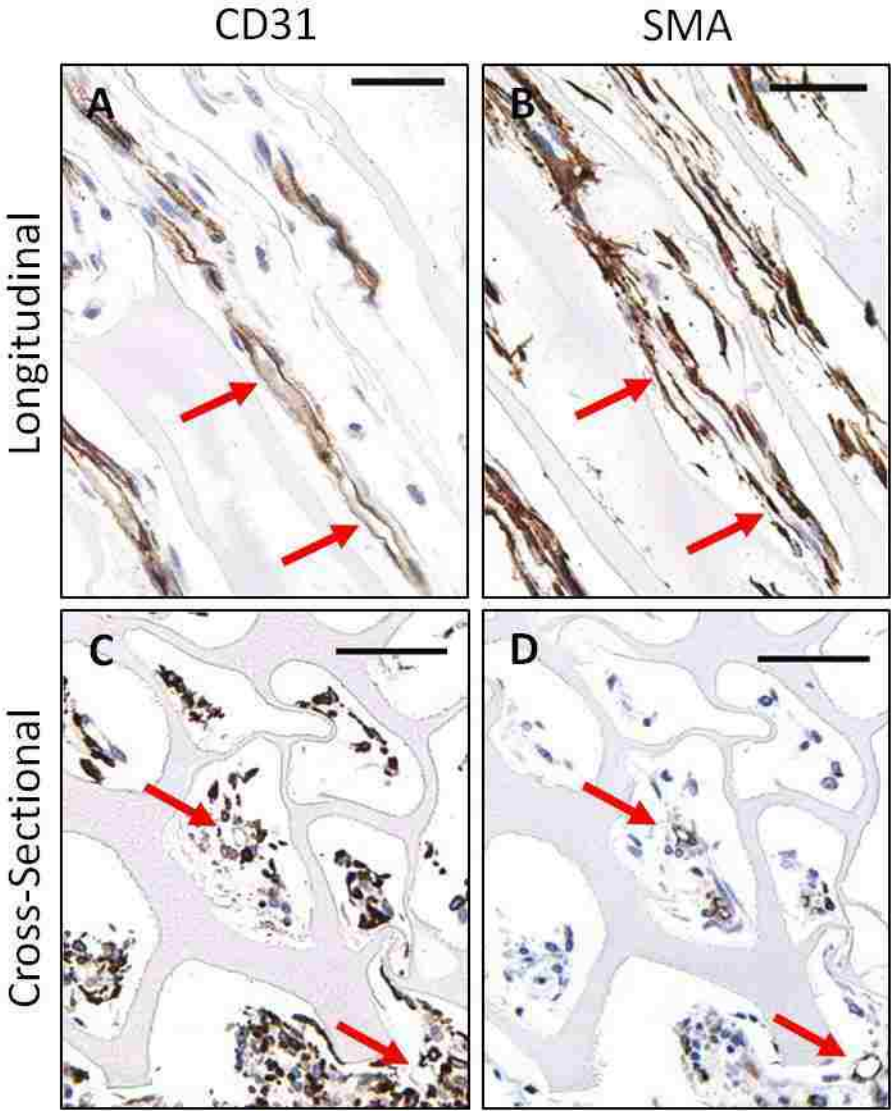

Figure 4.4. Pre-vascular network formation in human tri-cell scaffolds. Histological analysis of constructs 7 days after seeding shown in **(a, b)** longitudinal section and **(c, d)** cross-section. **(a, c)** Endothelial cells (CD31+) forming lumen structures within construct channels were surrounded by **(b, d)** cells staining for smooth muscle actin (SMA+), as indicated by red arrows. Scale bars = 50µm.

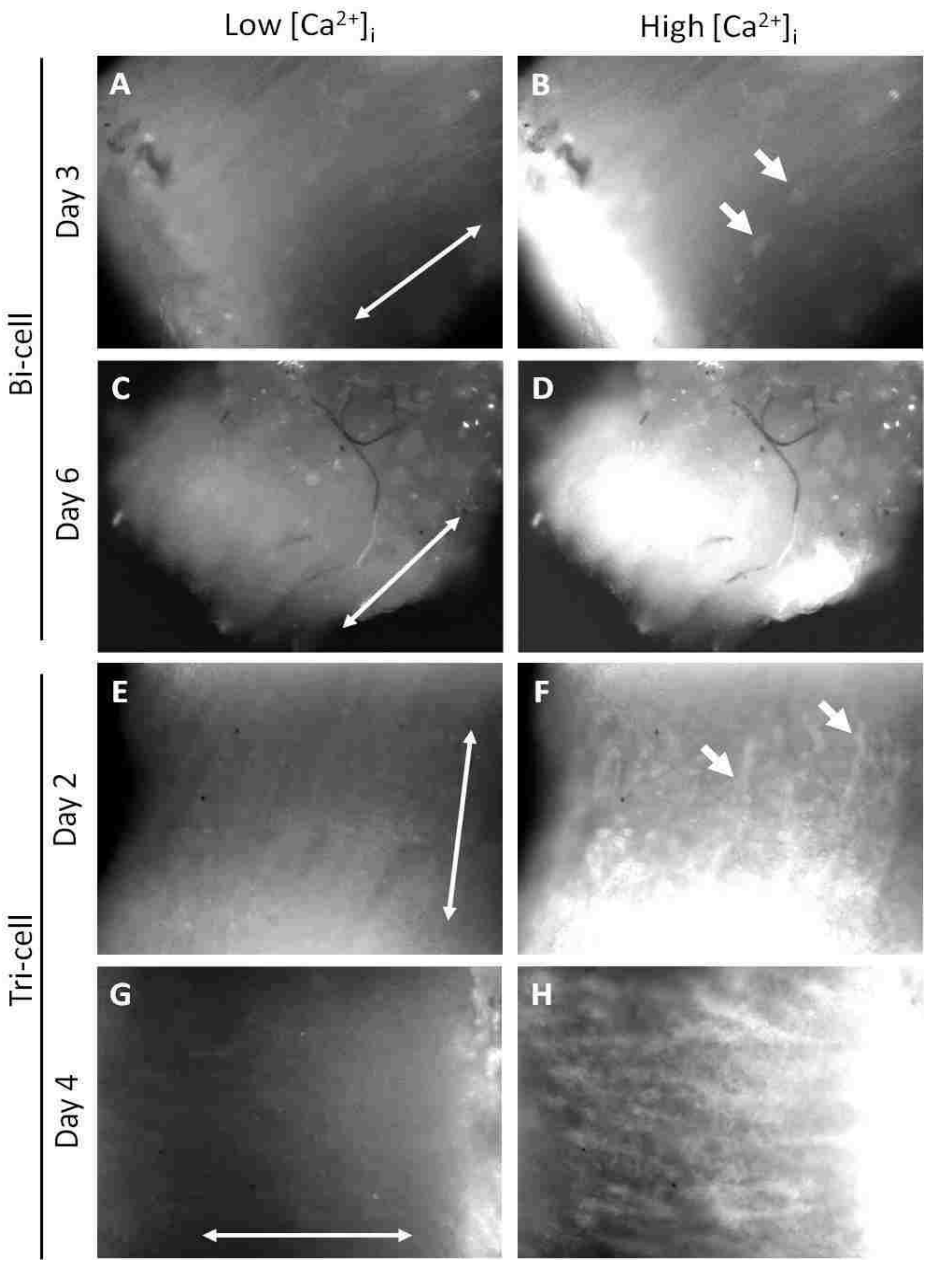

Figure 4.5. Bi-cell vs. tri-cell seeding of fibrin scaffolds. Human cell constructs with GCaMP3 cardiomyocytes showing rhythmic GCaMP3 signal in **(a, c, e, g)** low intracellular calcium ($[Ca^{2+}]_i$) and **(b, d, f, h)** high $[Ca^{2+}]_i$ states. Bi-cell seeded constructs after **(a, b)** 3 days and **(c, d)** 6 days of culture showing isolated islands of viable cardiomyocytes (white arrows in **(b)**) which remained isolated for the duration of the 2 week observation period. Tri-cell seeded constructs after **(e, f)** 2 days and **(g, h)** 4 days of culture showing synchronous lines of contracting cardiomyocytes (white arrows in **(f)**), which resulted in physical contraction of the scaffold in the direction of microchannel alignment. White double-headed arrows in **(a, c, e, g)** indicate the direction of microchannel alignment. 5x magnification.

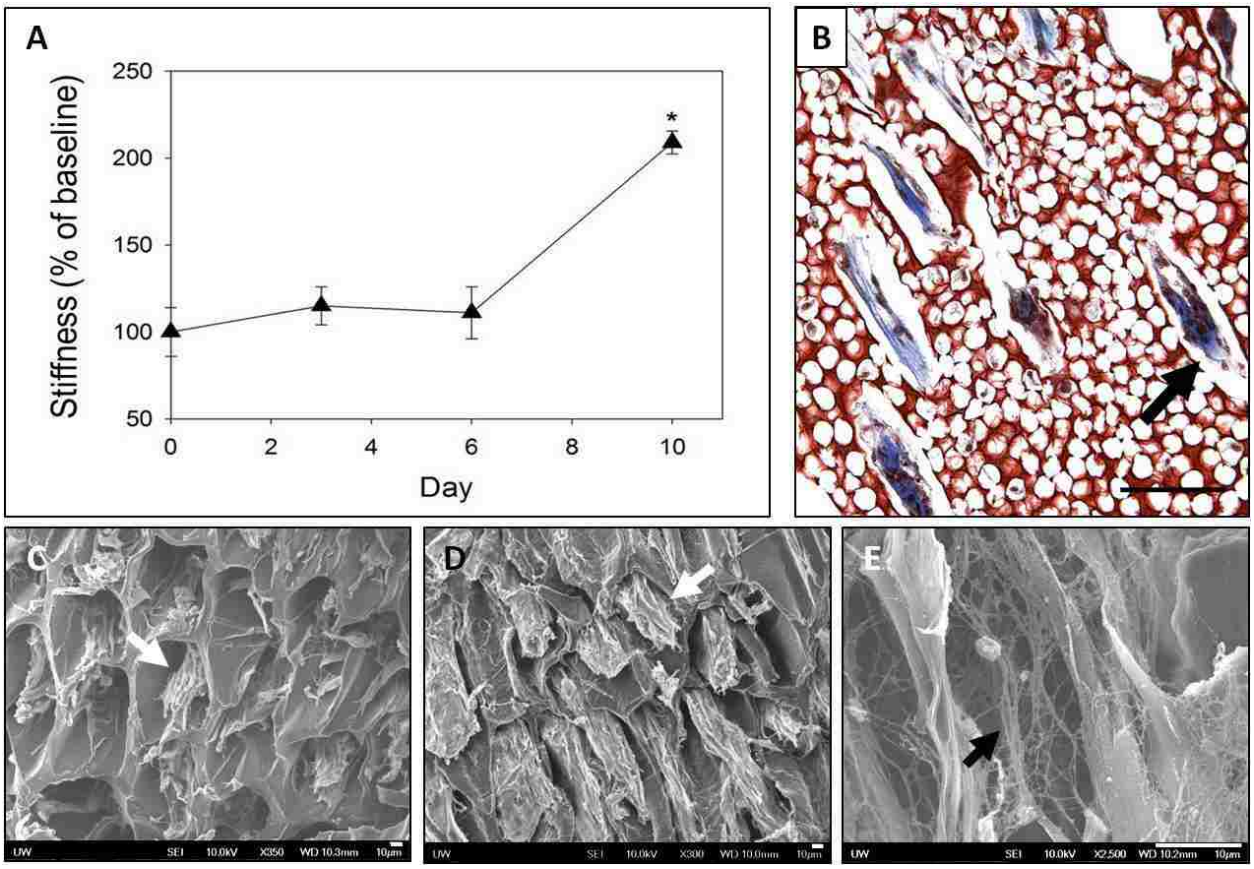

Figure 4.6. Tri-cell seeded construct mechanical properties. **(a)** Change in construct stiffness (% of baseline, Day 0 stiffness) of rat tri-cell seeded scaffolds over 10 days *in vitro*. ***** Statistically significant difference from Day 6 time point (Student's t-test, $p < 0.05$). **(b)** Masson's trichrome staining of 8 day cell-seeded construct indicating newly deposited collagen (black arrow) by cells within channels. SEM imaging of cell-seeded constructs after **(c, e)** 3 days and **(d)** 6 days of culture indicating cell seeding within construct channels (white arrows), with **(e)** fibrils of ECM deposition from seeded cells (black arrow). Scale bar in **(b)** = 100µm. Scale bars in **(c-e)** = 10µm.

Chapter 5:

Development of a Perfusion System for Improvement of Microtemplated Fibrin Scaffold Cell-Seeding

5.1. Introduction

The construction of the microtemplated fibrin scaffolds used in this project was done using modified techniques for templating high density fibrin in a microporous architecture, developed by Linnes *et al.*, and methods to construct a microchanneled and microporous architecture in pHEMA scaffolds, developed by Madden *et al.* (10, 11). These pHEMA constructs were seeded with cardiomyocytes using centrifugation to seed cells within the scaffold channels. Because the microtemplated fibrin scaffolds used for this project were constructed with the same architecture as these pHEMA scaffolds, centrifugation was the main method of cell-seeding utilized, as described in detail in Chapter 4. While it was demonstrated that these fibrin scaffolds could support cell seeding, survival, and organization *in vitro*, the efficiency of seeding in terms of the number of successfully seeded constructs and the overall distribution of cells within constructs was very poor with the centrifugation method. Despite continued optimization, it is estimated less than 20% of attempted scaffolds were actually seeded, and for those that were, cells were very often confined to one half of the construct (**Figure 5.1**). This inefficiency of seeding was most likely due to the fibrin material properties, as it is a much more compliant material than pHEMA and cannot withstand high centrifugal forces,

causing the fibrin scaffold to collapse during centrifugation and thus preventing efficient cell seeding. Because of these material properties, the centrifugation speeds used for the fibrin scaffolds needed to be much lower than those used for pHEMA constructs (11, 96), which may be another limiting factor. Therefore, it was determined that a new method of seeding was necessary in order to improve efficiency, distribution, and density of cell seeding within the microtemplated fibrin scaffolds.

Achieving high density and evenly distributed cell seeding within biomaterial scaffolds continues to be one of the major hurdles in tissue engineering (14, 135). Many different methods of cell seeding have been developed for various types of scaffold constructs, each with their own set of advantages and disadvantages. By far the most common method is passive seeding, in which a cell suspension is added to the surface of a scaffold, and seeding relies on gravity and cell migration into the interior regions of the construct (135-137). Variations on this method have included the use of adhesive coatings or the incorporation of cell-matrix cues within the scaffold material to promote increased cell penetration (137-139). While passive cell seeding is relatively simple, it is highly inefficient (10-25% of cells successfully seeded (136)) and there are major issues with achieving uniform cell distributions throughout the entirety of the constructs, especially when attempting to seed larger scaffolds.

To address these issues, many groups have developed dynamic methods of cell-seeding which are often customized for specific scaffold architectures and/or cell populations, with the goal of increasing the efficiency, uniformity, and reliability of cell seeding (135). For example, rotational seeding systems have been used to seed cardiac cells into porous alginate scaffolds, resulting in uniformly distributed cell seeding with 60-90% efficiency (14). These systems typically involve rotation of scaffolds submerged in a cell suspension, or incubation of scaffolds within a continually mixed suspension of cells, such as a spinner flask. Seeding efficiencies with this type of system have been reported to be anywhere from 38-90%, depending mainly on the rotational speeds and duration of seeding used (14, 136, 140).

Others have used vacuum pressure to force cells into scaffold pores, which has the advantages of being fairly efficient (60-90%) and rapid, but the effects on cell morphology and viability have not yet been fully established (141-143). Other methods of cell seeding include the use of electrostatic charging of scaffold surfaces to enhance cell adhesion to the material (137, 144), and the application of magnetic fields across scaffolds with the use of magnetic nanoparticles either within or on the surface of cells to be seeded (145-149). While these have been shown to be rapid and efficient methods of promoting cell penetration of scaffolds, they are not applicable to all tissue engineering constructs and the potential for long-term adverse effects on the cells is high.

For these reasons, many groups have investigated the use of perfusion to seed cells into scaffold constructs. Systems are often tailored specifically to particular scaffold architectures and dimensions, and can include pulsatile flow, the ability to change the direction of flow during seeding, and are sometimes built as bioreactors intended for construct incubation after the conclusion of seeding (150-154). Perfusion seeding has been shown to be an effective method of evenly distributing cells throughout constructs at higher densities than can be achieved with more static seeding methods (44, 151, 154). When C2C12 cells were seeded into collagen sponges using perfusion, a cell density comparable to native tissues and a spatially uniform distribution of cells was achieved (154). Similar results were shown with perfusion seeding of neonatal rat cardiomyocytes into channeled PGS scaffolds (44), and when perfusion was used to seed smooth muscle and endothelial cells into a porous PGA scaffold for a small diameter vascular graft (142). These studies demonstrate the potential for high efficiency seeding of larger scaffolds with the use of perfusion systems.

It was therefore hypothesized that a perfusion seeding system could be used to seed the microtemplated fibrin scaffolds with greater efficiency, more evenly distributed cells, and an overall higher density of cell seeding. The perfusion system would need to be designed for seeding fibrin

scaffolds of specific sizes (for example, 2mm diameter scaffolds like those used for centrifugation seeding), be able to maintain scaffold orientation during seeding in order to ensure scaffold channels are aligned with the direction of fluid flow, and be temperature controlled. Additionally, the seeding protocol would need to be optimized for cell survival, distribution, and efficiency of seeding.

5.2. Perfusion Seeding System Design

5.2.1. *Microtemplated Scaffold Void Fraction Estimation*

In order to make estimations of the shear stress cells would see during perfusion flow through the microtemplated scaffolds, it was first necessary to calculate the estimated void fraction of the scaffolds. This estimation was done for a scaffold with a height ($H_{scaffold}$) of 3mm and radius ($r_{scaffold}$) of 1mm, with microchannel radii ($r_{channel}$) of 30µm. The volume of the scaffold ($V_{scaffold}$) was therefore 9.4mm^3. Scaffold void fraction ($\varepsilon_{scaffold}$) was calculated as the sum of microchannel void fraction ($\varepsilon_{channels}$) and micropore void fraction (ε_{pores}). The number of microchannels (N) in a scaffold of these dimensions was calculated using **Equation A**:

$$N = \frac{\pi r_{scaffold}^2}{\pi r_{channel}^2} = \frac{\pi\,(1mm)^2}{\pi(0.06mm)^2} = 278 \qquad (\boldsymbol{Eq.A})$$

Void fraction of the microchannels was then calculated using **Equation B**:

$$\varepsilon_{channels} = \pi r_{channel}^2 H_{scaffold} N = \pi(0.03mm)^2(3mm)(278) = 2.36mm^3 \qquad (\boldsymbol{Eq.B})$$

The void fraction of the micropores was calculated using the previously determined porosity that results from the microporous templating technique (Linnes *et al.* 2007, approximately 74% overall porosity)(10) and **Equation C**:

$$\varepsilon_{pores} = (\%\, porosity)\left(V_{scaffold} - \varepsilon_{channels}\right)$$

$$= (74\%)(9.4mm^3 - 2.36mm^3) = 5.21mm^3 \qquad (\boldsymbol{Eq.C})$$

The void fraction of the microtemplated fibrin scaffolds ($\varepsilon_{scaffold}$) was therefore calculated to be approximately 80.5%.

5.2.2. *Shear Stress Estimation of Flow Through Scaffolds*

In order to estimate the amount of shear stress exerted on cells as they are perfused through the microtemplated fibrin scaffolds, it was first necessary to calculate the average fluid velocity through the voids of the scaffold (i.e., the channels and pores). The same scaffold dimensions were used as in the previous section. For the purposes of these calculations, the voids of the scaffold were assumed to be tortuous and follow a path length equal to 1.5 times the scaffold height (1.5*H)[1]. Average fluid velocity through the scaffold (U) was calculated for multiple volumetric flow rates (Q, shown in **Table 5.1**) using **Equation D**:

$$U = \frac{(1.5H)Q}{\varepsilon V_{scaffold}} \qquad (\boldsymbol{Eq.D})$$

Shear stress (τ_w) estimations were made assuming Poiseuille flow through the scaffold. The viscosity of the perfused solution (η) was assumed to be equal to that of water at 37°C (0.00069Pa·s)

[1] The path length of a tortuous porous scaffold would normally be estimated to be twice the scaffold height (2H), while the path length of the microchannels is equal to the scaffold height (1H). Therefore, an average of these two path lengths was used as the path length of the microtemplated scaffolds (1.5H).

(153), and an average of the pore and channel radii was used as the radius of the scaffold voids (R_c = 21.75µm)[2]. Shear stress was then calculated using **Equation E**:

$$\tau_w = \eta \frac{4U}{R_c} \qquad (\boldsymbol{Eq.E})$$

The resulting average fluid velocity (mL/min·mm^2) and shear stress (dyn/cm^2) estimates for each corresponding volumetric flow rate (mL/min) are shown in **Table 5.1**.

5.2.3. *Perfusion Seeding System Considerations & Design Iterations*

A perfusion seeding system for the microtemplated fibrin scaffolds was developed to be a method of improving seeding efficiency, seeded cell distribution, and cell density within these scaffolds. Considerations for the design of this system included biocompatibility and ability to sterilize all components that would come in contact with scaffolds and cells, the ability to control flow rates of the cell solutions through scaffolds, the ability to easily reverse flow direction, proper dimensions of tubing and components to ensure evenly distributed fluid flow through scaffolds while retaining scaffolds within a seeding chamber, the ability to remove air bubbles from the system, and a system designed for easy assembly and disassembly in a sterile environment so as not to disturb seeded constructs during removal.

The first three versions of the perfusion seeding loop were designed as open-ended systems containing a single seeding chamber (i.e., one scaffold could be seeded per loop), with the tubing loop connected to a peristaltic pump and the open ends of the loop placed in a cell reservoir (**Figure 5.2**). The perfusion loop and pump were kept in a 37^{o}C oven for the duration of seeding, which was approximately 30-60min total with the direction of flow changed every 15min. The major issue encountered with these

[2] Microchannel diameter is 60µm and the diameter of the micropores is 27µm, therefore an average of these two radii is used for R_c.

designs was the formation of bubbles in the tubing lines during the seeding protocol, and the lack of a means to de-bubble the system when needed. In addition, the open-ended tubing lines submerged in the cell reservoir caused a large degree of bubbling within this tube, which was detrimental to cell survival during seeding. Other issues included cell pellet formation within the reservoir resulting in fewer cells flowing through the scaffolds, contamination of the system during seeding due to the open-ended design which required parafilm to close the connection between the tubing ends and the cell reservoir, and difficulties with keeping the tubing system in an upright position to ensure proper fluid flow through the scaffolds while minimizing bubble formation.

To address these issues, the perfusion seeding system was redesigned based on a perfusion bioreactor system developed by Radisic *et al*. for the development of thick cardiac tissue constructs (154), which formed the basis for system versions 4-6. In these versions, the perfusion system was designed as a closed-loop system, which could be completely assembled and sealed off in a sterile environment, therefore ensuring sterility during the seeding protocol. Each perfusion loop now contained two seeding chambers, an injection site for delivery of media and cell suspensions, and a method of de-bubbling the lines as needed. By removing the cell reservoir from the system, these designs ensured the majority of cells would be flowed through scaffolds, and minimized the formation of bubbles during seeding. In addition, the newly designed perfusion loop could be connected to a peristaltic pump on top of an incubator, and the loop lines containing cells and scaffolds could be kept in an upright position inside the incubator. The three different versions of this closed-loop system were design iterations to address issues with tubing and connector dimensions which allowed leaks and movement of scaffolds out of the seeding chambers. Version 6 of the perfusion loop design is described by **Figure 5.3** and **Table 5.2**.

5.3. Materials & Methods

5.3.1. *Perfusion Seeding System Components & Assembly*

The perfusion seeding system was designed for use with a Gilson Minipuls 3 Peristaltic Pump (Gilson, Middleton, WI). All system components are described in **Table 5.2**. Gilson PVC tubing with 3.16mm ID (F117969) and 1.02mm ID (F117938, calibrated) were used (Gilson, Middleton, WI). Thermo Scientific Nalgene 180 PVC tubing with 3/32" ID x 5/32" OD x 1/32" wall thickness (Thermo Scientific #8000-0006) was used (Thermo Fisher Scientific, Waltham, MA). All tubing components were autoclavable. The 3-way stopcocks with Luer locks (SC3LL) were obtained from SAI Infusion Technologies (SAI Infusion Technologies, Libertyville, IL), and were sterilized with ETO. The IN-4000 Intermittent Injection Site to Male Luer Lock made of polyisoprene with an ABS acrylic body (VPS3901074N), and the Male Luer Integral Lock Ring to 500 series barb 1/16" (1.6mm) ID tubing made of white nylon (MTLL004-1) were from Value Plastics (Value Plastics, Fort Collins, CO), and were sterilized with ETO (though the white nylon can also be autoclaved). The 0.2µm syringe filters were from VWR International (Radnor, PA). The 1mL NORM-JECT syringes used to make Part J were from Henke Sass Wolf (Tuttlingen, Germany), and were cut to fit around Part A using a razor blade.

Each component was assigned a letter designation (**Figure 5.3**), and all parts were sterilized or came in sterile packaging before use except Part I and the two Part D components connected to each end of Part I, as these stayed connected to the peristaltic pump outside of the incubator and did not come in contact with any cell solution during the seeding procedure. Each sterile tubing component was rinsed with sterile dIH_20, and then Parts A-H were assembled in a sterile environment before each seeding experiment. Part E served as the seeding chamber, and scaffolds were inserted before attachment of Part E to the rest of the loop. By attaching Part H (sterile syringe filter) to close the ends of the open tubing system formed by Parts A-G, this portion of the perfusion loop remained sterile

during transfers between the tissue culture hood and incubator. When moving the sterile perfusion loop to the incubator, it was connected to the pump and Part J was attached at the necessary location along Part A to prevent collapse of this tubing component in the door seal of the incubator.

5.3.2. *Determination of Desirable Flow Rates*

Once version 6 of the perfusion system was designed and assembled, the flow rate through the system was determined by measuring the volume of water that was pumped through the perfusion loop each minute (mL/min) at different RPM settings on the Gilson peristaltic pump. It was found that the flow rate corresponded linearly with the RPM settings. Therefore, the range of RPM settings to test during the seeding protocol optimization was determined by the corresponding shear stress seen by cells (dyn/cm^2) calculated for different flow rates in the above section (**Table 5.1 & Figure 5.4**), with the goal of keeping the flow rates high enough to achieve cell seeding while maintaining shear stress below 2.4dyn/cm^2 to avoid cell damage (154).

5.3.3. *Fibrin Scaffold Construction*

Scaffold templates and fibrin scaffolds were constructed as described in Chapter 2. Briefly, the polymer templates were infiltrated with a 200mg/mL fibrinogen solution (bovine fibrinogen Type 1-S, Sigma-Aldrich, St. Louis, MO; in 0.9% NaCl) via centrifugation. The fibrinogen solution was pre-warmed in a 37^{o}C water bath for 45-90minutes to allow the fibrinogen to completely dissolve. After centrifuging the fibrinogen solution into the templates and after scraping all surfaces to remove excess fibrinogen, concentrated thrombin solution (13.25U/mL thrombin, Sigma-Aldrich, St. Louis, MO; 8.3mM $CaCl_2$; DMEM, Gibco, Grand Island, NY) warmed to 37^{o}C was used to polymerize the fibrinogen into fibrin around the polymer template overnight at room temperature. After scraping the exterior of the scaffolds to remove excess fibrin, the polymer template was dissolved with two 24 hour washes in a 90%

dichloromethane/10% hexanes solution followed by a 24h acetone wash on an orbital shaker at room temperature. Scaffolds were treated with 100% ethanol rinses for 1 week before rehydration with a graded ethanol series into sterile phosphate-buffered saline (PBS).

5.3.4. *Cell Culture*

Human umbilical vein endothelial cells (HUVECs, Lonza, Basel, Switzerland) were grown in culture according to standard protocols. HUVECs were fluorescently labeled 24 hours prior to seeding by incubating for 20min with a fluorescent lipophilic tracer dye (CM-DiI, Vybrant Cell-Labeling Solutions; Molecular Probes, Eugene, OR) at 5µL/mL in warmed culture medium, followed by three 5min washes in warmed medium.

5.3.5. *Perfusion Seeding of Microtemplated Scaffolds*

Fibrin scaffolds were rehydrated into sterile PBS, 2mm cylinders were cut with biopsy punches as described in previous chapters, and these prepared scaffolds were kept in seeding media for approximately 1hr before seeding. The perfusion seeding loop was assembled under sterile conditions with both stopcocks in the "closed" position (**Figure 5.3**), and 2mm scaffolds were inserted into the seeding chambers (Part E) (1 scaffold/chamber), ensuring scaffold channels were aligned with the direction of flow. Approximately 10µL of seeding media was added on top of the scaffold to prevent the fibrin material from drying out. Next, 2mL of seeding media was injected through the injection site (Part C) into the tubing above one seeding chamber (Part A). Both stopcocks were then opened to the "open 1" position (**Figure 5.3**) to allow the media to flow through the system, and the lines were gently de-bubbled as needed[3], after which the stopcocks were turned back to the "closed" position. The entire

[3] System de-bubbling was performed by attaching an empty 20mL syringe with Luer lock to Part H and gently pulling and pushing the media back and forth through the system (being careful not to allow media to reach Part H) until all bubbles were removed.

system was then attached to the peristaltic pump outside of the hood and the lines were placed in the incubator to control the temperature of the system during cell preparation.

Cells were trypsinized, counted, and resuspended at 2-4x10^6 cells/scaffold in 0.5mL of cell suspension per scaffold. A small aliquot of this cell suspension was taken for pre-seeding cell viability testing via trypan blue exclusion. The perfusion system was then taken out of the incubator and placed back in the sterile hood, ensuring the scaffold seeding chambers remained vertical (to prevent bubble formation in lines). For cell seeding, 0.5mL of the cell suspension was injected into Part A above each seeding chamber (stopcocks still in the "closed" position) before transferring the entire system back to the incubator and connecting it to the peristaltic pump. The stopcocks were then turned to the "open 2" position (**Figure 5.3**), the pump was turned on to the desired RPM (2-3.1 RPM, corresponding to 0.2-0.3mL/min), and run in one direction until the media in the corresponding line was lowered to the top of the stopcock above the first seeding chamber (connection between Part A and Part B). The pump was then stopped, and the direction of flow reversed until the media on the other side was lowered to the top of the stopcock above the second seeding chamber. This flow reversal was repeated until the desired total seeding time was reached (30-120 minutes), with the number of direction changes determined by the flow rate and duration of seeding being tested.

Upon completion of the seeding protocol, the perfusion system was detached from the pump and moved back into the sterile hood for disassembly. First, the stopcocks were turned to the "closed" position, and the tubing was disconnected between Part E and Part D. Seeded scaffolds were carefully removed from the seeding chambers with sterile tweezers one at a time, and placed directly into 2mL of warmed media in a 12-well plate. Aliquots of the cell solution from the perfusion lines were taken at this point for post-seeding cell viability testing via trypan blue exclusion.

5.3.6. *Assessment of Cell Viability & Perfusion-Seeded Scaffolds*

Cell viability was tested both pre- and post-seeding by taking an aliquot of cell suspension and diluting it 1:4 with 2 parts media and 1 part 0.4% trypan blue solution. The numbers of viable and non-viable cells were counted with a hemacytometer, and the percent viability was calculated. Live cell-seeded constructs containing CM-DiI-labeled HUVECs were imaged under fluorescent light 2-3 hours after seeding, and then immersion-fixed in MC fixative. Samples were processed, embedded in paraffin, and sectioned (5μm) for histology. Sections were cut at 4-5 different depths through each scaffold and stained with H&E to assess the distribution of cell seeding.

5.4. Results

5.4.1. *Determination of Optimal Seeding Duration*

For the first test of version 6 of the perfusion seeding system (Experimental Set I, **Table 5.3**), it was decided to try the lowest flow rate in the calculated range of optimal flow rates (0.2mL/min) using the same cell density as used for centrifugation seeding studies ($2x10^6$ cells/scaffold), and to try a short seeding duration (approximately 40min total). Fluorescent imaging of seeded scaffolds 2-3 hours after seeding indicated some sparsely distributed cells throughout the construct, with some channels seeded densely in areas but not for the entire length of the construct, and the majority of channels remained unseeded (**Figure 5.5a, b**). Therefore, the next test of the perfusion system repeated the same set of parameters except the seeding duration was increased to approximately 120 minutes total (Experimental Set II, **Table 5.3**). Results from this test showed a greater number of channels seeded with a higher density of cells, but the distribution of cells remained uneven throughout the construct as indicated by fluorescent imaging and confirmed by histological analysis (**Figure 5.5c**). Pre-seeding cell

viability was measured as 92%, and post-seeding viability was 75%, indicated a decrease of 17% over the 2 hour seeding protocol.

5.4.2. *Determination of Optimal Cell Seeding Density*

In an attempt to improve the overall density of cells seeded within constructs, the next experiment (Experimental Set III, **Table 5.3**) tested an increase in the total number of cells added to the perfusion lines ($4x10^6$ cells/scaffold) while using the low flow rate (0.2mL/min) and the longer seeding duration (120min). As shown in **Figure 5.5d & e**, this resulted in dense seeding in nearly all of the channels on the end of the scaffold that was seeded first, while the other end of the scaffold remained mostly empty. However, the cell viability dropped 32% over the course of this experiment (down from 95% to 63%), indicating a large degree of cell loss with this higher cell density parameter.

5.4.3. *Determination of Optimal Flow Rate*

For the final test of the perfusion system (Experimental Set IV, **Table 5.3**), the lower cell density ($2x10^6$ cells/scaffold) and longer seeding duration were used with the highest flow rate from the calculated range of optimal flow rates (0.3mL/min). The rational for this set of parameters was that a higher flow rate might improve cell distribution, while also allowing for a greater number of flow direction changes. Fluorescent imaging of live cell-seeded scaffolds indicated an even distribution of cell seeding within nearly all the construct channels, as indicated by both longitudinal and cross-sectional views (**Figure 5.5f, g**). These results were confirmed by H&E staining showing dense areas of cell seeding at all depths through the scaffold. In addition, the cell viability only decreased by 22% (down from 95% to 73%) over the duration of seeding.

5.5. Discussion

The main method of seeding used for the microtemplated fibrin scaffolds has been centrifugation, as described in detail in Chapter 4. However, the efficiency of seeding in terms of the number of successfully seeded constructs, as well as the overall distribution of seeding within constructs was very poor with this method. Despite continued optimization, it is estimated that less than 20% of attempted scaffolds were actually seeded, and for the fraction of these with a desirable degree of seeded cell density, cells were very often confined to approximately half of the construct. Therefore, it was determined that a new method was necessary in order to improve efficiency, distribution, and density of cell seeding within the microtemplated fibrin scaffolds.

The use of perfusion to seed cells into biomaterial scaffolds has been shown to be an effective method of evenly distributing cells throughout constructs at higher densities than can be achieved with more static seeding methods (44, 142, 151, 153, 154). When C2C12 cells were seeded into collagen sponges using perfusion, a cell density comparable to native tissues and a spatially uniform distribution of cells was achieved within scaffolds (154). Similar results were shown with perfusion seeding of neonatal rat cardiomyocytes into channeled PGS scaffolds (44). It was therefore hypothesized that a perfusion seeding system could be used to seed the microtemplated fibrin scaffolds with greater efficiency, more even distribution of cells, and an overall higher density of cell seeding.

Versions 1-3 of the seeding system were designed as open-loop systems in which the two open ends of tubing were submerged in a cell reservoir. This led to major issues with bubble formation in the lines and within the reservoir cell suspension, as well as difficulties maintaining sterility of the system during seeding. Therefore, versions 4-6 were redesigned as closed-loop systems in which the cell reservoir was removed, and components were added which allowed for maintenance of sterility during seeding (syringe filters, injection sites), improved control of flow direction (3-way stopcocks), and an

additional seeding chamber in each loop. Importantly, the closed-loop system also allowed for removal of bubbles from the seeding lines when necessary without requiring disassembly of any components. In addition, the final versions of the perfusion system were designed to attach to the peristaltic pump on top of the incubator so the perfusion loop would hang through the door seal of the incubator, allowing the seeding chambers to remain in an upright position for the duration of the seeding protocol (important for reduction of bubble formation during seeding). Another important design consideration was easy assembly and disassembly of all components in a sterile environment, with the intent of minimizing any disturbance of the cell-seeded constructs during removal from the seeding chambers. All of these design considerations were optimized through the iterative versions of the perfusion seeding system described in this chapter.

Once the finalized version of the system was designed, it was necessary to optimize the seeding protocol. The variables that were optimized for this system were the duration of seeding, the total number of cells per scaffold, and the flow rate of cells through the system. By increasing the duration of the seeding protocol from 30-40 minutes to approximately 2 hours, the total amount of cells that were retained within scaffolds was significantly increased, as indicated by fluorescent imaging and H&E staining. An increased amount of time for seeding increased the number of times the direction of flow was changed, therefore increasing the opportunities for unseeded cells to come in contact with the fibrin scaffold. When the total number of cells was increased from $2x10^6$ cells/scaffold to $4x10^6$ cells/scaffold, the density of cell seeding appeared to be significantly improved, but was limited to the "front end" of the scaffold which was seeded with the first flow direction. This higher density of cells most likely began to clog the scaffold channels, therefore preventing cells from flowing through the entire length of the scaffold. One consideration for future designs of the perfusion seeding loop would be to include cell injection sites both above and below each seeding chamber, so that both ends of the scaffolds would see this initial bolus of cell delivery at the beginning of the seeding protocol. However,

the large decrease in cell viability seen over during the seeding protocol with this high density of cells (a decrease of 32%) indicated that, without additional optimization of media conditions, there was substantial cell loss under these conditions.

While the amount of cells seeded within scaffolds improved with the increased seeding time, and the lower cell density showed improved cell viability retention during seeding, the issue of cell distribution within scaffolds still remained. When attempting to seed a high density of cells into a relatively larger scaffold, one of the major parameters to consider is the amount of hydrodynamic shear stress the cells experience while flowing through the construct. While small amounts of shear stress have been shown to have beneficial effects on cells, shear stresses above 2.4dyn/cm^2 have been shown to cause decreased cell functionality, dedifferentiation, and induction of apoptosis in cardiomyocytes (44, 152, 154). As this system was developed with the intention of being used to seed fibrin scaffolds with the tri-cell mixture in the future, the flow rates used for testing were determined by calculating the corresponding amount of shear stress they would inflict on the cells and maintaining this shear stress below this threshold level of 2.4dyn/cm^2. In addition, flow rates that were too low would be less likely to adequately flow cells through scaffolds. Based on these considerations, it was decided that flow rates in the range of 0.2-0.3mL/min would be tested. Cell seeding distribution remained suboptimal with the use of the low flow rate (0.2mL/min); therefore the highest flow rate in the test range (0.3mL/min) was used for the final optimization experiments. The hypothesis was that a higher flow rate (still below the shear stress threshold) would allow for more even distribution of cells, since the cells would flow further into (or all the way through) the scaffolds with each change in the direction of flow. This higher flow rate, combined with the optimal number of cells and longer seeding time showed the most desirable distribution and density of cell seeding within scaffolds when compared to any other combination of seeding parameters tested. These results correspond with literature studies indicating higher flow rates

for perfusion seeding result in more evenly distributed cells and more consistent seeding of biomaterial constructs (44, 154).

There are multiple parameters of the perfusion seeding protocol that will need to be further optimized for use with the tri-cell mixture. For example, it is likely that the composition of the seeding media will need to be changed, perhaps to include a buffer to help control the pH of the media for the duration of the seeding protocol. This will likely improve the overall cell viability during seeding. In addition, as with the centrifugation seeding optimization, it may be necessary to use a mixture of different media types when using multiple cells in the seeding mixture. It will most likely be necessary to use an agent to prevent cell clumping during seeding, such as DNAse (see Chapter 4), as this was a major issue that had to be addressed for the centrifugation seeding protocol. It will be extremely important to prevent cell clumping in the perfusion system in order to ensure even flow and seeding of scaffolds.

In addition to optimization of the seeding protocol, there are aspects of the perfusion system itself that could also be further optimized. One example mentioned above is the addition of a second injection site below each seeding chamber, which would allow a more equal number of cells to be seeded from each end of the scaffold initially. This could improve the overall seeding density and distribution of cells throughout the scaffolds. Another potential direction would be a design that includes more than two seeding chambers within a loop, but the media volume requirements and cell density within the tubing lines would have to be taken into consideration. With the current design, a total of eight scaffolds could potentially be seeded at once (2 scaffolds/loop, 4 loops can attach to the pump at one time). For future high-throughput *in vitro* testing and *in vivo* implant studies, it would be beneficial to have the ability of seeding more scaffolds at once.

With the development of this perfusion seeding system, a useful tool has been introduced which will allow future studies with cell-seeded scaffolds that were not possible with the current method of

seeding. Without an efficient method of seeding that was consistent from batch to batch, it was not possible to run controlled *in vitro* experiments on cellular constructs. In addition, an *in vivo* implant study of cell-seeded scaffolds would not be plausible without a means to prepare a large number of consistent implantable constructs. The goal of this project to develop a perfusion seeding system optimized for the microtemplated fibrin constructs was to provide a method of cell seeding that was efficient and which would promote an even distribution and high density of cells within scaffolds in order to allow for future studies of tri-cell seeded scaffold constructs.

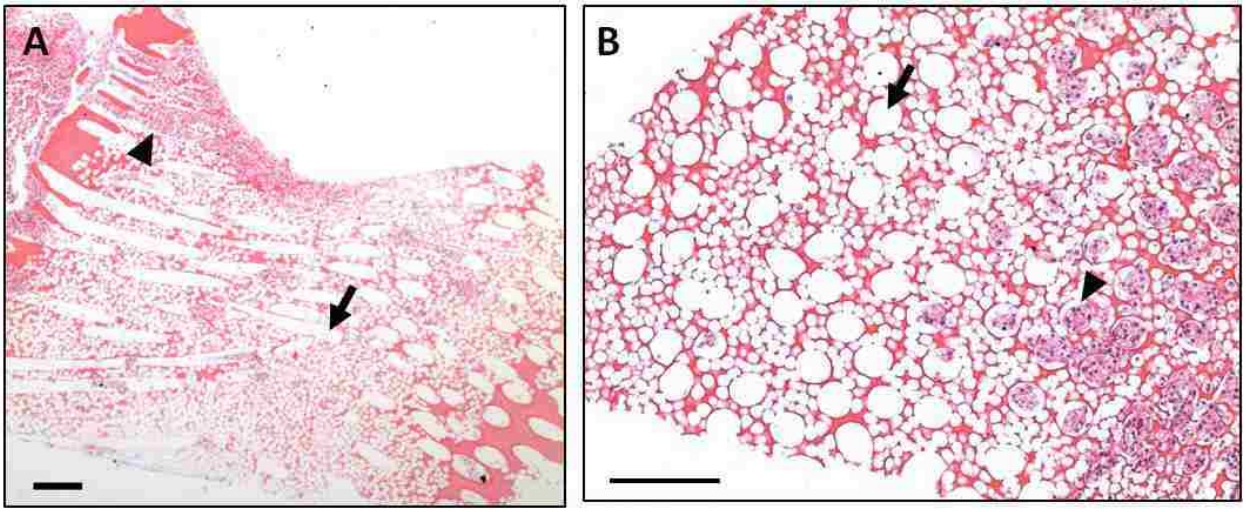

Figure 5.1. Representative H&E staining of centrifugation-seeded constructs demonstrating uneven distribution of cells obtained with this seeding method in **(a)** longitudinal section and **(b)** cross-section. Arrows indicate examples of unseeded channels, arrowheads indicate examples of densely seeded channels. Scale bars = 200µm.

Table 5.1. Estimated average fluid velocities (U) and shear stresses (τ_w) calculated at different volumetric flow rates (Q) for a solution of cells flowing through a microtemplated fibrin scaffold.

Q (mL/min)	U (mL/min·mm^2)	τ_w (dyn/cm^2)
0.05	0.0297	0.314
0.1	0.0594	0.629
0.2	0.119	1.26
0.6	0.357	3.77
1.0	0.594	6.29

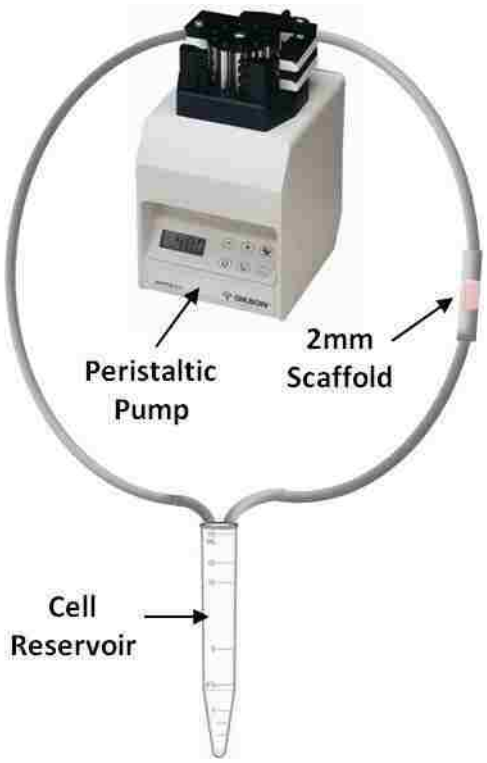

Figure 5.2. Diagram of the open-loop perfusion seeding system containing a single seeding chamber and a cell reservoir, representative of version 1-3 of the system design.

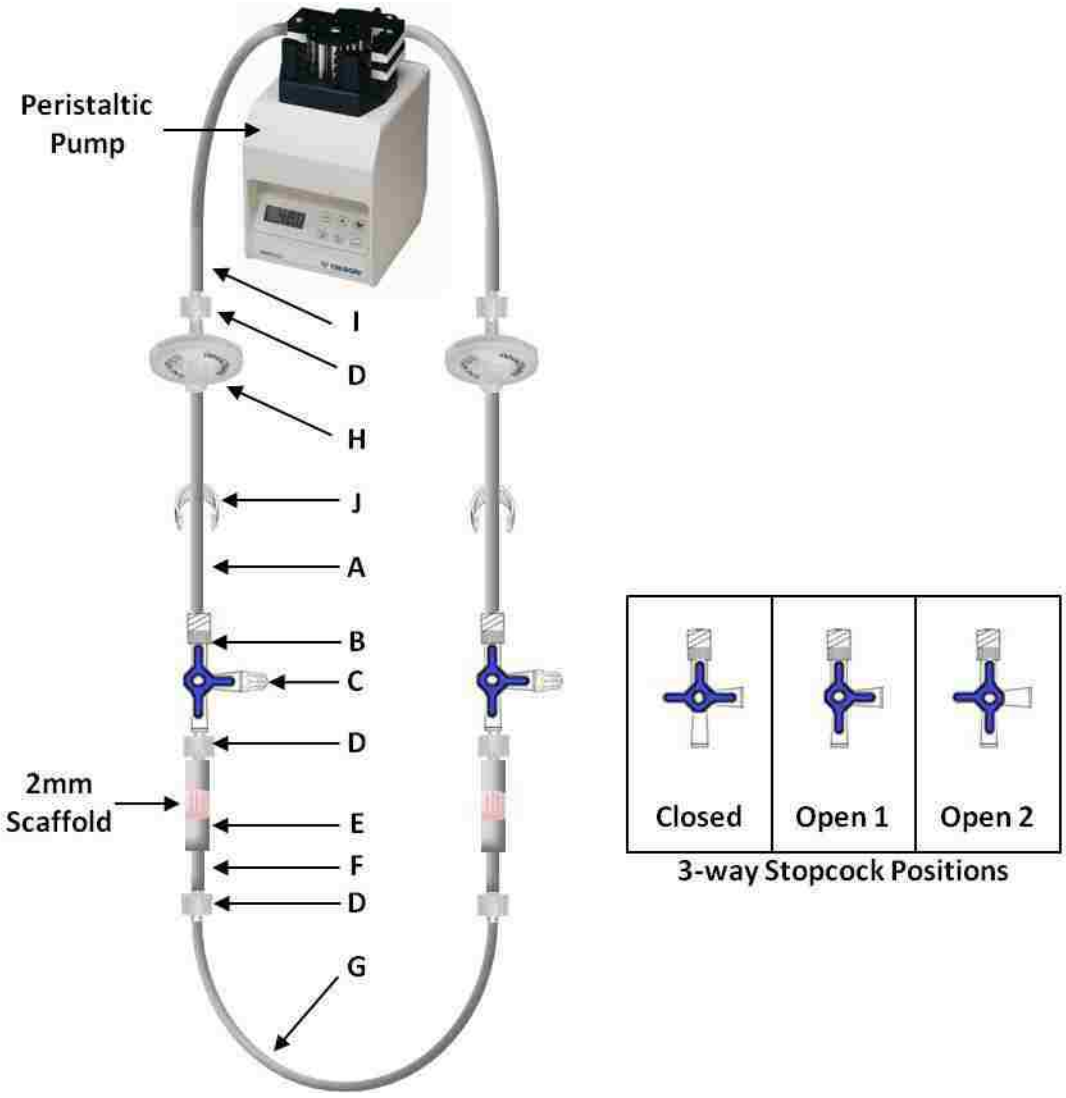

Figure 5.3. Diagram of the closed-loop perfusion seeding system containing two seeding chambers, demonstrating version 6 of the design. The cell solution is confined to components below Part H, and does not flow through Parts H or I. The three positions of the 3-way stopcock valve are also shown. "Closed" prevents flow from Part A to the seeding chamber; "Open 1" allows flow from Part A and from the injection site (Part C) to the seeding chamber; "Open 2" allows flow from Part A but not from the injection site (Part C) to the seeding chamber, which helps prevent the introduction of bubbles into the lines during the seeding protocol.

Table 5.2. Descriptions of each component of version 6 of the perfusion seeding system.

Part	Description	Dimensions	Method of Sterilization	Product Info	Total #
A	Clear PVC tubing	3.16mm ID, 12" length	Autoclave	Gilson #F117969	2
B	3-way stopcock with Luer lock, polycarbonate & polyethylene	N/A	ETO	SAI #SC3LL; VWR #89134-220	2
C	IN-4000 intermittent injection site to male Luer lock, polyisoprene w/ABS acrylic body	N/A	ETO	Value Plastics #VPS3901074N	2
D	Male Luer integral lock ring to 500 series barb, white nylon	Attaches to 1/16" (1.6mm) ID tubing	Autoclave or ETO	Value Plastics #MTLL004-1	6 (4 sterile)
E	Nalgene 180 clear PVC tubing (seeding chamber)	2.38mm (3/32") ID x 5/32" OD x 1/32" wall thickness, 1.5" long	Autoclave	Thermo Scientific #8000-0006; Fisher #14-176-192	2
F	Clear PVC tubing	1.02 mm ID, 1" length	Autoclave	Gilson #F117938	2
G	Clear PVC tubing	3.16mm ID, 3" length	Autoclave	Gilson #F117969	1
H	Syringe filter 0.2µm	N/A	Single-use	VWR #28145-477	2
I	Calibrated PVC tubing	1.02mm ID, standard length	Autoclave	Gilson #F117938	1
J	Tubing protector, cut from 1mL NORM-JECT syringe, c-shaped to hold Part A tubing open in incubator door seal	Approximately 1" length	N/A	HSW #4010.200V0	2

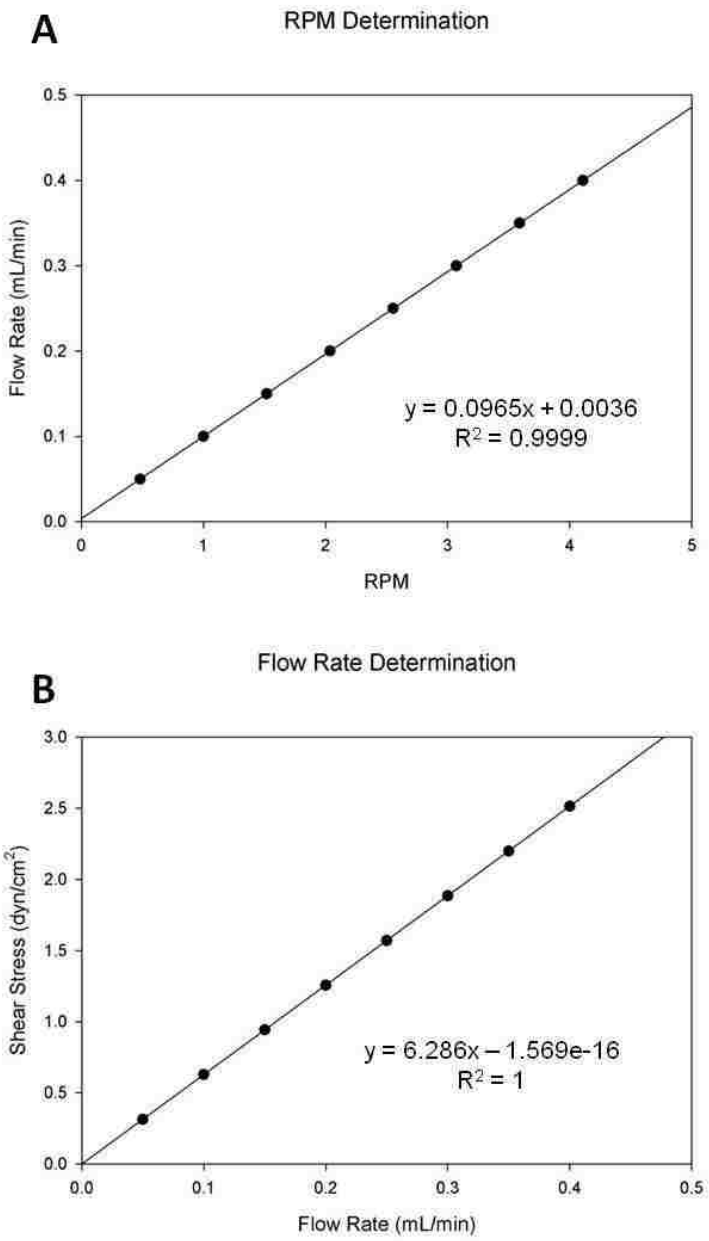

Figure 5.4. Determination of desirable flow rates for version 6 of the perfusion seeding system. **(a)** Flow rates (mL/min) measured for corresponding RPM settings on the peristaltic pump, and **(b)** calculated shear stresses (dyn/cm^2) for corresponding flow rates (mL/min).

Table 5.3. Experimental parameters optimized with version 6 of the perfusion seeding system with the resulting changes in cell viability.

Experimental Set	Flow Rate (mL/min)	Time (min)	Cells per Scaffold	Change in Cell Viability
I	0.2	30-40	2×10^6	N/A
II	0.2	**120**	2×10^6	-17%
III	0.2	120	**4×10^6**	-32%
IV	**0.3**	120	2×10^6	-22%

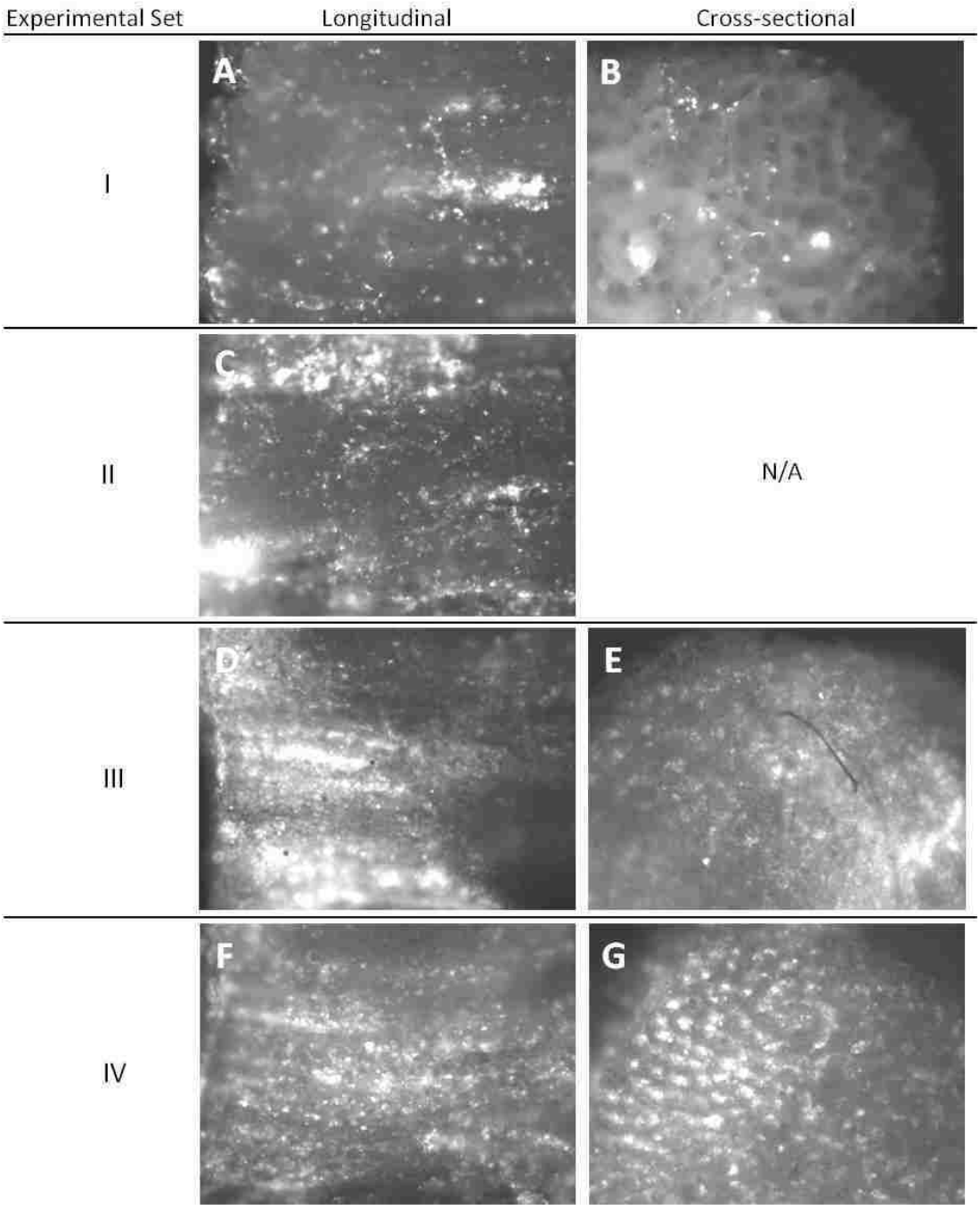

Figure 5.5. Imaging results for experimental sets I-IV of version 6 of the perfusion seeding system demonstrating cell seeding distributions and densities. Images are of live fluorescently-labeled endothelial cells seeded in microtemplated fibrin scaffolds in **(a,c,d,f)** longitudinal view with scaffold channels oriented horizontally, and **(b,e,g)** cross-sectional view. No cross-sectional view of experimental set II could be imaged due to entrapment of bubbles within the scaffold which caused it to float at the top of the culture medium.

Chapter 6:

Conclusions & Future Studies

6.1. Summary & Conclusions

The research presented in this dissertation describes the development of a novel fibrin scaffold with a microtemplated architecture, and material and degradation properties targeted for cardiac tissue engineering. Techniques for templating high density fibrin in a microporous architecture (10) and for templating synthetic polymers with a bimodal architecture (11) were combined and modified to develop a high density fibrin scaffold with this microchanneled and microporous architecture. The hypothesis was that this highly organized architecture would promote cell seeding into scaffolds and induce cellular organization and alignment mimicking the native myocardial tissue structure.

One of the major issues with using natural polymers for tissue engineering construct is that they generally have very low mechanical strength. By using the microtemplating technique, it was possible to develop a high density fibrin construct with much greater mechanical strength than fibrin gels, while still providing open channels and pores for cell infiltration. The initial stiffness of these microtemplated fibrin scaffolds was comparable to native cardiac tissues, averaging approximately 70-90kPa. However, without any additional material modifications, unmodified fibrin scaffolds degraded very quickly both *in vitro* and *in vivo*. It was hypothesized that an extended scaffold lifetime would be necessary for future cell-seeded implants in order to provide sufficient mechanical support to grafted cells before they could replace the fibrin scaffold with their own ECM. Therefore, material modifications were tested in an

attempt to prolong the scaffold lifetime. While these modifications did not affect the initial material stiffness, it was found that addition of FXIII or the MMP inhibitor galardin were able to improve scaffold stiffness retention at an intermediate level, while the addition of aprotinin (with or without FXIII) showed 70-80% stiffness retention over 10 days *in vitro*. These studies demonstrated the ability to tune the material degradation properties of the templated fibrin scaffolds.

An interesting finding of the preliminary acellular scaffold implant study was the apparent decrease in fibrous capsule thickness surrounding aprotinin implants, while effects of material modifications on scaffold degradation rates were inconclusive. Due to the small implant size required with the myocardial implantation method, and the limitation of a single implant per animal, it was decided that a more in depth implant study would be done using a subcutaneous implant model to further assess host tissue responses to the four different fibrin scaffold formulations (unmodified, FXIII, aprotinin, and FXIII + aprotinin). The results of this study indicated aprotinin significantly decreased scaffold degradation after two weeks of implantation. In addition, the extent of host vascular infiltration was significantly greater in aprotinin scaffolds, with a greater number of lumen structures reaching further into the interior of scaffold implants. Aprotinin release from scaffolds also decreased the extent of inflammation in the surrounding tissue, as indicated by a decreased amount of macrophages (CD68+ area) after 7 days and a decreased number of lumen structures (RECA-1+) after 14 days. Finally, a significantly thinner but apparently more cellular fibrous capsule was found surrounding aprotinin implants after 2 weeks when compared to unmodified scaffolds. Taken together, these results demonstrate that modification of the fibrin material by addition of the serine protease inhibitor has significant effects on the host tissue and promotes a more physiological healing response. These scaffold properties would be highly beneficial for implants that require a strong angiogenic response from the host in order to improve graft integration, as is the case with cardiac tissue constructs.

Cell seeding of microtemplated fibrin scaffolds proved to be the biggest challenge encountered over the course of this research, as was expected from the current tissue engineering literature. Centrifugation seeding was found to be superior to static seeding methods for the microchanneled fibrin architecture. Cell seeding with both rat and human cell mixtures demonstrated the scaffolds were able to support high density cell seeding and promote seeded cell survival and organization, as demonstrated by cardiomyocyte alignment and endothelial cell lumen structure formation within channels. In addition, histological analysis of cell-seeded constructs demonstrated the graft cells were depositing collagen within construct channels, indicating the cells could eventually replace the degrading fibrin scaffold with their own ECM. It was hypothesized that the use of a tri-cell mixture would improve overall cell survival and promote this type of cellular organization, and was designed to mimic the natural cell make-up of myocardial tissue. It was hypothesized that the development of a pre-vascular network within constructs would not only improve cardiomyocyte survival and organization *in vitro*, but that upon construct implantation it would promote a faster anastomosis with the host vasculature, thus improving the chances of overall graft survival and the ability to provide a therapeutic benefit.

While the centrifugation seeding method demonstrated the ability of the fibrin scaffolds to support cell seeding and organization as was hypothesized, issues with inefficient cell seeding, uneven cell distribution throughout constructs, and sub-optimal cell densities prevented further *in vitro* testing and cell-seeded implant studies. It was therefore determined that a new dynamic seeding method was needed in order to address these issues and allow for future studies of cellular constructs. The use of perfusion to seed larger biomaterial scaffolds has shown promising results in the literature, including for cardiac tissue engineering. The microchanneled architecture of the fibrin scaffolds lends itself well to seeding via perfusion flow of cells through the channels; therefore, a perfusion seeding system was developed and optimized for seeding of the microtemplated fibrin. Optimization of flow rates to minimize shear stress on seeded cells, duration of seeding, and cell seeding density was performed using

a single cell type (HUVEC) labeled with a fluorescent tracer dye in order to allow for quick assessment of seeding experiments. The most optimal set of parameters resulted in evenly distributed high density cell seeding throughout constructs, with a much greater seeding efficiency than was found with centrifugation methods. The perfusion seeding system is a useful tool that will allow for high-throughput studies of cell seeded constructs in the future.

In conclusion, the research in this dissertation describes the development, characterization, and optimization of high density microtemplated fibrin constructs designed for cardiac tissue engineering applications. Material properties, degradation profiles, and host tissue responses were investigated in order to develop a scaffold with mechanical properties suited for cardiac tissue engineering, and which would promote vascularization and a physiological healing response from the host tissue. The architecture of these scaffolds was designed to mimic the native cardiac ECM, with the goal of developing a construct that could support a high density of cardiomyocyte seeding and promote cellular alignment and organization, including the development of a pre-vascular network. The scaffold design and construct optimization resulting from this research should promote improved construct survival and integration with host tissue in future implant studies.

6.2. Future Studies

There are several directions of potential future studies for this research. For example, the dose of aprotinin studied was based upon optimization studies performed by Linnes *et al*. (10). Based on the significant effects of aprotinin on host tissue responses seen in the subcutaneous implant study described in Chapter 3, it would be interesting to perform a dosing study to determine whether there was a threshold level of aprotinin that could induce the same levels of host responses, and whether much higher doses of aprotinin would have any detrimental effects. Alternatively, the addition of

growth factors or other chemoactive molecules to the fibrin material could be an effective way to tailor the host response to implants. One hypothesis proposed for the macrophage response seen within aprotinin implants was the possibility of different macrophage phenotypes within and around scaffolds. Future studies investigating this phenomenon could provide important insight into the mechanisms of the differing host responses seen between unmodified and aprotinin scaffold implants.

The development of the perfusion seeding system tailored for the microtemplated fibrin constructs will allow for more efficient, evenly distributed, and high density cell seeding of scaffolds after future optimization for tri-cell seeding. Further improvement of seeding density will be necessary, and optimization of seeding and culture conditions that will further promote cellular organization (and perhaps function) in constructs would be beneficial. With the improved efficiency of seeding, it will be possible to perform high-throughput *in vitro* studies such as testing mechanical force production of synchronously contracting constructs and evaluating construct electrophysiological properties. Additionally, consistent cell seeding of constructs will allow further investigation of the significant differences seen between bi-cell and tri-cell constructs. Finally, since the design of the scaffold architecture, material and mechanical properties, and cell-seeding parameters were all intended to develop a construct that will improve graft survival and integration with host tissue upon implantation, it will be important to evaluate these constructs in an implantation model. Assessment of cell-seeded construct survival, integration, and effects on heart function will demonstrate the effectiveness of the overall construct design.

Bibliography

1. Go, A.S., Mozaffarian, D., Roger, V.L., Benjamin, E.J., Berry, J.D., Borden, W.B., Bravata, D.M., Dai, S., Ford, E.S., Fox, C.S., Franco, S., Fullerton, H.J., Gillespie, C., Hailpern, S.M., Heit, J.A., Howard, V.J., Huffman, M.D., Kissela, B.M., Kittner, S.J., Lackland, D.T., Lichtman, J.H., Lisabeth, L.D., Magid, D., Marcus, G.M., Marelli, A., Matchar, D.B., McGuire, D.K., Mohler, E.R., Moy, C.S., Mussolino, M.E., Nichol, G., Paynter, N.P., Schreiner, P.J., Sorlie, P.D., Stein, J., Turan, T.N., Virani, S.S., Wong, N.D., Woo, D., Turner, M.B., andSubcommittee, A.H.A.S.C.a.S.S. Heart disease and stroke statistics--2013 update: a report from the American Heart Association. Circulation **127**, e6, 2013.

2. Dobaczewski, M., Gonzalez-Quesada, C., andFrangogiannis, N.G. The extracellular matrix as a modulator of the inflammatory and reparative response following myocardial infarction. J Mol Cell Cardiol **48**, 504, 2010.

3. Dobaczewski, M., andFrangogiannis, N.G. Chemokines and cardiac fibrosis. Front Biosci (Schol Ed) **1**, 391, 2009.

4. Jawad, H., Ali, N.N., Lyon, A.R., Chen, Q.Z., Harding, S.E., andBoccaccini, A.R. Myocardial tissue engineering: a review. J Tissue Eng Regen Med **1**, 327, 2007.

5. Jawad, H., Lyon, A., Harding, S., Ali, N., andBoccaccini, A. Myocardial tissue engineering. Br Med Bull **87**, 31, 2008.

6. Laflamme, M.A., Zbinden, S., Epstein, S.E., andE., M.C. Cell-based therapy for myocardial ischemia and infarction: pathophysiological mechanisms. Annu Rev Pathol Mech Dis **2**, 307, 2007.

7. Taylor, D. From stem cells and cadaveric matrix to engineered organs. Curr Opin Biotechnol **20**, 598, 2009.

8. Sasagawa, T., Shimizu, T., Sekiya, S., Haraguchi, Y., Yamato, M., Sawa, Y., andOkano, T. Design of prevascularized three-dimensional cell-dense tissues using a cell sheet stacking manipulation technology. Biomaterials 2009.

9. Ott, H., Matthiesen, T., Goh, S., Black, L., Kren, S., Netoff, T., andTaylor, D. Perfusion-decellularized matrix: using nature's platform to engineer a bioartificial heart. Nat Med **14**, 213, 2008.

10. Linnes, M.P., Ratner, B.D., andGiachelli, C.M. A fibrinogen-based precision microporous scaffold for tissue engineering. Biomaterials **28**, 5298, 2007.

11. Madden, L.R., Mortisen, D.J., Sussman, E.M., Dupras, S.K., Fugate, J.A., Cuy, J.L., Hauch, K.D., Laflamme, M.A., Murry, C.E., andRatner, B.D. Proangiogenic scaffolds as functional templates for cardiac tissue engineering. Proc Natl Acad Sci U S A **107**, 15211, 2010.

12. Callegari, A., Bollini, S., Iop, L., Chiavegato, A., Torregrossa, G., Pozzobon, M., Gerosa, G., De Coppi, P., Elvassore, N., andSartore, S. Neovascularization induced by porous collagen scaffold implanted on intact and cryoinjured rat hearts. Biomaterials **28**, 5449, 2007.

13. Chiu, L.L., Radisic, M., andVunjak-Novakovic, G. Bioactive scaffolds for engineering vascularized cardiac tissues. Macromol Biosci **10**, 1286, 2010.

14. Dar, A., Shachar, M., Leor, J., andCohen, S. Optimization of cardiac cell seeding and distribution in 3D porous alginate scaffolds. Biotechnol Bioeng **80**, 305, 2002.

15. Galperin, A., Long, T.J., andRatner, B.D. Degradable, thermo-sensitive poly(N-isopropyl acrylamide)-based scaffolds with controlled porosity for tissue engineering applications. Biomacromolecules **11**, 2583, 2010.

16. Leor, J., Aboulafia-Etzion, S., Dar, A., Shapiro, L., Barbash, I.M., Battler, A., Granot, Y., andCohen, S. Bioengineered cardiac grafts: A new approach to repair the infarcted myocardium? Circulation **102**, III56, 2000.

17. Radisic, M., Park, H., Martens, T.P., Salazar-Lazaro, J.E., Geng, W., Wang, Y., Langer, R., Freed, L.E., andVunjak-Novakovic, G. Pre-treatment of synthetic elastomeric scaffolds by cardiac fibroblasts improves engineered heart tissue. J Biomed Mater Res A **86**, 713, 2008.

18. Zimmermann, W.H., Melnychenko, I., andEschenhagen, T. Engineered heart tissue for regeneration of diseased hearts. Biomaterials **25**, 1639, 2004.

19. Lakshmanan, R., Krishnan, U.M., andSethuraman, S. Living cardiac patch: the elixir for cardiac regeneration. Expert Opin Biol Ther **12**, 1623, 2012.

20. Laflamme, M.A., andMurry, C.E. Heart regeneration. Nature **473**, 326, 2011.

21. Zhang, G., andSuggs, L.J. Matrices and scaffolds for drug delivery in vascular tissue engineering. Adv Drug Deliv Rev **59**, 360, 2007.

22. Silva, E.A., Kim, E.S., Kong, H.J., andMooney, D.J. Material-based deployment enhances efficacy of endothelial progenitor cells. Proc Natl Acad Sci U S A **105**, 14347, 2008.

23. Hall, H. Modified fibrin hydrogel matrices: both, 3D-scaffolds and local and controlled release systems to stimulate angiogenesis. Curr Pharm Des **13**, 3597, 2007.

24. Trentin, D., Hall, H., Wechsler, S., andHubbell, J.A. Peptide-matrix-mediated gene transfer of an oxygen-insensitive hypoxia-inducible factor-1alpha variant for local induction of angiogenesis. Proc Natl Acad Sci U S A **103**, 2506, 2006.

25. Mirsadraee, S., Wilcox, H.E., Korossis, S.A., Kearney, J.N., Watterson, K.G., Fisher, J., andIngham, E. Development and characterization of an acellular human pericardial matrix for tissue engineering. Tissue Eng **12**, 763, 2006.

26. Anderson, J.M., Rodriguez, A., andChang, D.T. Foreign body reaction to biomaterials. Semin Immunol **20**, 86, 2008.

27. Anderson, J.M. Biological Responses to Materials. Annu Rev Mater Res **31**, 81, 2001.

28. Silverthorn, D. Human Physiology: An Integrated Approach. 3rd ed: Pearson/Benjamin Cummings; 2004.

29. Karamysheva, A.F. Mechanisms of angiogenesis. Biochemistry (Mosc) **73**, 751, 2008.

30. Jain, R.K. Molecular regulation of vessel maturation. Nat Med **9**, 685, 2003.

31. Kutryk, M.J., andStewart, D.J. Angiogenesis of the heart. Microsc Res Tech **60**, 138, 2003.

32. Ahn, A., Frishman, W.H., Gutwein, A., Passeri, J., andNelson, M. Therapeutic angiogenesis: a new treatment approach for ischemic heart disease--part I. Cardiol Rev **16**, 163, 2008.

33. Ding, Y.T., Kumar, S., andYu, D.C. The role of endothelial progenitor cells in tumour vasculogenesis. Pathobiology **75**, 265, 2008.

34. Khoo, C.P., Pozzilli, P., andAlison, M.R. Endothelial progenitor cells and their potential therapeutic applications. Regen Med **3**, 863, 2008.

35. Miller-Kasprzak, E., andJagodziński, P.P. Endothelial progenitor cells as a new agent contributing to vascular repair. Arch Immunol Ther Exp (Warsz) **55**, 247, 2007.

36. De Palma, M., andNaldini, L. Role of haematopoietic cells and endothelial progenitors in tumour angiogenesis. Biochim Biophys Acta **1766**, 159, 2006.

37. Jujo, K., Ii, M., andLosordo, D.W. Endothelial progenitor cells in neovascularization of infarcted myocardium. J Mol Cell Cardiol **45**, 530, 2008.

38. Goodwin, A.M. In vitro assays of angiogenesis for assessment of angiogenic and anti-angiogenic agents. Microvasc Res **74**, 172, 2007.

39. Kalluri, R. Basement membranes: structure, assembly and role in tumour angiogenesis. Nat Rev Cancer **3**, 422, 2003.

40. Hughes, C.C. Endothelial-stromal interactions in angiogenesis. Curr Opin Hematol **15**, 204, 2008.

41. Loffredo, F., andLee, R.T. Therapeutic vasculogenesis: it takes two. Circ Res **103**, 128, 2008.

42. Hoch, R.V., andSoriano, P. Roles of PDGF in animal development. Development **130**, 4769, 2003.

43. Baiguera, S., andRibatti, D. Endothelialization approaches for viable engineered tissues. Angiogenesis **16**, 1, 2013.

44. Maidhof, R., Marsano, A., Lee, E.J., andVunjak-Novakovic, G. Perfusion seeding of channeled elastomeric scaffolds with myocytes and endothelial cells for cardiac tissue engineering. Biotechnol Prog **26**, 565, 2010.

45. Radisic, M., Park, H., Chen, F., Salazar-Lazzaro, J.E., Wang, Y., Dennis, R., Langer, R., Freed, L.E., andVunjak-Novakovic, G. Biomimetic approach to cardiac tissue engineering: oxygen carriers and channeled scaffolds. Tissue Eng **12**, 2077, 2006.

46. Tulloch, N.L., Muskheli, V., Razumova, M.V., Korte, F.S., Regnier, M., Hauch, K.D., Pabon, L., Reinecke, H., andMurry, C.E. Growth of engineered human myocardium with mechanical loading and vascular coculture. Circ Res **109**, 47, 2011.

47. Black, A.F., Hudon, V., Damour, O., Germain, L., andAuger, F.A. A novel approach for studying angiogenesis: a human skin equivalent with a capillary-like network. Cell Biol Toxicol **15**, 81, 1999.

48. Hudon, V., Berthod, F., Black, A.F., Damour, O., Germain, L., andAuger, F.A. A tissue-engineered endothelialized dermis to study the modulation of angiogenic and angiostatic molecules on capillary-like tube formation in vitro. Br J Dermatol **148**, 1094, 2003.

49. Levenberg, S., Rouwkema, J., Macdonald, M., Garfein, E.S., Kohane, D.S., Darland, D.C., Marini, R., van Blitterswijk, C.A., Mulligan, R.C., D'Amore, P.A., andLanger, R. Engineering vascularized skeletal muscle tissue. Nat Biotechnol **23**, 879, 2005.

50. Sekine, H., Shimizu, T., Hobo, K., Sekiya, S., Yang, J., Yamato, M., Kurosawa, H., Kobayashi, E., andOkano, T. Endothelial cell coculture within tissue-engineered cardiomyocyte sheets enhances neovascularization and improves cardiac function of ischemic hearts. Circulation **118**, S145, 2008.

51. Black, A.F., Berthod, F., L'heureux, N., Germain, L., andAuger, F.A. In vitro reconstruction of a human capillary-like network in a tissue-engineered skin equivalent. FASEB J **12**, 1331, 1998.

52. Lesman, A., Habib, M., Caspi, O., Gepstein, A., Arbel, G., Levenberg, S., andGepstein, L. Transplantation of a tissue-engineered human vascularized cardiac muscle. Tissue Eng Part A **16**, 115, 2010.

53. Christman, K.L., Fok, H.H., Sievers, R.E., Fang, Q., andLee, R.J. Fibrin glue alone and skeletal myoblasts in a fibrin scaffold preserve cardiac function after myocardial infarction. Tissue Eng **10**, 403, 2004.

54. Ahmed, T.A., Griffith, M., andHincke, M. Characterization and inhibition of fibrin hydrogel-degrading enzymes during development of tissue engineering scaffolds. Tissue Eng **13**, 1469, 2007.

55. Ahmed, T.A., Dare, E.V., andHincke, M. Fibrin: A Versatile Scaffold for Tissue Engineering Applications. Tissue Eng Part B Rev **14**, 199, 2008.

56. Chen, X., Aledia, A.S., Ghajar, C.M., Griffith, C.K., Putnam, A.J., Hughes, C.C., andGeorge, S.C. Prevascularization of a fibrin-based tissue construct accelerates the formation of functional anastomosis with host vasculature. Tissue Eng Part A **15**, 1363, 2009.

57. Christman, K.L., Vardanian, A.J., Fang, Q., Sievers, R.E., Fok, H.H., andLee, R.J. Injectable fibrin scaffold improves cell transplant survival, reduces infarct expansion, and induces neovasculature formation in ischemic myocardium. J Am Coll Cardiol **44**, 654, 2004.

58. Chekanov, V., Akhtar, M., Tchekanov, G., Dangas, G., Shehzad, M.Z., Tio, F., Adamian, M., Colombo, A., Roubin, G., Leon, M.B., Moses, J.W., andKipshidze, N.N. Transplantation of autologous endothelial cells induces angiogenesis. Pacing Clin Electrophysiol **26**, 496, 2003.

59. Huang, Y.C., Khait, L., andBirla, R.K. Contractile three-dimensional bioengineered heart muscle for myocardial regeneration. J Biomed Mater Res A **80**, 719, 2007.

60. Ryu, J.H., Kim, I.K., Cho, S.W., Cho, M.C., Hwang, K.K., Piao, H., Piao, S., Lim, S.H., Hong, Y.S., Choi, C.Y., Yoo, K.J., andKim, B.S. Implantation of bone marrow mononuclear cells using injectable fibrin matrix enhances neovascularization in infarcted myocardium. Biomaterials **26**, 319, 2005.

61. Doolittle, R.F. Fibrinogen and fibrin. Annu Rev Biochem **53**, 195, 1984.

62. Hantgan, R., McDonagh, J., andHermans, J. Fibrin assembly. Ann N Y Acad Sci **408**, 344, 1983.

63. Hunter, S., Jones, P., Mitchell, A., Apweiler, R., Attwood, T.K., Bateman, A., Bernard, T., Binns, D., Bork, P., Burge, S., de Castro, E., Coggill, P., Corbett, M., Das, U., Daugherty, L., Duquenne, L., Finn, R.D., Fraser, M., Gough, J., Haft, D., Hulo, N., Kahn, D., Kelly, E., Letunic, I., Lonsdale, D., Lopez, R., Madera, M., Maslen, J., McAnulla, C., McDowall, J., McMenamin, C., Mi, H., Mutowo-Muellenet, P., Mulder, N., Natale, D., Orengo, C., Pesseat, S., Punta, M., Quinn, A.F., Rivoire, C., Sangrador-Vegas, A., Selengut, J.D., Sigrist, C.J., Scheremetjew, M., Tate, J., Thimmajanarthanan, M., Thomas, P.D., Wu, C.H., Yeats, C., andYong, S.Y. InterPro in 2011: new developments in the family and domain prediction database. Nucleic Acids Res **40**, D306, 2012.

64. Monroe, D.M., andHoffman, M. What does it take to make the perfect clot? Arterioscler Thromb Vasc Biol **26**, 41, 2006.

65. Noll, T., Wozniak, G., McCarson, K., Hajimohammad, A., Metzner, H.J., Inserte, J., Kummer, W., Hehrlein, F.W., andPiper, H.M. Effect of factor XIII on endothelial barrier function. J Exp Med **189**, 1373, 1999.

66. Lijnen, H.R. Elements of the fibrinolytic system. Ann N Y Acad Sci **936**, 226, 2001.

67. Kluft, C. The fibrinolytic system and thrombotic tendency. Pathophysiol Haemost Thromb **33**, 425, 2003.

68. Michel, J.B., Martin-Ventura, J.L., Egido, J., Sakalihasan, N., Treska, V., Lindholt, J., Allaire, E., Thorsteinsdottir, U., Cockerill, G., Swedenborg, J., andconsortium, F.t.F.E. Novel aspects of the pathogenesis of aneurysms of the abdominal aorta in humans. Cardiovasc Res 2010.

69. Creemers, E.E., Cleutjens, J.P., Smits, J.F., andDaemen, M.J. Matrix metalloproteinase inhibition after myocardial infarction: a new approach to prevent heart failure? Circ Res **89**, 201, 2001.

70. Cholewinski, E., Dietrich, M., Flanagan, T.C., Schmitz-Rode, T., andJockenhoevel, S. Tranexamic acid--an alternative to aprotinin in fibrin-based cardiovascular tissue engineering. Tissue Eng Part A **15**, 3645, 2009.

71. DeBlois, C., Côté, M.F., andDoillon, C.J. Heparin-fibroblast growth factor-fibrin complex: in vitro and in vivo applications to collagen-based materials. Biomaterials **15**, 665, 1994.

72. Clark, R.A. Fibrin is a many splendored thing. J Invest Dermatol **121**, xxi, 2003.

73. Odrljin, T.M., Francis, C.W., Sporn, L.A., Bunce, L.A., Marder, V.J., andSimpson-Haidaris, P.J. Heparin-binding domain of fibrin mediates its binding to endothelial cells. Arterioscler Thromb Vasc Biol **16**, 1544, 1996.

74. Odrljin, T.M., Shainoff, J.R., Lawrence, S.O., andSimpson-Haidaris, P.J. Thrombin cleavage enhances exposure of a heparin binding domain in the N-terminus of the fibrin beta chain. Blood **88**, 2050, 1996.

75. Houck, K.A., Leung, D.W., Rowland, A.M., Winer, J., andFerrara, N. Dual regulation of vascular endothelial growth factor bioavailability by genetic and proteolytic mechanisms. J Biol Chem **267**, 26031, 1992.

76. Bootle-Wilbraham, C., Tazzyman, S., Thompson, W., Stirk, C., andLewis, C. Fibrin fragment E stimulates the proliferation, migration and differentiation of human microvascular endothelial cells in vitro. Angiogenesis **4**, 269, 2001.

77. Ge, M., Ryan, T.J., Lum, H., andMalik, A.B. Fibrinogen degradation product fragment D increases endothelial monolayer permeability. Am J Physiol **261**, L283, 1991.

78. Ge, M., Tang, G., Ryan, T.J., andMalik, A.B. Fibrinogen degradation product fragment D induces endothelial cell detachment by activation of cell-mediated fibrinolysis. J Clin Invest **90**, 2508, 1992.

79. Naito, M., Stirk, C.M., Smith, E.B., andThompson, W.D. Smooth muscle cell outgrowth stimulated by fibrin degradation products. The potential role of fibrin fragment E in restenosis and atherogenesis. Thromb Res **98**, 165, 2000.

80. Thompson, W.D., Smith, E.B., Stirk, C.M., Marshall, F.I., Stout, A.J., andKocchar, A. Angiogenic activity of fibrin degradation products is located in fibrin fragment E. J Pathol **168**, 47, 1992.

81. Takei, A., Tashiro, Y., Nakashima, Y., andSueishi, K. Effects of fibrin on the angiogenesis in vitro of bovine endothelial cells in collagen gel. In Vitro Cell Dev Biol Anim **31**, 467, 1995.

82. Stevens, K., Pabon, L., Muskheli, V., andMurry, C. Scaffold-free human cardiac tissue patch created from embryonic stem cells. Tissue Eng Part A **15**, 1211, 2009.

83. Barsotti, M.C., Felice, F., Balbarini, A., andDi Stefano, R. Fibrin as a scaffold for cardiac tissue engineering. Biotechnol Appl Biochem **58**, 301, 2011.

84. Giraud, M.N., Ayuni, E., Cook, S., Siepe, M., Carrel, T.P., andTevaearai, H.T. Hydrogel-based engineered skeletal muscle grafts normalize heart function early after myocardial infarction. Artif Organs **32**, 692, 2008.

85. Kreutziger, K.L., Piroddi, N., Belus, A., Poggesi, C., andRegnier, M. Ca^{2+}-binding kinetics of troponin C influence force generation kinetics in cardiac muscle. Biophysical Journal **92**, 477a, 2007.

86. Gillis, T.E., Martyn, D.A., Rivera, A.J., andRegnier, M. Investigation of thin filament near-neighbour regulatory unit interactions during force development in skinned cardiac and skeletal muscle. J Physiol **580**, 561, 2007.

87. Moreno-Gonzalez, A., Korte, F.S., Dai, J., Chen, K., Ho, B., Reinecke, H., Murry, C.E., andRegnier, M. Cell therapy enhances function of remote non-infarcted myocardium. J Mol Cell Cardiol **47**, 603, 2009.

88. Lahmers, S., Wu, Y., Call, D.R., Labeit, S., andGranzier, H. Developmental control of titin isoform expression and passive stiffness in fetal and neonatal myocardium. Circ Res **94**, 505, 2004.

89. Bagoly, Z., Koncz, Z., Hársfalvi, J., andMuszbek, L. Factor XIII, clot structure, thrombosis. Thromb Res **129**, 382, 2012.

90. Takagi, J., Kasahara, K., Sekiya, F., Inada, Y., andSaito, Y. Subunit B of factor XIII is present in bovine platelets. Thromb Res **50**, 767, 1988.

91. Hickerson, W.L., Nur, I., andMeidler, R. A comparison of the mechanical, kinetic, and biochemical properties of fibrin clots formed with two different fibrin sealants. Blood Coagul Fibrinolysis **22**, 19, 2011.

92. Standeven, K.F., Carter, A.M., Grant, P.J., Weisel, J.W., Chernysh, I., Masova, L., Lord, S.T., andAriëns, R.A. Functional analysis of fibrin {gamma}-chain cross-linking by activated factor XIII: determination of a cross-linking pattern that maximizes clot stiffness. Blood **110**, 902, 2007.

93. Akpalo, E., Bidault, L., Boissière, M., Vancaeyzeele, C., Fichet, O., andLarreta-Garde, V. Fibrin-polyethylene oxide interpenetrating polymer networks: new self-supported biomaterials combining the properties of both protein gel and synthetic polymer. Acta Biomater **7**, 2418, 2011.

94. McEvoy, M.D., Reeves, S.T., Reves, J.G., andSpinale, F.G. Aprotinin in cardiac surgery: a review of conventional and novel mechanisms of action. Anesth Analg **105**, 949, 2007.

95. Bull, D.A., andMaurer, J. Aprotinin and preservation of myocardial function after ischemia-reperfusion injury. Ann Thorac Surg **75**, S735, 2003.

96. Thomson, K.S., Korte, F.S., Giachelli, C.M., Ratner, B.D., Regnier, M., andScatena, M. Prevascularized Microtemplated Fibrin Scaffolds for Cardiac Tissue Engineering Applications. Tissue Eng Part A 2013.

97. Naderi, H., Matin, M.M., andBahrami, A.R. Review paper: critical issues in tissue engineering: biomaterials, cell sources, angiogenesis, and drug delivery systems. J Biomater Appl **26**, 383, 2011.

98. Cosson, M., Debodinance, P., Boukerrou, M., Chauvet, M.P., Lobry, P., Crépin, G., andEgo, A. Mechanical properties of synthetic implants used in the repair of prolapse and urinary incontinence in women: which is the ideal material? Int Urogynecol J Pelvic Floor Dysfunct **14**, 169, 2003.

99. Kidd, K.R., Nagle, R.B., andWilliams, S.K. Angiogenesis and neovascularization associated with extracellular matrix-modified porous implants. J Biomed Mater Res **59**, 366, 2002.

100. Christman, K.L., Vardanian, A.J., Fang, Q., Sievers, R.E., Fok, H.H., andLee, R.J. Injectable fibrin scaffold improves cell transplant survival, reduces infarct expansion, and induces neovasculature formation in ischemic myocardium. Journal of the American College of Cardiology **44**, 654, 2004.

101. Jockenhoevel, S., Zund, G., Hoerstrup, S.P., Chalabi, K., Sachweh, J.S., Demircan, L., Messmer, B.J., andTurina, M. Fibrin gel -- advantages of a new scaffold in cardiovascular tissue engineering. Eur J Cardiothorac Surg **19**, 424, 2001.

102. Stevens, K., Kreutziger, K., Dupras, S., Korte, F., Regnier, M., Muskheli, V., Nourse, M., Bendixen, K., Reinecke, H., andMurry, C. Physiological function and transplantation of scaffold-free and vascularized human cardiac muscle tissue. Proc Natl Acad Sci U S A **106**, 16568, 2009.

103. Koutsioumpa, M., Hatziapostolou, M., Mikelis, C., Koolwijk, P., andPapadimitriou, E. Aprotinin stimulates angiogenesis and human endothelial cell migration through the growth factor pleiotrophin and its receptor protein tyrosine phosphatase beta/zeta. Eur J Pharmacol **602**, 245, 2009.

104. Buser, Z., Kuelling, F., Liu, J., Liebenberg, E., Thorne, K.J., Coughlin, D., andLotz, J.C. Biological and biomechanical effects of fibrin injection into porcine intervertebral discs. Spine (Phila Pa 1976) **36**, E1201, 2011.

105. Lorentz, K.M., Kontos, S., Frey, P., andHubbell, J.A. Engineered aprotinin for improved stability of fibrin biomaterials. Biomaterials **32**, 430, 2011.

106. Ye, Q., Zünd, G., Benedikt, P., Jockenhoevel, S., Hoerstrup, S.P., Sakyama, S., Hubbell, J.A., andTurina, M. Fibrin gel as a three dimensional matrix in cardiovascular tissue engineering. Eur J Cardiothorac Surg **17**, 587, 2000.

107. Smith, J.D., Chen, A., Ernst, L.A., Waggoner, A.S., andCampbell, P.G. Immobilization of aprotinin to fibrinogen as a novel method for controlling degradation of fibrin gels. Bioconjug Chem **18**, 695, 2007.

108. Fritz, H., andWunderer, G. Biochemistry and applications of aprotinin, the kallikrein inhibitor from bovine organs. Arzneimittelforschung **33**, 479, 1983.

109. Carmona, P., Molina, M., andRodríguez-Casado, A. Raman study of the thermal behaviour and conformational stability of basic pancreatic trypsin inhibitor. Eur Biophys J **32**, 137, 2003.

110. Marshall AJ, I.C., Barker T, Sage EH, Hauch KD, Ratner BD. . ; . Biomaterials with tightly controlled poresize that promote vascular in-growth. *Polym Preprints* **45: 100-101.**2004.

111. Dvorak, H.F., Harvey, V.S., Estrella, P., Brown, L.F., McDonagh, J., andDvorak, A.M. Fibrin containing gels induce angiogenesis. Implications for tumor stroma generation and wound healing. Lab Invest **57**, 673, 1987.

112. van Hinsbergh, V.W., Collen, A., andKoolwijk, P. Role of fibrin matrix in angiogenesis. Ann N Y Acad Sci **936**, 426, 2001.

113. Jurasz, P., Santos-Martinez, M.J., Radomska, A., andRadomski, M.W. Generation of platelet angiostatin mediated by urokinase plasminogen activator: effects on angiogenesis. J Thromb Haemost **4**, 1095, 2006.

114. Radziwon-Balicka, A., Moncada de la Rosa, C., Zielnik, B., Doroszko, A., andJurasz, P. Temporal and pharmacological characterization of angiostatin release and generation by human platelets: implications for endothelial cell migration. PLoS One **8**, e59281, 2013.

115. Hill, G.E., Diego, R.P., Stammers, A.H., Huffman, S.M., andPohorecki, R. Aprotinin enhances the endogenous release of interleukin-10 after cardiac operations. Ann Thorac Surg **65**, 66, 1998.

116. McEvoy, M.D., Taylor, A.G., Zavadzkas, J.A., Mains, I.M., Ford, R.L., Stroud, R.E., Jeffords, L.B., Beck, C.U., Reeves, S.T., andSpinale, F.G. Aprotinin exerts differential and dose-dependent effects on myocardial contractility, oxidative stress, and cytokine release after ischemia-reperfusion. Ann Thorac Surg **86**, 568, 2008.

117. Asimakopoulos, G., Lidington, E.A., Mason, J., Haskard, D.O., Taylor, K.M., andLandis, R.C. Effect of aprotinin on endothelial cell activation. J Thorac Cardiovasc Surg **122**, 123, 2001.

118. Hill, G.E., Pohorecki, R., Alonso, A., Rennard, S.I., andRobbins, R.A. Aprotinin reduces interleukin-8 production and lung neutrophil accumulation after cardiopulmonary bypass. Anesth Analg **83**, 696, 1996.

119. Brown, B.N., Valentin, J.E., Stewart-Akers, A.M., McCabe, G.P., andBadylak, S.F. Macrophage phenotype and remodeling outcomes in response to biologic scaffolds with and without a cellular component. Biomaterials **30**, 1482, 2009.

120. Lee, C.G., Homer, R.J., Zhu, Z., Lanone, S., Wang, X., Koteliansky, V., Shipley, J.M., Gotwals, P., Noble, P., Chen, Q., Senior, R.M., andElias, J.A. Interleukin-13 induces tissue fibrosis by selectively stimulating and activating transforming growth factor beta(1). J Exp Med **194**, 809, 2001.

121. Rolfe, B., Mooney, J., Zhange, B., Jahnke, S., Le, S.-J., Chau, Y.-Q., Huang, Q., Wang, H., Campbell, G., andCampbell, J. The Fibrotic Response to Implanted Biomaterials: Implications for Tissue Engineering, Regenerative Medicine and Tissue Engineering. In: Eberli D., ed.2011.

122. McDevitt, T.C., Angello, J.C., Whitney, M.L., Reinecke, H., Hauschka, S.D., Murry, C.E., andStayton, P.S. In vitro generation of differentiated cardiac myofibers on micropatterned laminin surfaces. J Biomed Mater Res **60**, 472, 2002.

123. Black, L.D., Meyers, J.D., Weinbaum, J.S., Shvelidze, Y.A., andTranquillo, R.T. Cell-induced alignment augments twitch force in fibrin gel-based engineered myocardium via gap junction modification. Tissue Eng Part A 2009.

124. Melero-Martin, J.M., De Obaldia, M.E., Kang, S.Y., Khan, Z.A., Yuan, L., Oettgen, P., andBischoff, J. Engineering robust and functional vascular networks in vivo with human adult and cord blood-derived progenitor cells. Circ Res **103**, 194, 2008.

125. Davis, G.E., Koh, W., andStratman, A.N. Mechanisms controlling human endothelial lumen formation and tube assembly in three-dimensional extracellular matrices. Birth Defects Res C Embryo Today **81**, 270, 2007.

126. Caspi, O., Lesman, A., Basevitch, Y., Gepstein, A., Arbel, G., Habib, I.H., Gepstein, L., andLevenberg, S. Tissue engineering of vascularized cardiac muscle from human embryonic stem cells. Circ Res **100**, 263, 2007.

127. Liu, X., Simpson, J., Brunt, K., Ward, C., Hall, S., Kinobe, R., Barrette, V., Tse, M., Pang, S., Pachori, A., Dzau, V., Ogunyankin, K., andMelo, L. Preemptive heme oxygenase-1 gene delivery reveals reduced mortality and preservation of left ventricular function 1 yr after acute myocardial infarction. Am J Physiol Heart Circ Physiol **293**, H48, 2007.

128. Liu, X., Pachori, A., Ward, C., Davis, J., Gnecchi, M., Kong, D., Zhang, L., Murduck, J., Yet, S., Perrella, M., Pratt, R., Dzau, V., andMelo, L. Heme oxygenase-1 (HO-1) inhibits postmyocardial infarct remodeling and restores ventricular function. FASEB J **20**, 207, 2006.

129. Rodriguez, A.G., Han, S.J., Regnier, M., andSniadecki, N.J. Substrate stiffness increases twitch power of neonatal cardiomyocytes in correlation with changes in myofibril structure and intracellular calcium. Biophys J **101**, 2455, 2011.

130. Shiba, Y., Fernandes, S., Zhu, W.Z., Filice, D., Muskheli, V., Kim, J., Palpant, N.J., Gantz, J., Moyes, K.W., Reinecke, H., Van Biber, B., Dardas, T., Mignone, J.L., Izawa, A., Hanna, R., Viswanathan, M., Gold, J.D., Kotlikoff, M.I., Sarvazyan, N., Kay, M.W., Murry, C.E., andLaflamme, M.A. Human ES-cell-derived cardiomyocytes electrically couple and suppress arrhythmias in injured hearts. Nature **489**, 322, 2012.

131. Robey, T.E., Saiget, M.K., Reinecke, H., andMurry, C.E. Systems approaches to preventing transplanted cell death in cardiac repair. J Mol Cell Cardiol **45**, 567, 2008.

132. Brauker, J., Martinson, L.A., Hill, R.S., Young, S.K., Carr-Brendel, V.E., andJohnson, R.C. Neovascularization of immunoisolation membranes: the effect of membrane architecture and encapsulated tissue. Transplant Proc **24**, 2924, 1992.

133. Brauker, J.H., Carr-Brendel, V.E., Martinson, L.A., Crudele, J., Johnston, W.D., andJohnson, R.C. Neovascularization of synthetic membranes directed by membrane microarchitecture. J Biomed Mater Res **29**, 1517, 1995.

134. Marshall AJ, I.C., Barker T, Sage EH, Hauch KD, Ratner BD. . ; . Biomaterials with tightly controlled poresize that promote vascular in-growth. *Polym Preprints* **45: 100-101.)**2004.

135. Villalona, G.A., Udelsman, B., Duncan, D.R., McGillicuddy, E., Sawh-Martinez, R.F., Hibino, N., Painter, C., Mirensky, T., Erickson, B., Shinoka, T., andBreuer, C.K. Cell-seeding techniques in vascular tissue engineering. Tissue Eng Part B Rev **16**, 341, 2010.

136. Roh, J.D., Nelson, G.N., Udelsman, B.V., Brennan, M.P., Lockhart, B., Fong, P.M., Lopez-Soler, R.I., Saltzman, W.M., andBreuer, C.K. Centrifugal seeding increases seeding efficiency and cellular distribution of bone marrow stromal cells in porous biodegradable scaffolds. Tissue Eng **13**, 2743, 2007.

137. Pawlowski, K.J., Rittgers, S.E., Schmidt, S.P., andBowlin, G.L. Endothelial cell seeding of polymeric vascular grafts. Front Biosci **9**, 1412, 2004.

138. Sagnella, S., Anderson, E., Sanabria, N., Marchant, R.E., andKottke-Marchant, K. Human endothelial cell interaction with biomimetic surfactant polymers containing Peptide ligands from the heparin binding domain of fibronectin. Tissue Eng **11**, 226, 2005.

139. Salacinski, H.J., Tiwari, A., Hamilton, G., andSeifalian, A.M. Cellular engineering of vascular bypass grafts: role of chemical coatings for enhancing endothelial cell attachment. Med Biol Eng Comput **39**, 609, 2001.

140. Hsu, S.H., Tsai, I.J., Lin, D.J., andChen, D.C. The effect of dynamic culture conditions on endothelial cell seeding and retention on small diameter polyurethane vascular grafts. Med Eng Phys **27**, 267, 2005.

141. Nieponice, A., Soletti, L., Guan, J., Deasy, B.M., Huard, J., Wagner, W.R., andVorp, D.A. Development of a tissue-engineered vascular graft combining a biodegradable scaffold, muscle-derived stem cells and a rotational vacuum seeding technique. Biomaterials **29**, 825, 2008.

142. Williams, C., andWick, T.M. Perfusion bioreactor for small diameter tissue-engineered arteries. Tissue Eng **10**, 930, 2004.

143. van Wachem, P.B., Stronck, J.W., Koers-Zuideveld, R., Dijk, F., andWildevuur, C.R. Vacuum cell seeding: a new method for the fast application of an evenly distributed cell layer on porous vascular grafts. Biomaterials **11**, 602, 1990.

144. Bowlin, G.L., Meyer, A., Fields, C., Cassano, A., Makhoul, R.G., Allen, C., andRittgers, S.E. The persistence of electrostatically seeded endothelial cells lining a small diameter expanded polytetrafluoroethylene vascular graft. J Biomater Appl **16**, 157, 2001.

145. Tiwari, A., Punshon, G., Kidane, A., Hamilton, G., andSeifalian, A.M. Magnetic beads (Dynabead) toxicity to endothelial cells at high bead concentration: implication for tissue engineering of vascular prosthesis. Cell Biol Toxicol **19**, 265, 2003.

146. Perea, H., Aigner, J., Heverhagen, J.T., Hopfner, U., andWintermantel, E. Vascular tissue engineering with magnetic nanoparticles: seeing deeper. J Tissue Eng Regen Med **1**, 318, 2007.

147. Perea, H., Aigner, J., Hopfner, U., andWintermantel, E. Direct magnetic tubular cell seeding: a novel approach for vascular tissue engineering. Cells Tissues Organs **183**, 156, 2006.

148. Shimizu, K., Ito, A., Lee, J.K., Yoshida, T., Miwa, K., Ishiguro, H., Numaguchi, Y., Murohara, T., Kodama, I., andHonda, H. Construction of multi-layered cardiomyocyte sheets using magnetite nanoparticles and magnetic force. Biotechnol Bioeng **96**, 803, 2007.

149. Shimizu, K., Ito, A., andHonda, H. Enhanced cell-seeding into 3D porous scaffolds by use of magnetite nanoparticles. J Biomed Mater Res B Appl Biomater **77**, 265, 2006.

150. Niklason, L.E., Gao, J., Abbott, W.M., Hirschi, K.K., Houser, S., Marini, R., andLanger, R. Functional arteries grown in vitro. Science **284**, 489, 1999.

151. Zhao, F., andMa, T. Perfusion bioreactor system for human mesenchymal stem cell tissue engineering: dynamic cell seeding and construct development. Biotechnol Bioeng **91**, 482, 2005.

152. Inoguchi, H., Tanaka, T., Maehara, Y., andMatsuda, T. The effect of gradually graded shear stress on the morphological integrity of a huvec-seeded compliant small-diameter vascular graft. Biomaterials **28**, 486, 2007.

153. Brown, M.A., Iyer, R.K., andRadisic, M. Pulsatile perfusion bioreactor for cardiac tissue engineering. Biotechnol Prog **24**, 907, 2008.

154. Radisic, M., Marsano, A., Maidhof, R., Wang, Y., andVunjak-Novakovic, G. Cardiac tissue engineering using perfusion bioreactor systems. Nat Protoc **3**, 719, 2008.